David Magalhães Sousa
Licenciatura em Química Aplicada

SOLUTION PROCESSED QUANTUM DOT PHOTODETECTORS

Dissertação para obtenção do Grau de Mestre em
Engenharia de Materiais

Orientador: Doutor Manuel João de Moura Dias Mendes, Pós-Doc CENIMAT, FCT-UNL
Co-orientador: Professor Doutor João Carlos dos Santos Silva e Pereira de Lima, Professor Associado, FCT-UNL

Presidente: Professor Doutor Hugo Manuel Brito Águas, Professor Auxiliar, FCT-UNL
Arguente: Doutor César António Tonicha Laia, Investigador Auxiliar, FCT-UNL
Vogal: Doutor Manuel João de Moura Dias Mendes, Pós-Doc CENIMAT, FCT-UNL

FACULDADE DE CIÊNCIAS E TECNOLOGIA
UNIVERSIDADE NOVA DE LISBOA

Setembro 2015

Aos meus insubstituíveis pais e irmão

Agradecimentos

Ao meu orientador Manuel João Mendes, que no inicio da tese me guiou para um tema deveras interessante e que me proporcionou a entrada neste gigante mundo das pequeníssimas coisas.

Ao meu co-orientador João Carlos Lima que, ao longo de 7 anos de convivência, se esforçou por me ensinar a lidar com a ciência e com o mundo académico.

À Professora Isabel Ferreira por me ter apoiado e incentivado a prosseguir quando me sentia menos motivado.

Ao pessoal do CENIMAT e do CEMOP que me ajudou quando precisei de pequenas artimanhas e artefactos.

À Tatiana por me ter dado ânimo naqueles dias em que queria largar tudo e ir trabalhar para um restaurante de fast-food, não me deixando desistir. <3

Aos meus pais que, apesar de não perceberem patavina da minha tese, me apoiaram vibrando com todos os meus êxitos e sofrendo com os meus fracassos, nunca duvidando das minhas capacidades.

Ao meu irmão que pelos seus "não percebi nada, explica outra vez!" que me obrigou a reformular vezes sem conta os meus raciocínios na tentativa de os tornar acessíceis a um leigo.

Ao meu avô que queria sempre saber qual era a minha ocupação, por me ver tantas horas ligado à "maquineta" e que pouco antes de eu terminar esta tese nos deixou, possivelmente para ir estudar química e materiais astrais.

À "o meu dono! o meu dono! o meu dono!" Kira, ao "se te aproximas eu rosno" Gibbs e ao "não quero saber de ti... se calhar quero" Mitsu, pela dedicada e terna companhia nas longas tardes e noites em frente ao computador.

Este trabalho foi suportado pelos projectos **PTDC/AAG-TEC/2721/2012** e **ERC-CoG-2014-CapTherPV**.

Your wings, though ruined,
are not without purpose.
Take hold of them as you leap,
and they will carry you across
this chasm

Elder God, Legacy of Kain, 1999

Abstract

To find sustainable solutions for the production of energy, it is necessary to create photovoltaic technologies that make every photon count. To pursue this necessity, in the present work photodetectors of zinc oxide embedded with nano-structured materials, that significantly raise the conversion of solar energy to electric energy, were developed.

The novelty of this work is on the development of processing methodologies in which all steps are in solution: quantum dots synthesis, passivation of their surface and sol-gel deposition.

The quantum dot solutions with different capping agents were characterized by UV-visible absorption spectroscopy, spectrofluorimetry, dynamic light scattering and transmission electron microscopy. The obtained quantum dots have dimensions between 2 and 3nm. These particles were suspended in zinc acetate solutions and used to produce doped zinc oxide films with embedded quantum dots, whose electric response was tested.

The produced nano-structured zinc oxide materials have a superior performance than the bulk, in terms of the produced photo-current. This indicates that an intermediate band material should have been produced that acts as a photovoltaic medium for solar cells. The results are currently being compiled in a scientific article, that is being prepared for possible submission to Energy and Environmental Science or Nanoscale journals.

Resumo

Encontrar soluções sustentáveis para a produção de energia leva à necessidade de criar tecnologias fotovoltaicas onde todos os fotões contem. É neste âmbito que se insere o presente trabalho, onde se desenvolveram foto-detetores de óxido de zinco usando materiais nano-estruturados, que aumentam significativamente a conversão de energia solar em corrente elétrica.

A novidade do trabalho está no desenvolvimento de metodologias de processamento em que todos os passos são em solução: síntese de pontos quânticos, passivação da superfície e deposição sol-gel.

As soluções de pontos quânticos com diferentes agentes estabilizantes foram caracterizadas por espectroscopia de absorção UV-visível, espectrofluorimetria, dispersão de luz dinâmica e microscopia eletrónica de transmissão. Os pontos quânticos obtidos têm dimensões entre 2 e 3nm. Estas partículas foram suspensas em soluções de acetato de zinco e utilizadas para produzir filmes de óxido de zinco com pontos quânticos embebidos, que foram testados relativamente à resposta elétrica.

Os materiais nano-estruturados de óxido de zinco produzidos têm um desempenho superior à massa, relativamente à foto-corrente produzida. Tal indica que se produziu um material de banda intermédia que deverá servir como meio fotovoltaico eficiente em células solares. Os resultados estão a ser compilados para submissão na revista Energy and Environmental Science ou Nanoscale.

Abbreviations and Symbols

α	- Absortion coefficient
λ	- Wavelength
Ω	- Ohm unit
3-MT	- 3-Methylthiophene
AN	- Acetonitrile
Bpy	- 2,2'-Bipyridine
CB	- Conduction band
CQD	- Colloidal quantum dot
Cys	- L-Cysteine
DC	- Direct current
DLS	- Dynamic light scattering
e^-	- Electron
eV	- Electronvolt
IB	- Intermediate band
IBSC	- Intermediate band solar cell
IBPVD	- Intermediate band photovoltaic device
IQE	- Internal quantum efficiency
MEH-PPV	- Poly[2-methoxy-5-(2-ethylhexyloxy)-1,4-phenylenevinylene]
NaAce	- Sodium acetate trihydrate
NIR	- Near-infrared
PV	- Photovoltaic
PI	- Polydispersity index
Py	- Pyridine
QD	- Quantum dot
QDSC	- Quantum dot solar cell
RI	- Refractive index
SEM	- Scanning electron microscopy
TEM	- Transmission electron microscopy
TCO	- Transparent conductive oxide
VB	- Valence band
ZnAce	- Zinc acetate dihydrate

Contents

List of Figures

List of Tables

Objective

The objective of the present work is to develop novel nano-structured hybrid materials based on semiconductor quantum dots for the construction of photodetectors, which can be entirely processed in a series of chemical solution and can exhibit improved broadband sensitivity.

Based on published strategies for the quantum dot synthesis, we decided to go a step further in testing different conditions, capping agents, stabilizing agents and solvents. Additionally, a new deposition method was introduced for a more homogeneous deposition of the films, containing the nano-structured hybrid materials.

The final goal was to demonstrate that nanostructured hybrid materials could perform better at longer wavelength, with respect to the host matrix (zinc oxide). In this sense, the goal was fully reached.

1. Introduction

1.1. Motivation

As the world marches into drastic climate changes, due to emissions of greenhouse gases, and the oil output is falling while the price will rise beyond sustainability, it is our duty to develop cleaner and cheaper sources of energy, like renewable ones.[1, 2, 3]

One of the steps to mitigate these changes, is to directly harvest one of the most abundant energy sources: the Sun. Enough usable solar energy reaches the earth: an astonishing $3.6 * 10^4$ TW, to serve our 17 TW needs.[4] The major problems, associated to the solar energy harvesting, are the price and efficiency of the photovoltaic (PV) cells. Much technology has been developed, since the 20th century, mostly based on conventional crystalline silicon wafer devices.

On the turn of the century, new PV technologies are being developed with a common purpose: to make every photon count. I.e. to allow a better exploitation of the wide spectrum of sunlight and, thereby, boost the solar cells conversion efficiency. Nanotechnology has been a major driver of this development, since it allows structuring the PV materials at almost atomic scale and, in this way, form artificial media enabling a more optimized light-matter interaction. Two of the most investigated PV concepts employing nanostructured materials are: the intermediate band solar cell (IBSC) and the quantum dot solar cell (QDSC). These types of architectures enable the capturing of lower energy photons, due to quantum effect - explained on section 1.3.4, leading to higher efficiencies.[5] IBSC's quantum dot (QD) layers are epitaxially grown from a crystalline substrate, with a lattice constant similar to the QD's, and require expensive and complex production methods. QDSCs, although being solution processed, suffer from lack of efficiency on electron (e^-) transport. The electrons hop from dot-to-dot, as shown in Figure 1.1, adapted from [6], leading to lower carrier mobilities.[7]

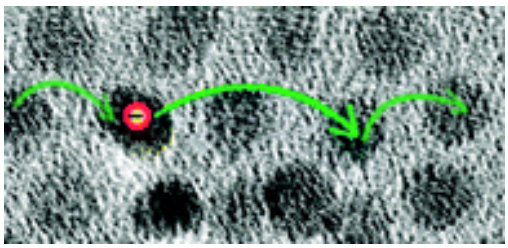

Figure 1.1: Illustration of an electron hopping from a QD to another neighboring QD. Adapted from Liu et al., 2010.

The focus of this project will be the development of solution-processed colloidal quantum dot (CQD) photodetector devices, to test several combinations of different QD materials and oxide matrices. The first approach consists in testing different capping agent, their spectral response, and the CQDs' behaviour in the sol-gel precursor solution.

Solution-processed quantum dots can be sprayed onto many kinds of surfaces, via scalable and low cost processes[8]. This enables roll-to-roll manufacturing, cutting the economic barrier of the production of solar cells. Instead of depositing the QDs on the photovoltaic device's semiconductor surface, they can easily be embedded into the semiconductor which acts as the host. An immediate consequence of having the QDs surrounded by a conductive matrix, is the efficiency improvement due to a better carrier transport (i.e. less electric resistivity), since the electrons will not be transfered through tunneling effect or hopping, but through the conduction band of the matrix medium.[7] Proof of concept experiments could be performed using arrays of photodetectors built in the same platform (see Figure 1.2). This would allow fast sequential testing of the photoresponse of several different combinations of CQDs and matrix materials, to rapidly

determine the preferential physical properties for PV application.

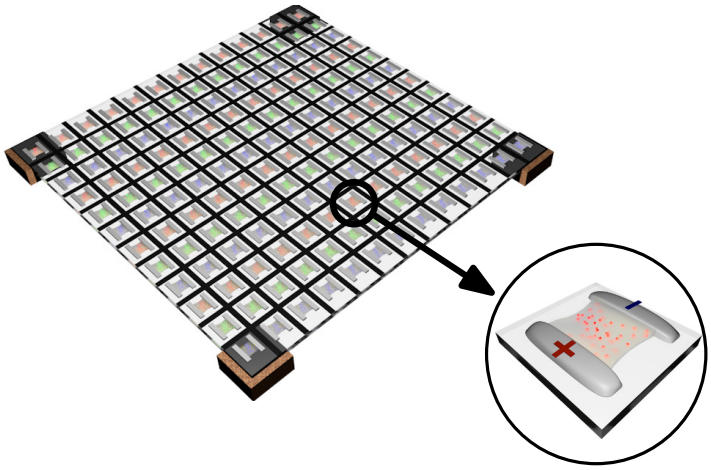

Figure 1.2: Proposed model of an array of solution-processed quantum dot photodetector devices, with a zoom on a single cell. The red plus and the blue minus indicate the corresponding polarity of the deposited contacts and the red shinning dots correspond to the embedded CQDs in a transparent conductive oxide (TCO) matrix. The array's purpose is to quickly test several combinations of QD's (with different sizes and materials) and matrices (varying the material and doping).

1.2. State of Art

A polymer-nanocrystal composite photodetector was built in 1996, composed of photoconductive polymer poly[2-methoxy-5-(2-ethylhexyloxy)-1,4-phenylenevinylene] (MEH-PPV) and a mixture of CdSe and CdS QDs. These devices exhibited limited spectral sensivity, due to the polymer and nanocrystals' limited absorption, from the visible up to 650 nm.[9]

In 2005, Mcdonald's group improved the latter device, by sensitizing the polymer towards longer wavelenghts into the infrared with PbS QDs.[10]

Another interesting development, in 2009, was the fabrication of a nanocomposite photodetector composed of a mesoporous titanium dioxide (TiO_2) matrix, impregnated with CdSe quantum dots. It is possible to observe in Figure 1.3, adapted from [11], the CdSe QDs, involved by the titanium dioxide matrix. Both components were solution-processed. The matrix was prepared by sol-gel reaction and the QDs were embedded into it. As described by the group, the QDs capture the photons and excite the electrons to the conduction band of the titanium dioxide. Driven by the applied electric field, the excited carriers are conducted to the contacts, creating current. They also reported that the size of the pores of the titanium dioxide matrix, inflicted a blue-shift to the photoluminescence of the QDs, due to a higher confinement.[11]

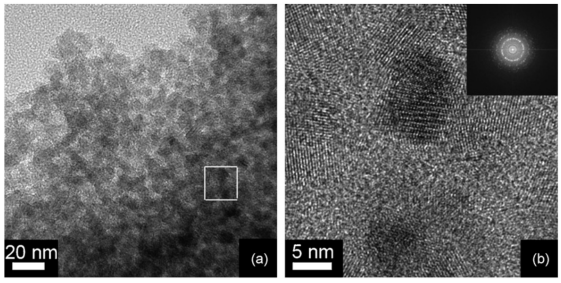

Figure 1.3: High resolution transmission electronic microscopy of the mesoporous titanium dioxide matrix, embedded with CdSe QDs. (b) corresponds to the amplification of the section, represented as a white square, in (a). The atomic planes of the CdSe QDs can be appreciated in the image, revealing their crystalline structure.

In a similar fashion to the TiO_2/CdSe device, a photodetector, represented in Figure 1.4, adapted from [12], composed of a zinc oxide matrix embedded with CdSe or CdS QDs was developed. The ZnO/CdSe blend device showed a promising internal quantum efficiency (IQE), fraction of absorbed photons that are converted to electrons, of 49%.[12]

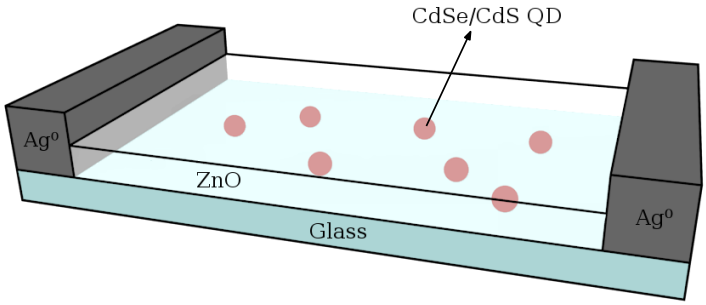

Figure 1.4: Schematic representation of the photodetector device, fabricated by White et al., 2013.

In the following sections the basic principles of the photovoltaic effect and the quantum dots will be presented.

1.3. Background Theory

1.3.1. Photovoltaic Effect

The photovoltaic effect is the conversion of absorbed photons to direct current (DC) electrical power. Typical PV cells are composed of semiconductor materials that have a valence band (VB) and a conduction band (CB), both separated by a given energy, usually expressed in electronvolt (eV), known as bandgap. The photovoltaic effect occurs when a photon collides with a VB electron and, if the photon has energy above the bandgap, the electron jumps to an excited state in the CB. If the semiconductor is connected to a positive contact, the electron begins it's journey to the external load, for example a battery, and then back to the negative contact, that delivers the traveler to the semiconductor's VB. The hole , on the other hand, sails on the opposite direction. Figure 1.5 is a schematic representation of a solar cell and an electron's and hole's closed circuits, for better understanding.[13]

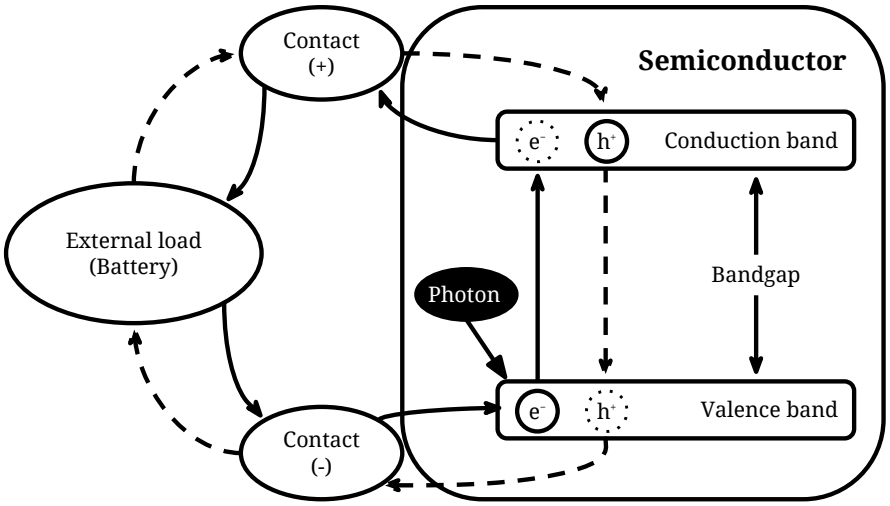

Figure 1.5: Schematic representation of a solar cell, its semiconductor's energy levels and an electron's and hole's closed circuit, excited by a photon.

1.3.2. Photodetector

A photodetector is, by definition, a device that is capable of detecting incident light (photons). There are several kinds of structures, like photodiodes, photogates, etc. The simplest structure was chosen: the photoconductor. The device is composed of a semiconductor and two contacts, as shown in Figure 1.4. When light hits the surface of the semiconductor, an electron-hole pair forms, known as exciton. If an external electric field is applied to the device, the electron will drift to the positive contact, while the hole will go to the negative one. This effect generates current.[14]

1.3.3. Intermediate Band

An intermediate band photovoltaic device has the architecture of a conventional solar cell, with an added feature: a band in between the semiconductor's VB and CB, originated from a second material. This band is denominated as intermediate band (IB) and confers the conjuncture three absorption coefficients (α), corresponding to the three electronic transitions: from VB to CB (α_{VC}), from VB to IB (α_{VI}) and from IB to CB (α_{IC}), as shown in Figure 1.6.[15]

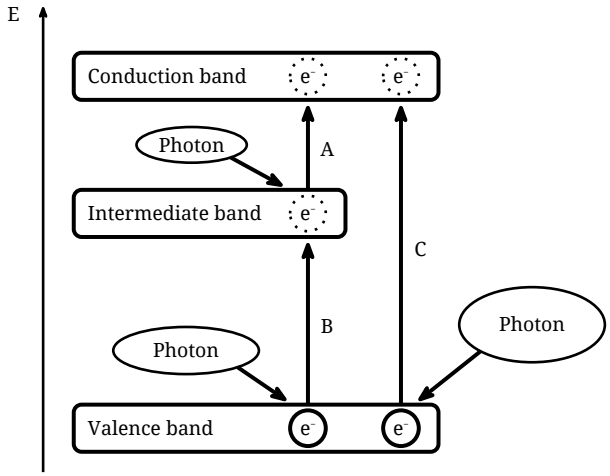

Figure 1.6: Diagram of semiconductor's energy levels, coupled with a material that supplies the intermediate band. A - electronic transition corresponding to α_{IC}; B - electronic transition corresponding to α_{VI}; C - electronic transition corresponding to α_{VC}.

The optimal IBSC has a bandgap of 1.95eV, subdivided into 0.71eV and 1.24eV subbandgaps.[16] Having a 1.95eV bandgap means that the matrix material will only absorb photons with equal, or greater, energy - Figure 1.6, transition C. The intermediate band will enable the capturing of lower energy photons - Figure 1.6, transitions A and B, proportionating a predicted maximum of 63,2% of conversion efficiency. This is possible due to a better exploitation of the solar radiation spectrum; as the solar cells are able to absorb a greater range of photon energies below the bandgap of the semiconductor matrix. For comparison, the conventional Si single-junction wafer cell can only achieve a theoretical maximum of 40,7% of efficiency.[16]

1.3.4. Quantum Dots

The name "quantum dot" was first given by Mark Reed's group, after observing them, through scanning electron microscopy (SEM), in GaAs nanostructures.[17]

The QDs' size range is up to tens of nanometers and they exhibit different properties from the bulk material. One effect derived from reducing a particle to the nanoscale is the quantum confinement. This effect manifests itself when the diameter of a particle reaches the value of electrons' de Broglie wavelength. As a result, a discrete energy level

structure is obtained, as opposed to the band-like structure in bulk materials. Further reduction of the nanoparticle's size leads to a stronger confinement and, consequently, to a raise in the bandgap's energy.[18] This permits the energy matching between donor and acceptor materials, to enhance the efficiency of photovoltaic devices. By adjusting the QD's size, it is possible to tune the semiconductor's bandgap to match the photons' energy across most of the solar spectrum. Conventional bulk semiconductors, whose bandgap is fixed, cannot grasp the same matching.[19] Figure 1.7 illustrates the latter explanation.

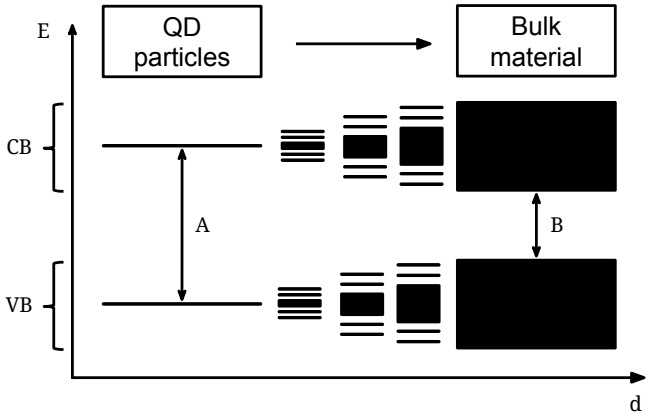

Figure 1.7: Illustration of the relation between bandgap energy and particle diameter, from QD size to bulk. As the particle size decreases, the bandgap increases from B to A.

1.3.5. Colloidal QDs

Expensive machinery is required to grow epitaxial QDs, like those usually employed in IBSCs [20, 21, 22], and their properties, like size, shape and composition, are hard to control. The synthesis of colloidal quantum dots (CQD), on the other hand, involves inexpensive wet lab material and is executed in simple steps. CQDs are QDs chemically fabricated through solution processes, involving salt precursors and capping agents. These agents, typically organic compounds or polymers, envelope the QDs to stabilize, solubilize and prevent further aggregation. This way, it is possible to control the QD's size and obtain a variety of colors, due to the quantization effect described in section 1.3.4. Smaller particles tend to emit purple/blue colors. This effect is known as blueshift. Bigger particles emit orange/red colors - redshift.[23, 24] Figure 1.8, adapted from Wikipedia [25], shows the relation between CQD's size and the emitted color of the corresponding suspension, under irradiation.

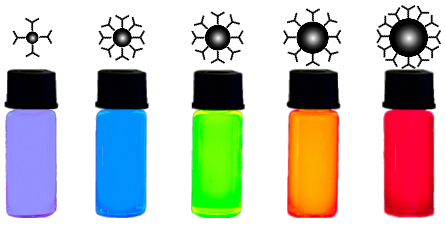

Figure 1.8: Relation between the size of the CQDs, with capping agents involving them, and the emitted color of the corresponding suspension, under irradiation.

If possible, the capping agent should be removed, after embedding the CQDs in the matrix, to reduce the resistance to the flow of electron from the QD to the matrix, or leave them on the QDs' surface if they can transport charges efficiently.

2. Materials and Methods

In this study, CdSe quantum dots were synthesized and capped with 2,2'-bipyridine, or simply bipyridine (Bpy), Pyridine (Py), 3-methylthiophene (3-MT), sodium acetate trihydrate (NaAce), L-cysteine (Cys) or zinc acetate dihydrate (ZnAce). zinc oxide precursor solutions were prepared and deposited, with or without embedded CQD, by means of spray pyrolysis and spin-coating. All reagents were used as received, without further purification. Unless otherwise stated, any mentioned compound or solvent has an equivalent degree of purity to puriss p.a.. and were bought from Sigma-Aldrich.

2.1. Synthesis

2.1.1. Zinc Oxide Sol-gel Precursors

The precursor was prepared as described by White et al. [12]. In a capped vial, 1g of zinc acetate dihydrate, reagent grade, 278mg of 2-ethanolamine, ≥98%, (about 7 drops) and 10mL of 2-methoxyethanol, ReagentPlus ≥99,0% with 50ppm BHT, further refereed as methoxyethanol, were mixed in the described order. The dissolution was carried at 80°C with vigorous stirring, for 1h. This solution was used on the experiment described in section 2.1.2.2. Three more batches were prepared for the experiment with the six different capping agents, for the dynamic light scattering (DLS) spectra acquisition and the spin-coat sol-gel depositions. These solutions will be further referred as ZnORG. As for methoxyethanol it will be referred as simply ORG. An aqueous zinc oxide sol-gel precursor solution was also prepared, for the spray pyrolysis deposition, consisting of 100mL of Milli-Q water, referred simply as water from here on, 4,390g of glacial acetic acid and 4,392g of zinc acetate dihydrate[26].

2.1.2. Cadmium Selenide Colloidal Quantum Dots

A Lumidot® CdSe kit was purchased from Sigma-Aldrich. 0,2mL of each Lumidot sample was dissolved in either 0,3mL of ORG or ZnORG. All flasks were protected from light with aluminium foil and capped with rubber septas, excluding the QDs' capping procedure and the following steps.

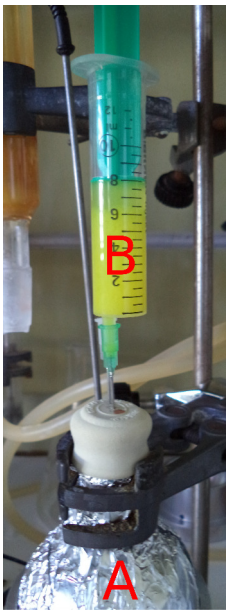

Figure 2.1: Experimental apparatus of CdSe CQD reaction vessel (A) and a syringe with freshly synthesized CdSe CQD (B).

2.1.2.1. Testing Different Capping Agents

Following a typical low temperature synthesis of CdSe [12], 37,30mg of selenium, ~100 mesh ≥99,5% trace metals basis, and 244,51mg of sodium sulfite, ≥98%, were mixed in 20mL of water. The mixture was heated to 100°C and refluxed for 1h. This solution was named sodium selenosulfate. To obtain the cadmium source, 532,90mg of cadmium acetate dihydrate, purum p.a. ≥98,0% (KT), was dissolved in 50mL of water and heated to 35°C for 15min. The sodium selenosulfate's temperature was lowered to 80°C and the syringe was heated for 5min in an oven, at 100°C. After injecting the sodium selenosulfate into the cadmium solution, the mixture was kept at 35°C and stirring for 2h.

To cap the CdSe QDs, a series of six falcon tubes with bipyridine, Alfa Aesar ACS ≥98%, pyridine, Merck p.a., 3-methylthiophene, ≥98%, sodium acetate trihydrate, Panreac PA-ACS-ISO, L-cysteine, non-animal source cell culture tested, and zinc acetate dihydrate were prepared, each with the equivalent to 192,1mmol of bipyridine dissolved in 3mL of acetone, PA. The exact weights of each capping agent is described in Table I in Appendix A. The tubes were named

according to the capping agent. To each tube, 8mL of CdSe CQD were introduced with the help of a syringe (Figure 2.1). A seventh tube was also prepared, named X, containing only 3mL of acetone, as a reference. Immediately after adding 8mL of the CdSe CQDs' suspension to each tube, they were subjected to shaking on a vortex, JANKE & KUNKEL IKA-Labortechnik VF2, for 10min. The washing cycle was done three times and consisted in centrifuging the tubes at 3000RPM, for 3min, in a Tehthica CENTRIC 150 centrifuge, decanting, refilling with 10mL of water and using the vortex to resuspend the pellet. After decanting, acetonitrile (AN), p.a., was added to all tubes, except the reference one, and suspended using an ultrasounds bath, Elmasonic 100H, for 30min, and then characterized, without diluting. All tubes were decanted again and put under vacuum, to remove the remaining AN. After drying, 1mg of each capped CdSe QD was weighted to eppendorfs and suspended, with the aid of an ultrasounds bath for 30min, in ORG solution. The latter process was repeated but this time they were suspended in ZnORG. Both ORG and ZnORG solution had a final concentration of 1mg/mL of capped CdSe CQDs. The prepared suspensions were then characterized. A table with the exact weights of CdSe CQDs can be found in Table II in Appendix A.

2.1.2.2. Evolution of 2,2'Bypridine Capped CdSe CQDs with Time

Another synthesis was done varying the reaction time and using bipyridine, dissolved in acetone, as the capping agent. The procedure was the same as before, varying slightly on the reactant weights: selenium - 37,3mg, sodium sulfide - 243,8mg, cadmium acetate dihydrate - 536,9mg. After 2h of reaction, 8mL of the CdSe CQDs' suspension was added to a falcon tube with 31,5mg of bipyridine in 3mL of acetone. After 5h and 40min, 8mL of the CdSe CQDs' suspension was added to a falcon tube with 31,0mg of bipyridine in 3mL of acetone. After 28h and 30min, 8mL of the CdSe CQDs' suspension was added to a falcon tube with 30,4mg of bipyridine in 3mL of acetone. The same washing, drying and suspension procedures were applied. In a similar fashion to the previous representation, the weights of bipyridine capped CdSe QDs used for optical characterization are displayed in Table III in Appendix A. Both ORG and ZnORG solution had a final concentration of 2mg/mL of capped CdSe CQDs.

2.1.2.3. CdSe CQDs capped with Molten 2,2'Bipyridine

A different experiment was attempted with bipyridine. 100mg were weighted to a 15mL falcon tube. The lower part of the tube was submerged into Baysilone® oil, as seen in Figure 2.2, with the cap closed. The oil's temperature was raised to 100°C, while slowly agitating the bipyridine with a magnet stirrer.

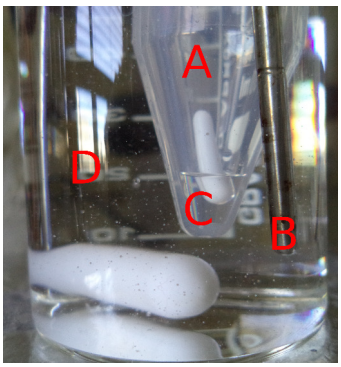

Figure 2.2: Apparatus for the CdSe CQD phase transfer to bipyridine. A - falcon tube with a stirrer. B - thermocouple. C - molten bipyridine. D - cup with Baysilone® oil and a stirrer.

After the bipyridine melted, 1mL of CdSe CQDs' suspension, after 2h of reaction, was slowly added at 35°C, without letting the bipyridine solidify. The stirring was

put on maximum speed for 1h at 100°C. The tube was then cooled down to room temperature and manually shaken, just enough to release three or four drops from the molten bipyridine to the upper aqueous phase. After the bipyridine instantaneously froze, the supernatant water was decanted. 1mL of water was added to the tube and then decanted. The tube was put under vacuum, to remove the remaining water.

2.2. Film Deposition

2.2.1. Spin-coat

The parameters tested were similar to the ones used by White et al.[12] The gorilla glass 2,5cm*2,5cm substrates were rinsed with acetone, dried with a air jet and cleaned with lint-free paper. 0,3mL of ZnORG solution was dispensed to the substrate in each deposition, before the spinning started. The rotation speed used were 1500RPM, 2500RPM, 3500RPM and 4500RPM, and for each rotation speed the following dwelling times were tested: 15s, 20s, 25s and 30s. The used acceleration ramp was of 10s. The deposited films were baked in a simple tube furnace at 180°C for 5min, with a heating ramp of 30min.

2.2.2. Spray Pyrolysis

An airbrush, Dexter, was used in pair with an airbrush compressor, HS08-5 from ROHS PAHS, that has three levels of pressure, ranging from 1,5bar (level 1) to 3,1bar (level 3). The substrates were cleaned with lint-free paper embedded in isopropanol and sprayed with an air jet, to remove the excess liquid. Schematics of the airbrush and heat plate positioning are represented in Figure 2.3.

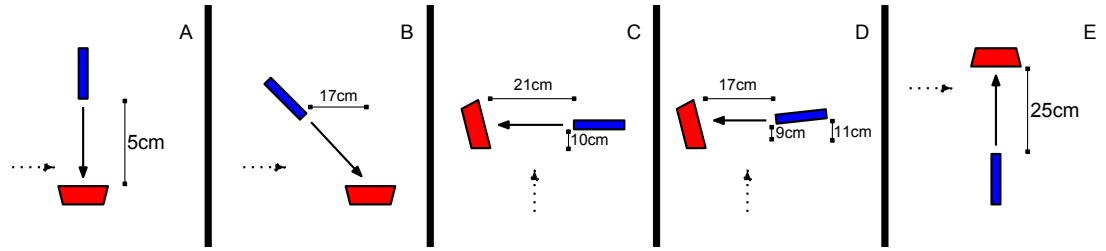

Figure 2.3: Schematics of the airbrush and heat plate positioning used for the spray pyrolysis deposition. The airbrush is represented in blue, the heat plate in red, the spray trajectory by a full black arrow and the fume hood air intake by a dashed black arrow. The letters identify the corresponding scheme.

In all schemes, a series of parameters, adapted from [26], were tested, like the volume of solution used or deposition time, the opening of the flux regulator of the airbrush and the pump's level. On scheme E, a total of 0,8mL of the aqueous zinc acetate dihydrate solution was used. The solution was dispensed with quick poofs, intercalated by no less than 10s of no spray, with a pressure of 1,5bar, the airbrush's flux regulator with one and a half turns and the heat plate stabilized at 180°C. Using the latter parameters, 4mg of L-cysteine capped CdSe CQDs where added to 0,7mL of the aqueous solution of zinc acetate dihydrate, the mixture was put on a ultrasounds bath for 10min and then sprayed onto a substrate. The deposition of the solution without the CQDs was replicated. Aluminium contacts, 1cm apart, were evaporated onto the surface of the surface of both films, with and without the L-cysteine capped CdSe CQDs, by evaporation.

2.3. Characterization

2.3.1. Cadmium Selenide Colloidal Quantum Dots

All absorption spectra were taken in a quartz cell with a 2mm optical path and a capacity of 0,7mL. For the absorption spectra, double-beam spectrometers were used and the baseline was done with both sample and reference compartments empty. The

emission spectra were taken in a cell with the same dimensions but with clear sides. The absorption spectra of the CdSe CQD, from the experiment described in section 2.1.2.2, dispersed in methoxyethanol, with and without zinc acetate dihydrate, ranging from 200nm to 2000nm, was recorded in a spectrophotometer Cary 5000. The absorption spectra of the CdSe CQD from the experiment described in section 2.1.2.1, in ORG and ZnORG, ranging from 200nm to 800nm, was measured in a spectrophotometer, Cary 100 Bio. The emission spectra of the CdSe CQD in AN, with a slit of 2nm, ORG and ZnORG, with a slit of 4nm, was measured in a HORIBA spectrofluorometer, model iHR 320. All spectra recording was done at room temperature. The characterizations were also performed on the Lumidot described in Section 2.1.2, in order to compare the results with standard commercial CQDs. For the full list of parameters reported by the devices, refer to Table V for the absorption spectra in AN, Table VI and Table VII for the absorption spectra in ORG and ZnORG, for the experiments described in section 2.1.2.1 and the experiments described in section 2.1.2.2 respectively.

The DLS spectra was done in a Horiba SZ-100, using a a quartz cell with clear sides, 2mm wide and with a 1cm optical path length, and to acquire the zeta potential a AGILE Carbon Zeta Potential Cell. All tests were done at 25°C.

Solutions of 0,01mg.mL^{-1} to 0,03mg.mL^{-1} of the synthesized QCDs in ethanol were prepared and the transmission electron microscopy (TEM) images were acquired from an Hitachi H-8100, using a grid of copper as support.

2.3.2. Film Deposition and Photo-response Measurement

The films deposited by spin-coating were characterized in a Shimadzu UV-3101PC spectrophotometer, using a integrating sphere. The films deposited by spray pyrolysis were characterized in a PG Instruments Ltd spectrophotometer, model T90+ UV/Vis. To test the photo-response, the electric conductance of the films was measured in the range of voltage between -10V and 10V, with a 500mV step, in ambient light. The test was repeated by illuminating the films with a white LED flashlight, held at around 5cm from the film's surface, and 254nm and 366nm wavelength light, from common laboratory UV lamps, held at around 15cm from the films' surface.

3. Results and Discussion

3.1. General Considerations

Pyridine and some thiol compounds[27, 28] are usually chosen as capping agents, but due to their volatility, toxicity and strongly unpleasant smell, a series of other capping agents were tested.

All the CdSe CQDs' suspensions formed a deposit, after 24h, when suspended in methoxyethanol without zinc acetate dihydrate. Although the solutions did not form stable colloids, every capping agent, except zinc acetate dihydrate, performed well at chemically stabilizing the CdSe QDs. In the next sections, the individual characteristics of uncapped and bipyridine, L-cysteine and zinc acetate dihydrate capped CdSe CQDs will be discussed. Subsequently, dedicated DLS and TEM sections are presented. The remaining capping agents are included in the comparison section since their proprieties are similar to the bipyridine capped CdSe CQDs. Finally, the results of the film depositions are shown in the last section.

All spectra were normalized, unless otherwise stated.

3.2. No Capping Agent

In the absence of a capping agent, the CdSe CQDs allowed to grow for 2h sustain their typical yellow color as can be seen in Figure 3.1-A.

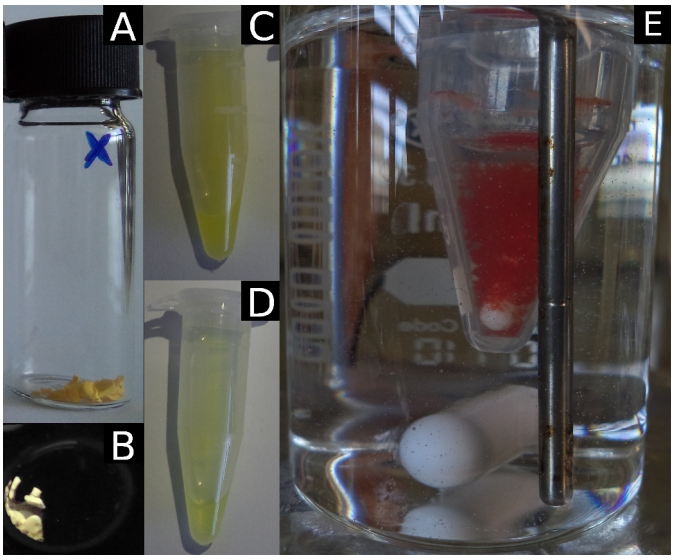

Figure 3.1: Photographies of uncapped CdSe CQDs: dried and inside a vial under normal light (A), dried and under the irradiation of an UV lamp with excitation at wavelength of 366nm (B), inside eppendorfs with the CQDs suspended in methoxyethanol (C), in methoxyethanol with zinc acetate dihydrate (D) and inside a falcon tube, suspended in water, in an oil bath at 100°C (E).

The dried CQDs retain their fluorescence under the UV lamp (B) and it is also possible to temporarily suspend them in methoxyethanol, with observable precipitates, (C) and for longer periods in methoxyethanol with zinc acetate dihydrate (D), which remains transparent.

For an application that requires heating the CQDs, like a spray-deposition or spin-coating; which requires the film to be sintered by prolonged baking, the uncapped ones will fail to retain their sizes and quickly aggregate. The growth is visibly noticeable because the CQDs undergo a color change from yellow to red, in a matter of seconds. A photography of the latter outcome is depicted in Figure 3.1-E. It is therefore a nonviable solution for depositions that requires higher temperatures. Note that bipyridine capped CdSe CQDs were heated at the same temperature for 1h and they did not grow; their

yellow color remained stable. This proves that the capping agents are fundamental for chemical stabilization of the CdSe CQDs.

The absorption and emission spectra of the uncapped CdSe CQDs can be found in Figure 3.2. The absorption spectrum of uncapped CdSe CQDs suspended in methoxyethanol was corrected using the algorithm proposed by Castanho et al.[29], to correct the scattered light.

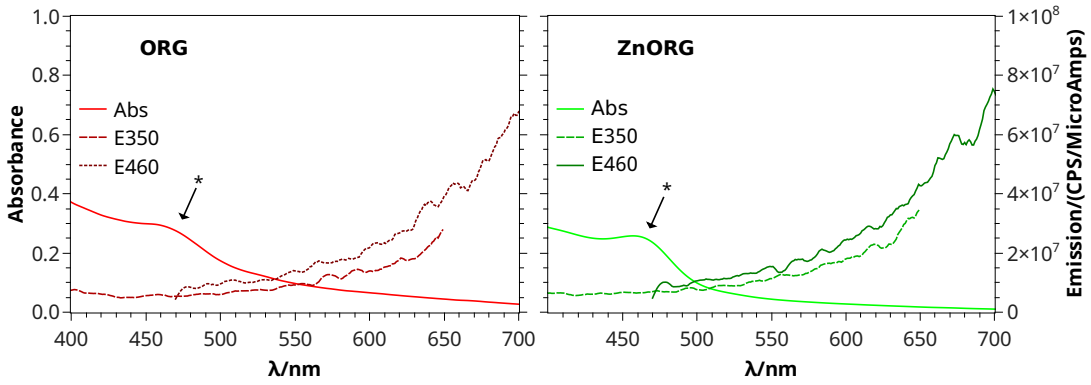

Figure 3.2: Absorption spectrum of diluted 1:10 uncapped CdSe CQDs, dispersed in methoxyethanol, on the left and on the right, diluted 1:2 and dispersed in methoxyethanol with zinc acetate dihydrate. The emission spectra were performed with a slit of 4nm, in right angle mode and the suspension was not diluted. The emission spectra were not normalized. * - First absorption peak corresponding to the confined ground-state (bandgap) of the CQDs. Emission using 350nm (E350) or 460nm (E460) wavelength excitation.

3.3. 2,2'Bipyridine as Capping Agent

Bipyridine is a toxic compound but, since it is a solid at room temperature and odorless, it does not pose the same risks as pyridine. To our knowledge, bipyridine has never been used as a capping agent, which constitutes a novel achievement in this thesis.

3.3.1. Testing Different Capping Agents

The UV-Vis absorption spectra of the bipyridine capped CdSe CQDs from the experiment described in section 2.1.2.1, dispersed in methoxyethanol, after 2h of reaction, is displayed in Figure 3.3.

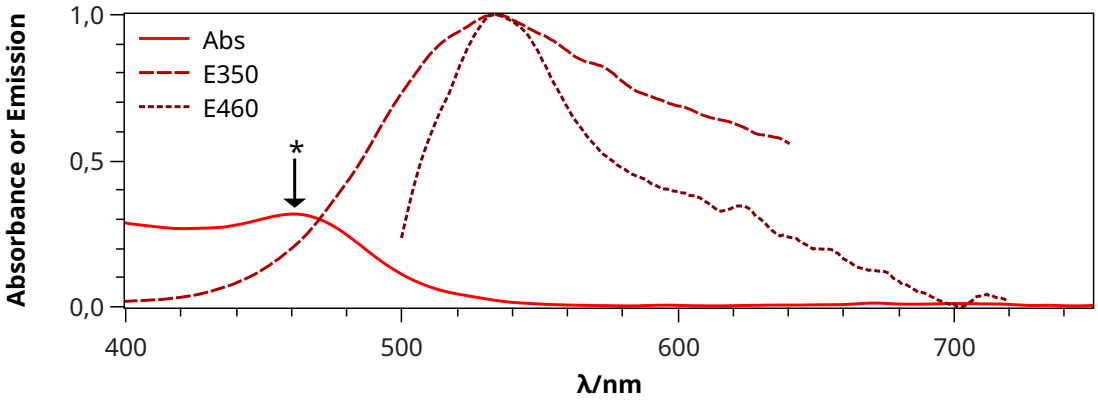

Figure 3.3: Absorption spectrum of diluted 1:10 bipyridine capped CdSe CQDs, from the experiment described in section 2.1.2.1, dispersed in methoxyethanol. The emission spectra were performed with a slit of 4nm, in right angle mode and the suspension was not diluted. * - First absorption peak corresponding to the confined ground-state (bandgap) of the CQDs.

To determine the first absorption peak, the absorption spectrum data of the bipyridine capped CdSe CQDs dispersed in methoxyethanol was subjected to a spectral derivative of the Abs with respect to the wavelength. The result is show in Figure 3.4, comprising the corresponding absorption spectrum and the smoothed spectral derivative. The absorption peaks from the remaining tested capping agents were also determined with the spectral derivative and can be found in Appendix B.

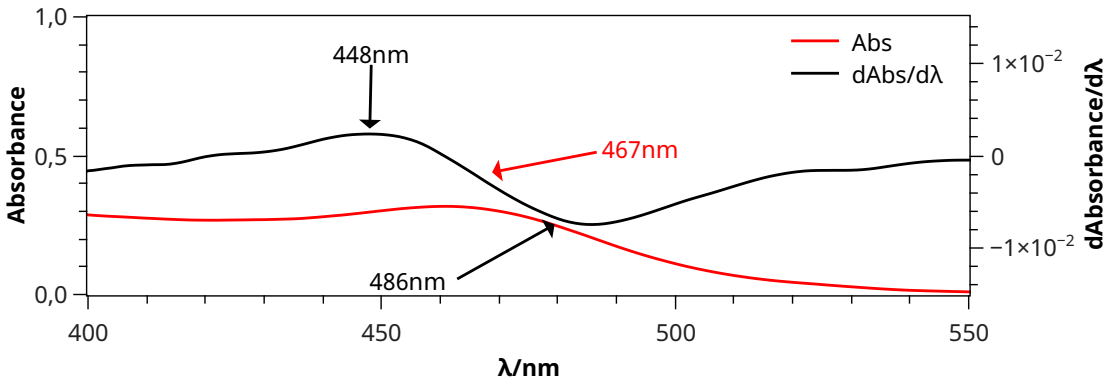

Figure 3.4: Absorption spectrum of diluted 1:10 bipyridine capped CdSe CQDs, dispersed in methoxyethanol, and the smoothed spectral derivative. The algorithm applied for smoothing was Savitzky-Golay with a polynomial order of 9 and with 25 points to the right and to the left. The black arrows indicate both maximum and minimum of the plot's derivate, and the red arrow indicates the inflection point, considered to be equidistant to the maximum and minimum, which occurs at the absorption peak of the first confined state.

The first absorption peak, of the CQDs suspended in methoxyethanol, is estimated to be λ=463nm; while the peak of the suspended CQDs in methoxyethanol with zinc acetate dihydrate is estimated to be λ=465nm, as shown in Figure VII in Appendix B.

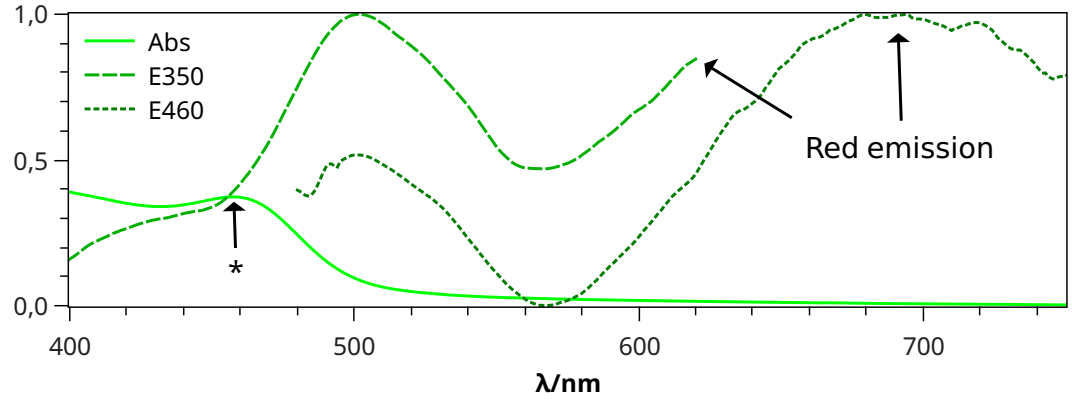

Figure 3.5: Absorption spectrum of diluted 1:2 bipyridine capped CdSe CQDs, from the experiment described in section 2.1.2.1, dispersed in methoxyethanol with zinc acetate dihydrate. The emission spectra were performed with a slit of 4nm, in right angle mode and the suspension was not diluted.

The suspension in methoxyethanol, when irradiated by a UV lamp, presents a more greenish yellow. The CQDs suspended in methoxyethanol with zinc acetate dihydrate, emit a yellow color (580nm) with a whitish tenuity; similar to dolly color. The emission at 580nm is not predominant, as can be seen in Figure 3.5. This means that the color the observed is merely the perception of the sum of two colors: the more energetic emission with a spring green color, at 500nm, and a lesser energetic emission with a solid red color, at 700nm.

3.3.2. Evolution of Bypridine Capped CdSe CQDs with Time

From the experiment described in section 2.1.2.2, the absorption spectra of bipyridine capped CdSe CQDs is displayed in Figure 3.6. The NIR portion of the spectra were omitted since it only showed the absorption peaks of the solvent.

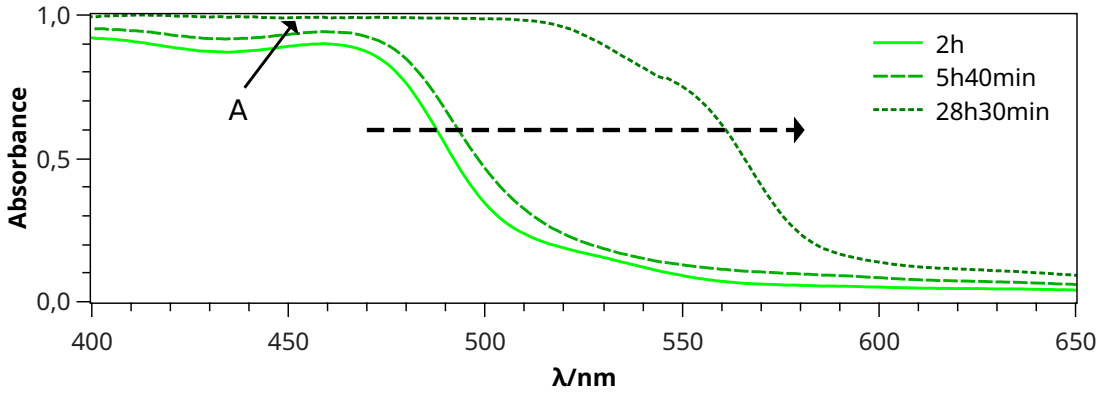

Figure 3.6: Absorption spectra of bipyridine capped CdSe CQDs, from the experiment described in section 2.1.2.2, dispersed in either methoxyethanol or methoxyethanol with zinc acetate dihydrate. The dashed black arrow indicates the peak's progression based on the reaction time. A - flat absorption area.

The CQDs dispersed in methoxyethanol with zinc acetate dihydrate appeared to be limpid and translucent, allowing to distinctly observe the first absorption band from the CdSe CQDs. Although the absorption first peaks from the samples with 2h and 5h 46min reaction times are very close to each other, 458nm and 459nm, respectively, the peak from the sample with 28h 30min reaction time is at 548nm. This indicates that the reaction time frame needed, to control the absorption peak of the CdSe CQDs, is 24h. A second observation is that the bigger particles tend to be less stable in the dispersion, forming aggregates and contributing to more light scattering.

The flat absorption area, indicated by A, is the typical absorption behavior of semiconductors, after the first absorption peak; its band-gap.

The emission spectra are represented in Figure 3.7.

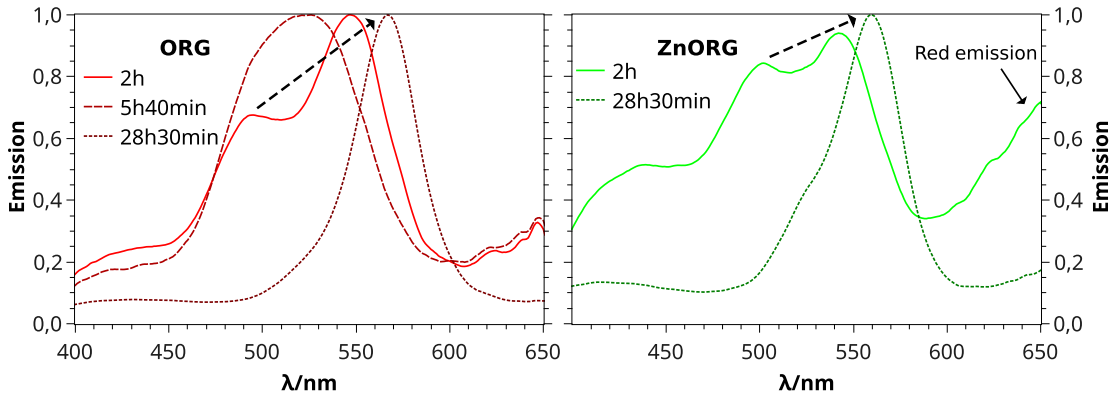

Figure 3.7: Emission spectra of bipyridine capped CdSe CQDs, from the experiment described in section 2.1.2.2, dispersed in methoxyethanol, on the left, and in methoxyethanol with zinc acetate dihydrate, on the right. The excitation wavelength is 350nm. The dashed black arrow indicates the peak's progression based on the reaction time.

The sample with 28h 30min reaction time dispersed in methoxyethanol emits at 568nm, which is higher than its 2h and 5h 40min counterparts, that respectively emit

at 500nm, considering the first emission band, and 530nm. This is in accordance with the quantum confinement effect.

The dual emission present in the 2h sample seems to fade, as the CQDs grow bigger, giving rise to a single emission band. Smaller particles' emission can be easily overwhelmed by their surface defects, as opposed to the bigger particles, whose ratio between the roughness' high and particle's size tend to be lower, diminishing the effect of the surface defects on the emission.

3.3.3. CdSe CQDs capped with Molten 2,2'Bipyridine

The third experiment was a typical extraction from an aqueous to an organic phase. The organic phase corresponds to molten bipyridine (Figure 3.8-A) and the aqueous phase is the orange suspension of uncapped CdSe CQDs (Figure 3.8-B). A change of color on the organic phase is observed in Figure 3.8-C, indicating that the QDs were being extracted from the aqueous phase to the bipyridine. After 10min, the QDs were fully transfered to the bipyridine and the aqueous phase became visibly limpid. It was possible to observe some red precipitate on the interface between the phases, although the molten bipyridine remained yellow, indicating that aggregated QDs tend to remain on the interface. Even after 1h in the oil bath, at 100°C and under stirring, the molten bipyridine remained vivid yellow, suggesting that even at high temperatures the CdSe QDs capped with bipyridine are stable and, therefore, do not grow.

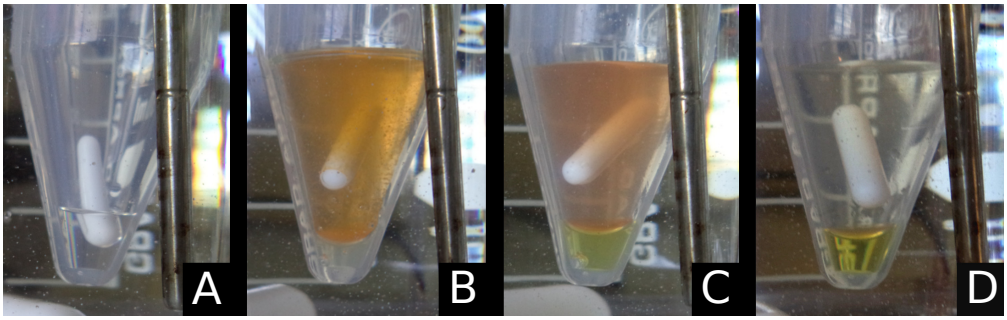

Figure 3.8: Time-lapse pictures of the solventless capping of CdSe QDs experiment. A - 100mg of molten bipyridine. B - molten bipyridine with 1mL of uncapped CdSe CQD. C - CQD phase transfer after 2min. D - total phase transfer after 10min. The falcon tube was immersed in Baysilone® oil at 100°C.

After leaving the tube at room temperature, the molten bipyridine with the CdSe QDs remained liquid, well below its melting point, not due to freezing-point depression but due to supercooling. By slightly shaking the two phases, some bipyridine bubbles were released to the upper phase. As soon as they fell back to the lower phase and joined it, the bipyridine instantly solidified, trapping the CdSe QDs. After removing the upper aqueous phase, a suspension of white bipyridine crystallites slowly started to form, leading to the removal of excess capping agent.

The formed solid kept the typical yellow fluorescence under the UV lamp and a yellow to whitish color.

This experiment was conducted in an attempt to suppress the washing cycles, required to remove the secondary product sodium selenosulfate, after adding the capping agents, to avoid the loss of CdSe QDs. Summarizing, this procedure proportionates a one-step CQD capping and washing.

3.4. L-Cysteine as Capping Agent

L-Cysteine has been previously used in other works as a successful capping agent [27, 30]. It is a non-toxic, almost odorless compound and, therefore, easier to handle. The absorption and emission spectra are presented in Figure 3.9, for the L-cysteine capped CdSe CQDs dispersed in methoxyethanol and methoxyethanol with zinc acetate dihydrate, respectively on the left and right. These absorption spectra were corrected using the algorithm proposed by Castanho et al.[29], to correct the absorbed light due to scattering.

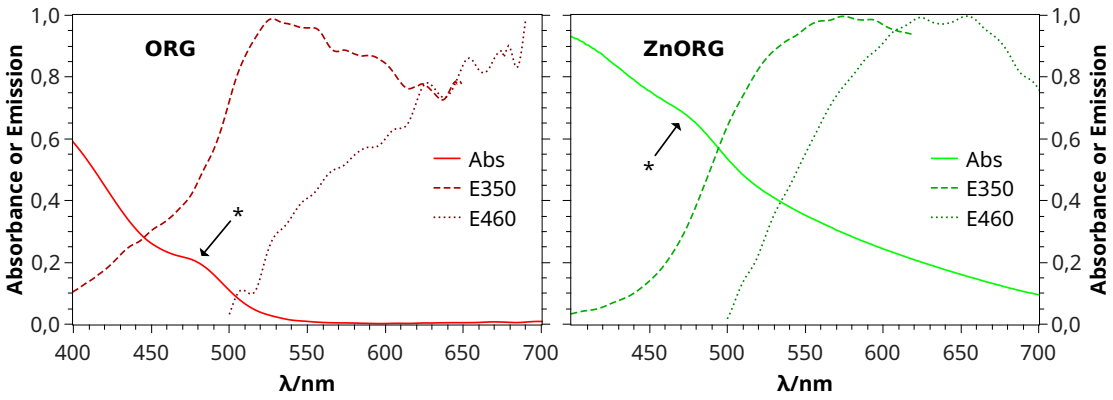

Figure 3.9: Absorption spectrum of diluted 1:10 L-cysteine capped CdSe CQDs, dispersed in methoxyethanol on the left and, on the right, diluted 1:2 and dispersed in methoxyethanol with zinc acetate dihydrate. The emission spectra were performed with a slit of 4nm, in right angle mode and the solution was not diluted. * - First absorption peak corresponding to the confined ground-state (bandgap) of the CQDs.

The first absorption peak is estimated to be at 482nm, as shown in Figure XV in Appendix B, for the CQDs dispersed in methoxyethanol and at 478nm dispersed in methoxyethanol with zinc acetate dihydrate, as shown in Figure XIV in Appendix B. These are rough estimations because the absorption spectra are showing the effect of scattered light.

There is no significant difference between the CQDs dispersions absorption spectra, in methoxyethanol or methoxyethanol with zinc acetate dihydrate. Unlike the other capping agents, the introduction of zinc cation does not influence the CQDs colloidal stability. The suspension remains with visible aggregates. The zinc cation is known to form zinc fingers[33], which are complexes of protein-zinc cation with the purpose of stabilizing the fold. An example of a Cys_2His_2-zinc complex and zinc complexed with the L-cysteine capped CdSe CQD analogously to the zinc finger system, is shown in Figure 3.10.

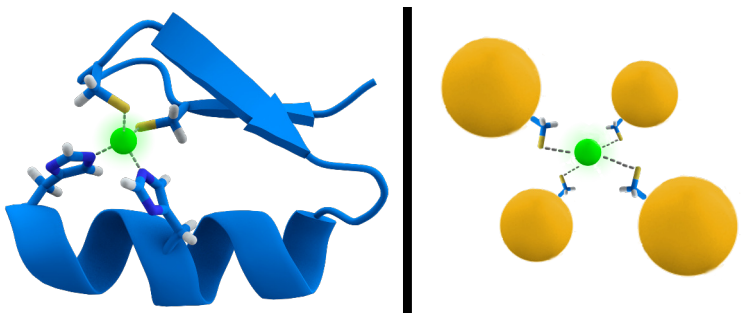

Figure 3.10: Representation of a Cys_2His_2 zinc finger motif, on the left, and zinc (green sphere) complexed with the L-cysteine of the CQDs (yellow spheres), on the right. The zinc finger motif is a courtesy of Thomas Splettstoesser, Wikimedia Commons, downloaded in August of 2015.

Considering the affinity of zinc cations to L-cysteine residues, an analogous complexing system occurs with the L-cysteine capping the CdSe QDs. By forming the complex, the CQDs start to link themselves and form aggregates, precipitating out of the solution.[34, 35]

3.5. Zinc Acetate Dihydrate as Capping Agent

An interesting behavior occurred when the zinc acetate dihydrate was mixed with the uncapped CdSe QDs. The suspension started to turn vivid red, indicating that the QDs were fused together; forming bigger nanoparticles, because a size increases red-shifts the first absorption state, i.e. it lowers the QD's bandgap. After drying and suspending the red dust in methoxyethanol, the suspension became milky, like other capped CQDs, but kept red and did not grow any further. The zinc acetate dihydrate capped CQDs suspended in methoxyethanol with zinc acetate dihydrate, on the contrary, formed a dark brown pellet, overnight. A picture of the zinc acetate dihydrate capped CdSe CQDs suspended in methoxyethanol (A) and methoxyethanol with zinc acetate dihydrate (B) is show in Figure 3.11, to illustrate the difference in stability.

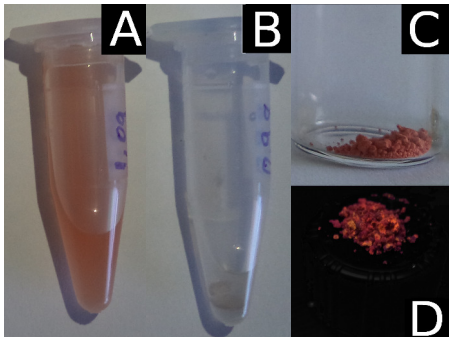

Figure 3.11: Photography of the zinc acetate dihydrate capped CdSe CQDs dispersed in methoxyethanol (A), in methoxyethanol with zinc acetate dihydrate (B), the dried form under normal light (C) and under UV lamp at excitation wavelength of 366nm (D).

The absorption spectra and corresponding emissions of the zinc acetate dihydrate capped CdSe CQDs, dispersed in methoxyethanol and methoxyethanol with zinc acetate dihydrate respectively, are represented in Figure 3.12. The algorithm, used previously and described in reference [29], was applied to correct the scattering. The selected fitting range had to be between 650nm and 800nm, since these particles absorb at around 550nm. Although the dried form of the zinc acetate dihydrate capped CdSe CQDS kept some reddish fluorescence (Figure 3.11-D), the emission spectra, of the zinc acetate dihydrate capped CdSe CQDs dispersed in methoxyethanol reveal almost no emission, comparatively to those dispersed in methoxyethanol with zinc acetate dihydrate which have a very high emission in the 650nm range.

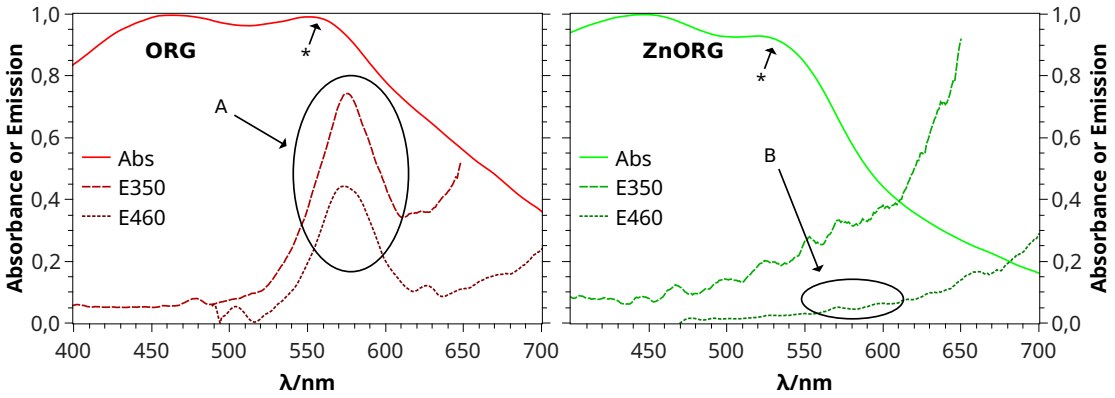

Figure 3.12: Absorption spectrum of diluted 1:10 zinc acetate dihydrate capped CdSe CQDs, dispersed in methoxyethanol, on the left and on the right, diluted 1:2 and dispersed in methoxyethanol with zinc acetate dihydrate. The emission spectra were performed with a slit of 4nm, in right angle mode and the suspension was not diluted. A - First emission peaks. B - No visible emission peaks. * - First absorption peak corresponding to the confined ground-state (bandgap) of the CQDs.

The first absorption peak is estimated to be at λ=563nm, for the CQDs dispersed in methoxyethanol and at λ=542nm dispersed in methoxyethanol with zinc acetate dihydrate, as shown in Figure XVII and Figure XVI, respectively, in Appendix B. This red-shift of the first absorption peak, relatively to the other capping agents, indicates that the CdSe QDs are not chemically stable with zinc acetate dihydrate as a capping agent.

3.6. Lumidot®

Commercial solutions of CdSe CQDs (named Lumidot) samples were purchased with the purpose of comparing them to the synthesized CQDs. Their high quality can be confirmed by the well defined emission peaks, observed in Figure 3.13 and Figure 3.14, which is in agreement with the data supplied by Sigma-Aldrich.[38]

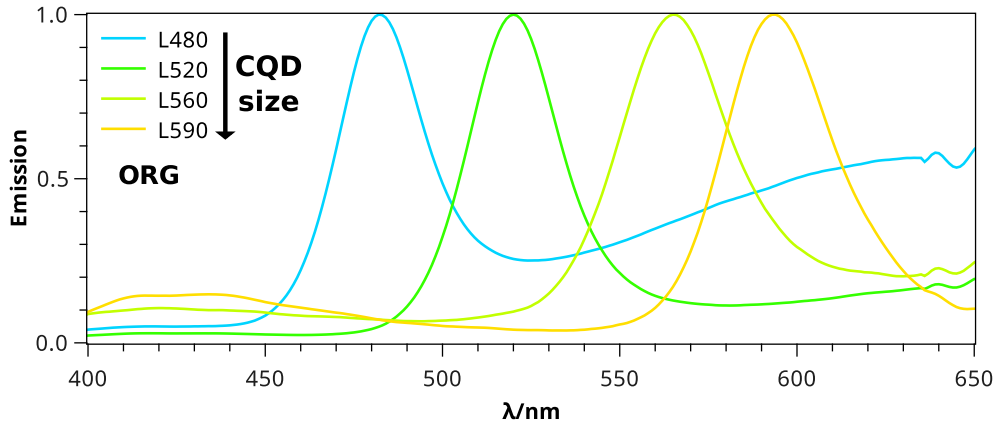

Figure 3.13: Emission spectra of Lumidot samples dispersed in methoxyethanol. The emission spectra were performed with a slit of 4nm, in right angle mode and the solution was not diluted.

The samples are referred as L###, given that the λ of the emission peak of the sample is described by the three consecutive #. The L480 sample has a higher red emission than the other samples. This emission peak red-shifts and gradually fades as the CQDs become bigger. On Figure 3.14, in the presence of the zinc salt the samples' red emission is greatly enhanced. In the L480 sample case, it overwhelms the first emission peak. The L590 sample's emission spectra are not altered by the presence of the cation.

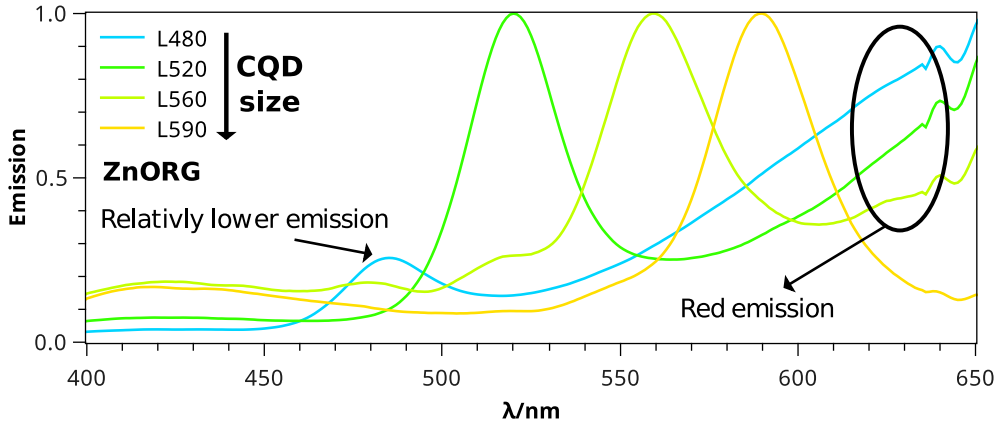

Figure 3.14: Emission spectra of Lumidot samples dispersed in methoxyethanol with zinc acetate dihydrate. The emission spectra were performed with a slit of 4nm, in right angle mode and the solution was not diluted.

The absorption spectra of the Lumidot samples, dispersed in methoxyethanol and methoxyethanol with zinc acetate dihydrate, are represented in Figure 3.15 and Figure 3.16, respectively. The samples L560 and L590 started to form a precipitate and it was not possible to obtain the spectra. The same flat absorption area is observed as in the bipyridine capped CdSe CQDs.

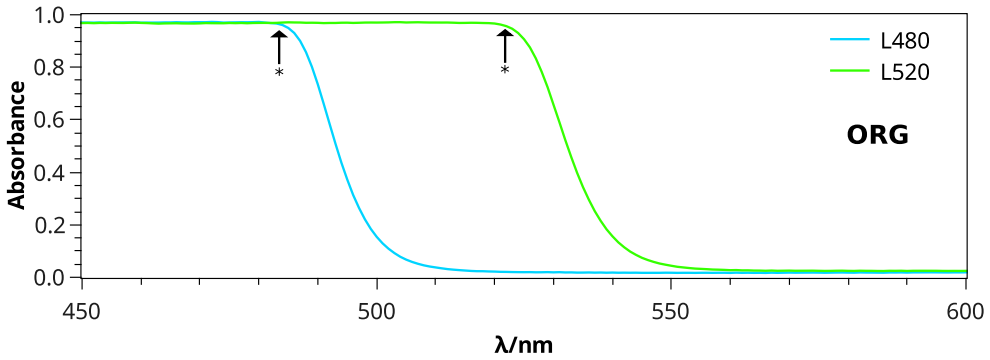

Figure 3.15: Absorption spectra of Lumidot samples dispersed in methoxyethanol. * - First absorption peak

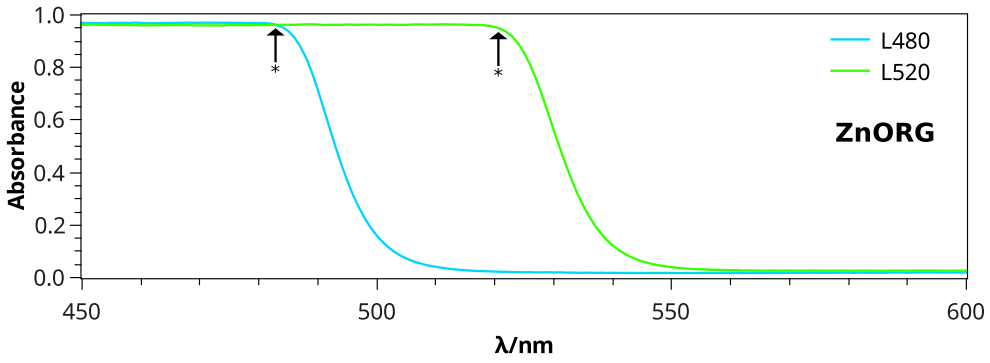

Figure 3.16: Absorption spectra of Lumidot samples dispersed in methoxyethanol with zinc acetate dihydrate. * - First absorption peak corresponding to the confined ground-state (bandgap) of the CQDs.

Below, in Table 3.1, is represented the measured emission and absorption peaks of the Lumidot samples suspended in methoxyethanol and methoxyethanol with zinc acetate dihydrate. To determine the QDs' size, the empirical Equation 3.6 can be used, given that the first absorptions peaks are within the advised by Yu et al[39]. D corresponds to the size of a quantum dot and λ is the first absorption peak.

$$D = (1.6122 \times 10^{-9})\lambda^4 - (2.6575 \times 10^{-6})\lambda^3 + (1.6242 \times 10^{-3})\lambda^2 - 0.4277\lambda + 41.57 \quad (3.1)$$

The emission and absorption peaks were determined graphically.

Table 3.1: Table with the first absorption peaks (Abs_1), calculated CdSe CQD's size (Calc. size) and measured emission peak with excitation at 350nm (E_{350nm}) of the Lumidot samples dispersed in methoxyethanol with zinc acetate dihydrate (ZnORG) and in methoxyethanol (ORG). Ind - indeterminable.

	ZnORG			
	L480	**L520**	**L560**	**L590**
Abs_1/nm	478	516	Ind	Ind
Calc. size/nm	2.16	2.51	Ind	Ind
E_{350nm}/nm	482	520	567	593
	ORG			
	L480	**L520**	**L560**	**L590**
Abs_1/nm	479	516	Ind	Ind
Calc. size/nm	2.17	2.51	Ind	Ind
E_{350nm}/nm	485	518	560	588

The most interesting propriety of the Lumidot samples is that the Stokes shift is practically absent. This can be do to the existence of zero-phonon transitions; transitions that do not generate phonons and do not lose energy[40]. Comparing both emission spectra, 3.13 and Figure 3.14, a loss of emission on the first emission peak is observable, specially on the samples L480 and L520. The Lumidot CQDs' surface is stabilized with hexadecylamine ligands which might have some affinity to the Zn^{2+}, leading to the destabilization of the CQDs, consequently aggregating and loosing emission. Although there is a loss of emission on the first peak, the second peak's emission is enhanced by the Zn^{2+}, as happens on the synthesized CQDs.

3.7. Dynamic Light Scattering (DLS) Measurements

For a brief explanation of the terms associated to the DLS analysis, please refer to the white paper, published by Malvern Instruments Worldwide.[41]

To ascertain if the solutions without CQDs had any particles in them, a DLS analysis was done and the results are shown in Figure 3.17.

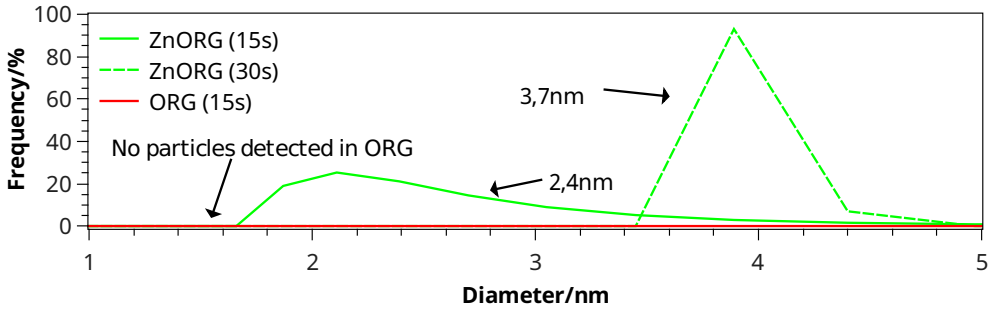

Figure 3.17: DLS spectra of methoxyethanol (ORG) and methoxyethanol with zinc acetate dihydrate (ZnORG) solutions in a quartz cell with all transparent sides, 2mm wide and with a 1cm optical path length. The solution was previously filtered with a 0,22μm filter. The signal accumulation times are 30s for the ZnORG solution and 15s for both solutions, at 25°C.

The methoxyethanol solution reveals no particles, as expected. The methoxyethanol with zinc acetate dihydrate solution spectra indicate that there are particles with sizes ranging from 2,4nm to 3,7nm. Curiously, the size of the zinc acetate dihydrate crystallites are the same as the calculated size of the CdSe CQDs. These zinc acetate dihydrate particles can be confounded with the signal from the CdSe CQDs particles.

The DLS spectra of uncapped CdSe CQDs (X) and capped with bipyridine, L-cysteine and zinc acetate dihydrate, dispersed in methoxyethanol and methoxyethanol with zinc

acetate dihydrate media, are represented in Figure 3.18.

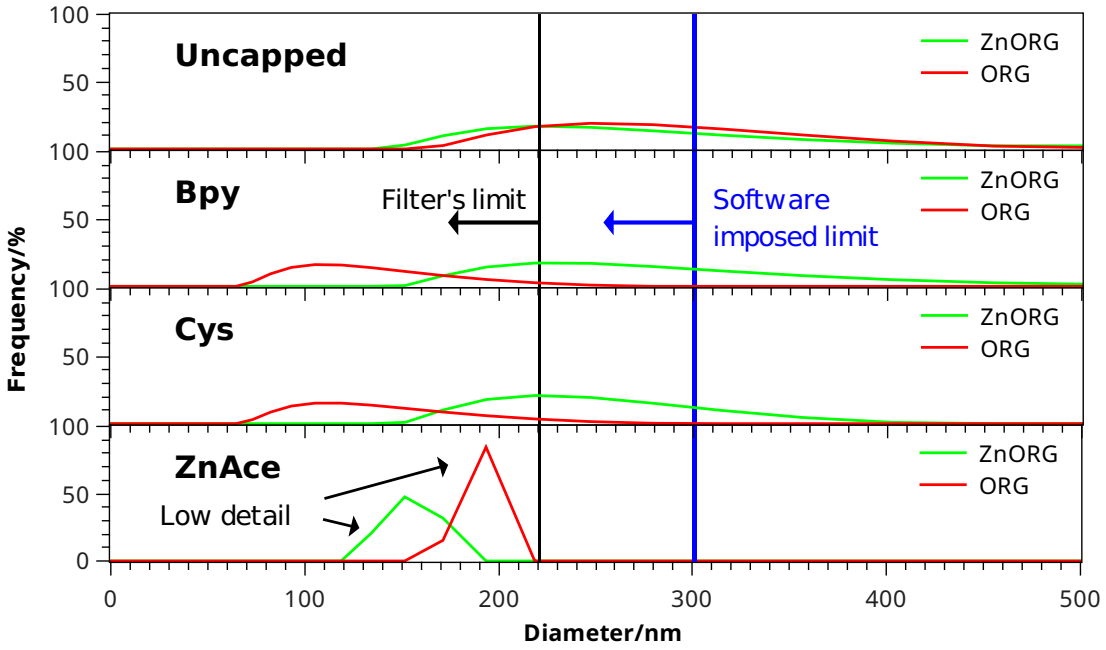

Figure 3.18: DLS spectra of uncapped and capped with bipyridine, L-cysteine and zinc acetate dihydrate CdSe CQDs, dispersed in methoxyethanol with zinc acetate dihydrate and methoxyethanol. The solution was previously filtered with a 0,22μm filter. The black barrier represents the filter's pore size upper limit and the blue barrier is software imposed upper limit of 300nm. A quartz cell with all transparent sides, 2mm wide and with a 1cm optical path length was used. The signal accumulation time is 30s, at 25°C.

Table 3.2 contemplates the hydrodynamic size and polydispersity index (PI), processed from the DLS analysis, for uncapped and capped with bipyridine, L-cysteine and zinc acetate dihydrate CdSe CQDs, in methoxyethanol with zinc acetate dihydrate and methoxyethanol media.

Table 3.2: Table with the data processed from the DLS analysis for uncapped and capped with bipyridine, L-cysteine and zinc acetate dihydrate CdSe CQDs, dispersed in methoxyethanol with zinc acetate dihydrate and methoxyethanol with zinc acetate dihydrate media. The samples were previously filtered with a 0,22μm filter and all measurements were done at 25°C, in a quartz cell with all transparent sides, 2mm wide and with a 1cm optical path length and with a signal accumulation time is 30s. *The peak size data is the weighted mean between two peaks: 115,2nm and 473,7nm.

				ZnORG			
	X	**Bpy**	**Cys**	**ZnAce**	**Py**	**3-MT**	**NaAce**
Peak size/nm	243,8	250,0	226,5	145,2	181,1	187,6	197,0
PI	0,589	0,611	0,454	1,238	0,507	0,634	0,429
				ORG			
	X	**Bpy**	**Cys**	**ZnAce**	**Py**	**3-MT**	**NaAce**
Peak size/nm	259,3	118,1	121,8	178,8	132,3	130,0*	98,9
PI	0,607	0,343	0,418	1,493	0,444	0,586	0,443

The remaining DLS spectra of the pyridine, 3-methylthiophene and sodium acetate trihydrate capped CdSe CQDs are similar to the bipyridine and L-cysteine capped CdSe CQDs' and can be found in Appendix B in the DLS spectra section. The latter section also contains the correlation graphics and the residuals corresponding to the samples studied in this section, with the data shown with the same sequence as Table 3.2.

The fact that solutions of CdSe CQDs dispersed in methoxyethanol with zinc acetate

dihydrate media are translucent, compared to the dispersed in methoxyethanol, lead to a first impression that the colloids are smaller and more stable in methoxyethanol with zinc acetate dihydrate. The data supplied by the table above negates that fact, since the capped CdSe CQDs, except the zinc acetate dihydrate capped, show higher polydispersity and bigger colloids. The zinc cation can interact with the capping agents by forming complexes and leaving them unprotected, as happens with the uncapped CdSe CQDs.

The zeta potential was determined for methoxyethanol with zinc acetate dihydrate solution, sodium acetate trihydrate capped CdSe CQDs in methoxyethanol and methoxyethanol with zinc acetate dihydrate, to determine if the CQDs exhibit a surface charge. The result are presented in Figure XXXIV and the full data can be found in Table VIII, in Appendix B. All samples exhibit no mensurable charge, indicating that the zinc acetate dihydrate crystallites and CQDs have a neutral surface.

Given that the DLS analysis gives an hydrodynamic size of particles, this value is naturally higher than the individual CQDs' diameter because DLS mainly detects the nanoparticles aggregates. So, the peaks observed in Figure 3.18 correspond to the aggregate sizes rather than the real CQD sizes. Another problem, associated with this technique, is the fact that if a big particle, i.e. an aggregate, passes in front of the sensor, the signal is saturated and it becomes harder to detect smaller particles, especially quantum dots, whose sizes range from 1nm to around 20nm. The TEM images, on the next section, will help revealing the size of the unaggregated CQDs.

3.8. Transmission Electron Microscopy (TEM)

The images from the TEM analysis are in accordance with the DLS data. Independently of the capping agent used, the particles form aggregates with diameters ranging from 100nm to 200nm, as the ones seen in Figure 3.19-A.

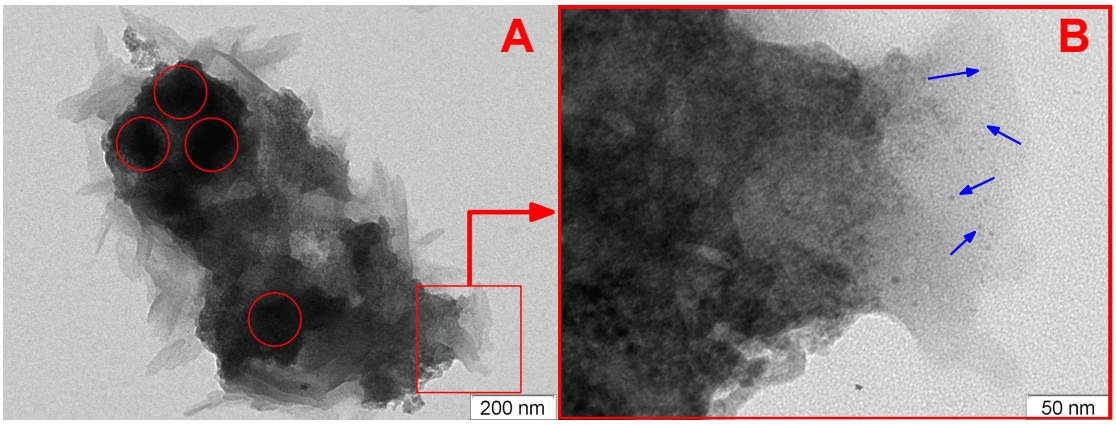

Figure 3.19: TEM image of uncapped CdSe CQDs. A - the red circles depict the aggregates with diameters ranging from 100nm to 200nm. B - zoomed image of the area represented by a red square in A. The blue arrows point to particles with diameters ranging from 2nm to 3nm. The CQDs were suspended in absolute ethanol, with the aid of ultrasounds, and deposited on a copper grid.

The presence of particles with diameters ranging from 2nm to 3nm is visually confirmed by TEM images, depicted by the blue arrows in Figure 3.19-B. It is also confirmed by the absorption and emission spectral peaks, that were previously presented, as predicted by the quantum confinement theory.

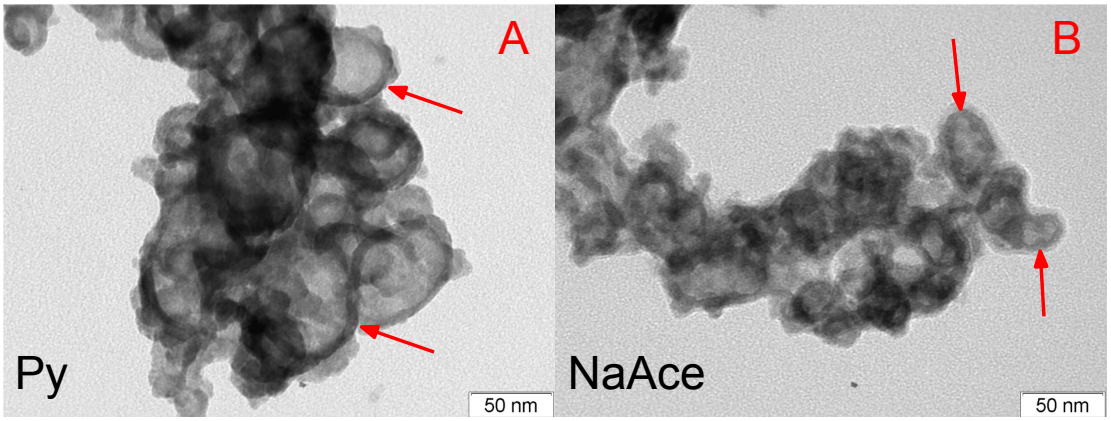

Figure 3.20: A - TEM image of pyridine capped CdSe CQDs. B - TEM image of sodium acetate trihydrate capped CdSe CQDs. The red arrows point to the structures that envelop the aggregates. The CQDs were suspended in absolute ethanol, with the aid of ultrasounds, and deposited on a copper grid.

The TEM images pertaining to both pyridine and sodium acetate trihydrate capped CdSe CQDs are represented in Figure 3.20-A and Figure 3.20-B, respectively. Odd structures delimiting the aggregates are observed in both images, shown by the red arrows, particularly noticeable pyridine capped CdSe CQDs' image.

The route used to synthesize these CdSe CQDs can take up to 48 hours to achieve the size of up 3nm, similarly to the ones found in Figure XXXV, giving the red colour. The use of the zinc acetate dihydrate salt as a capping agent accelerated the CQDs' growth to a matter of minutes.

The absorption bely present in the absorption spectra of the bipyridine capped CdSe CQDs, from the experiment described in section 2.1.2.2, reacted for 28h and 30min (Figure 3.6), and in the absorption spectra of the zinc acetate dihydrate capped CdSe CQDs (Figure 3.12-ZnORG), are similar. It is safe to assume that the distribution of the CQDs size is similar. The use of zinc acetate dihydrate as a capping agent poses as an alternative to hasten the growth of the CdSe CQDs, granting the possibility of obtaining 3nm CdSe CQDs in around 2h, instead of 48h.

3.9. Global Comparison and Discussion of Results

In Figure 3.21 resides a photography of all the CdSe CQDs from the experiment described in section 2.1.2.1 under visible light and, on the bottom, under an UV lamp with an excitation wavelength of 366nm. The photographies were subject to color removal to facilitate the visualization of CQDs dusts' colors. A comparison between the original photographies can be found in Appendix B; Figure XXXVI corresponding to the vials under visible light and Figure XXXVII to the vials under UV light.

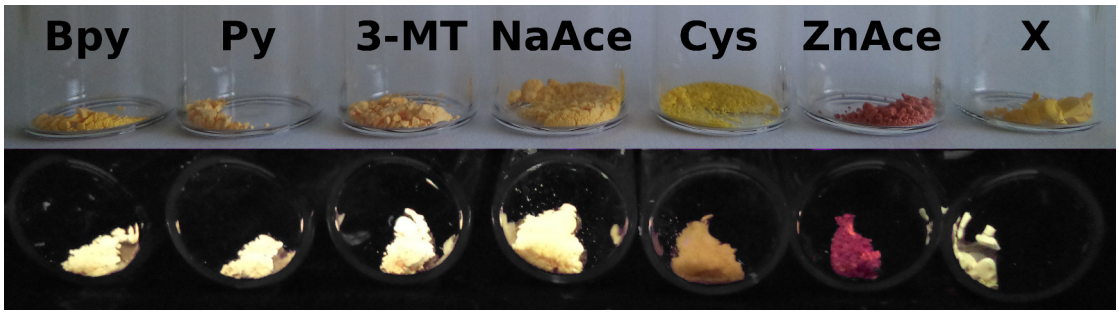

Figure 3.21: Photography of the synthesized CQDs from the experiment described in section 2.1.2.1, under visible light (top) and under UV light (bottom). The excitation wavelength is 366nm.

Using the data provided from the experiment described in section 2.1.2.2, it is possible to determine which capping agent performed better at prohibiting the CdSe CQDs from growing further. The difference between the two peaks from the absorption spectra of the 2h and 5h and 40min samples, reveal that in a 3h and 40min time frame of reaction, the absorption peak shift is 1nm. This corresponds to an estimated growth of around 9 picometers, which is a very low growth. On this basis, the time span between the capping agents additions can be approximated to zero and the absorption peak shifts can be attributed to the initial performance of the capping agents. A comprehensive list of the relation between the CdSe CQDs' absorption peaks, peaks' shift relatively to Bpy, and the estimated CQD's sizes, for each capping agent, is found in Table 3.3. The first absorption peak data for pyridine, 3-methylthiophene, sodium acetate trihydrate capped CQDs and uncapped ones, dispersed in methoxyethanol and in methoxyethanol with zinc acetate dihydrate, were determined with the help of the derivates of the absorption spectra, found in Appendix B. The emission peaks were determined graphically or through the maximum value in the plot's data. It is tempting to evaluate quantitatively the relation between the reaction time and the CQDs' size but more data would be needed between the 2h-28h reaction time frame.

Table 3.3: Table with the first absorption peaks (Abs_1), the peaks' shift relatively to Bpy (ΔAbs_1), calculated CdSe CQD's size (Calc. size), first (E_1), second (E_2) and third (E_3) emission peaks, with 350nm ($E_{n;350nm}$) and 460nm excitation light ($E_{n;460nm}$), for each capping agent, dispersed in methoxyethanol with zinc acetate dihydrate (ZnORG) and methoxyethanol (ORG) solution. Ind - indeterminable. Red - red emission

				ZnORG			
	Bpy	**Py**	**3-MT**	**NaAce**	**Cys**	**ZnAce**	**X**
Abs_1/nm	463	463	463	465	478	542	465
ΔAbs_1/nm	0	0	0	+2	+15	+88	+2
Calc. size/nm	2,05	2,05	2,05	2,06	2,16	2,90	2,06
$E_{1;350nm}$/nm	501	502	488	497	Ind	Red	Ind
$E_{1;460nm}$/nm	501	496	496	497	Ind	Ind	Ind
$E_{2;350nm}$/nm	526	535	538	538	Ind	Ind	Ind
$E_{2;460nm}$/nm	532	533	537	536	Ind	Ind	Ind
$E_{3;460nm}$/nm	688	693	700	703	624	Ind	Red
				ORG			
	Bpy	**Py**	**3-MT**	**NaAce**	**Cys**	**ZnAce**	**X**
Abs_1/nm	467	465	466	465	484	563	468
ΔAbs_1/nm	0	-2	-1	-2	+17	+99	+1
Calc. size/nm	2,08	2,06	2,07	2,06	2,21	3,33	2,08
$E_{1;350nm}$/nm	512	512	497	505	Ind	576	Ind
$E_{1;460nm}$/nm	506	505	503	504	Ind	574	Ind
$E_{2;350nm}$/nm	534	535	539	540	Ind	Red	Ind
$E_{2;460nm}$/nm	534	538	540	540	Ind	Red	Red

All capping agents appear to stabilize the CdSe QDs, since their absorption peaks appear to be similar. However, as predicted by the CQDs colors, the most unstable capping agent is zinc acetate dihydrate. To determine if the acetate had any role as a stabilizer, NaAce was used as a capping agent. Since the absorption peak of the NaAce capped CdSe CQDs is similar to the other capped CQDs, the responsible for the quantum dot fusion is the zinc cation.

The calculated CdSe CQDs' sizes are in agreement with the sizes obtained from the TEM images.

Chen et al. reported that CQDs synthesized in aqueous medium have a full width

at half-maximum, on the emission spectrum, of 100nm and that the ones synthesized in TOPO, at higher temperatures, is between 25nm and 30nm. This difference is due to a larger number of surface defects on the CQDs synthesized in aqueous medium.[36] The full width at half-maximum of the synthesized CQDs is around 100nm, higher than the Lumidot samples', indicating that this synthesis method produces QDs with surface defects.

3.10. Film Deposition and Photo-response Measurements

3.10.1. Spin-coat

The deposited films revealed to be visibly grainy and very heterogeneous, independently of the parameters used. The transmittance spectra for the various depositions are represented in Figure 3.22.

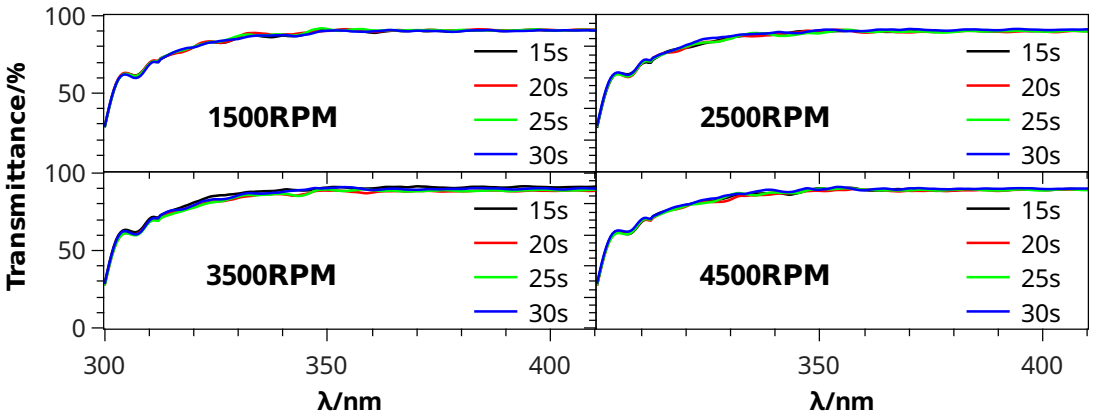

Figure 3.22: Transmittance spectra of the films deposited by spin-coat method, with different rotation speed and dwelling times. The spectra were taken using an integration sphere. The algorithm applied for smoothing was Savitzky-Golay with a polynomial order of 9 and with 25 points to the right and to the left.

There is no difference in transmittance between rotation speeds or dwelling times variation, suggesting that the film thickness is independent of these parameters. Nonetheless, given that the films produced by spin-coating were highly heterogeneous, the spray pyrolysis coating method was used.

3.10.2. Spray Pyrolysis

The transmittance spectra of the films deposited using scheme E, described in Figure 2.3. is represented in Figure 3.23. The replica was tested to ensure the reproducibility of the deposition using scheme E.

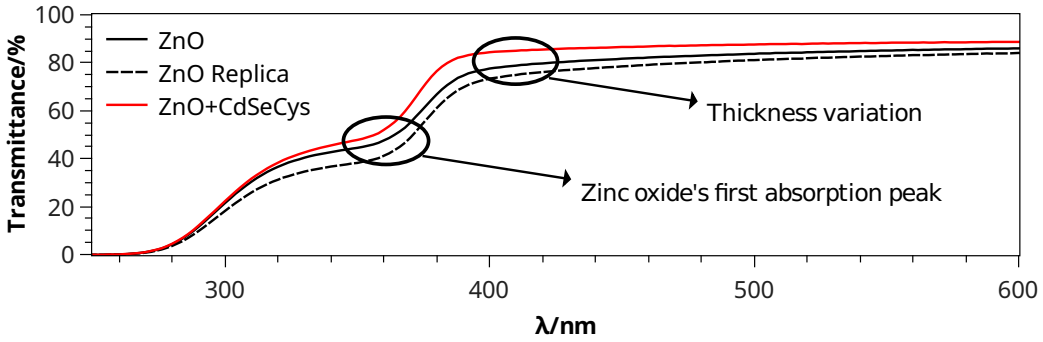

Figure 3.23: Transmittance spectra of the films deposited by spray pyrolysis method, using the scheme E. The algorithm applied for smoothing was Savitzky-Golay with a polynomial order of 9 and with 25 points to the right and to the left. The black circle to the left indicates the first absorption peak of the zinc oxide, corresponding to its bandgap, and the black circle to the right indicates the variation in film thickness.

The films obtained by spray pyrolysis were visibly homogeneous but, depending on the airbrush's positioning, the films surface consistently had some spots with slightly more material than others. After testing all the positioning schemes, the one that resulted in a less heterogeneous film, was the scheme were the airbrush is pointing upwards to the heat plate and the nozzle is 25cm away from the heat plate's surface, which corresponds to the scheme E in Figure 2.3. The film with the most interesting proprieties, apparent surface homogeneity and no light scattering, was the one obtained before the airbrush's nozzle was completely obstructed. This indicates that the best films can be obtained with a smaller nozzle than the one used. However, it is hard to keep the nozzle unobstructed until the deposition is complete.

The spectra of the films show that the method used is reproducible, with a transmittance variation of up to 15%. The difference between the films without the CQDs and the one with might be due the variation in composition of the dispensed solution. An loss of transmittance was expected in the 500nm region, since the Cys capped CdSe CQDs absorb light in that wavelength. After the deposition, the airbrush's container had a navy blue dust deposit, suggesting that the acidic aqueous media is not the ideal for dispersing the CdSe CQDs.

3.10.3. Current-Voltage Characteristic Curve Measurement

The current-voltage characteristic curves of the films deposited by spray, without and with L-cysteine capped CdSe CQDs, are represented in Figure 3.24, for each type of irradiation used.

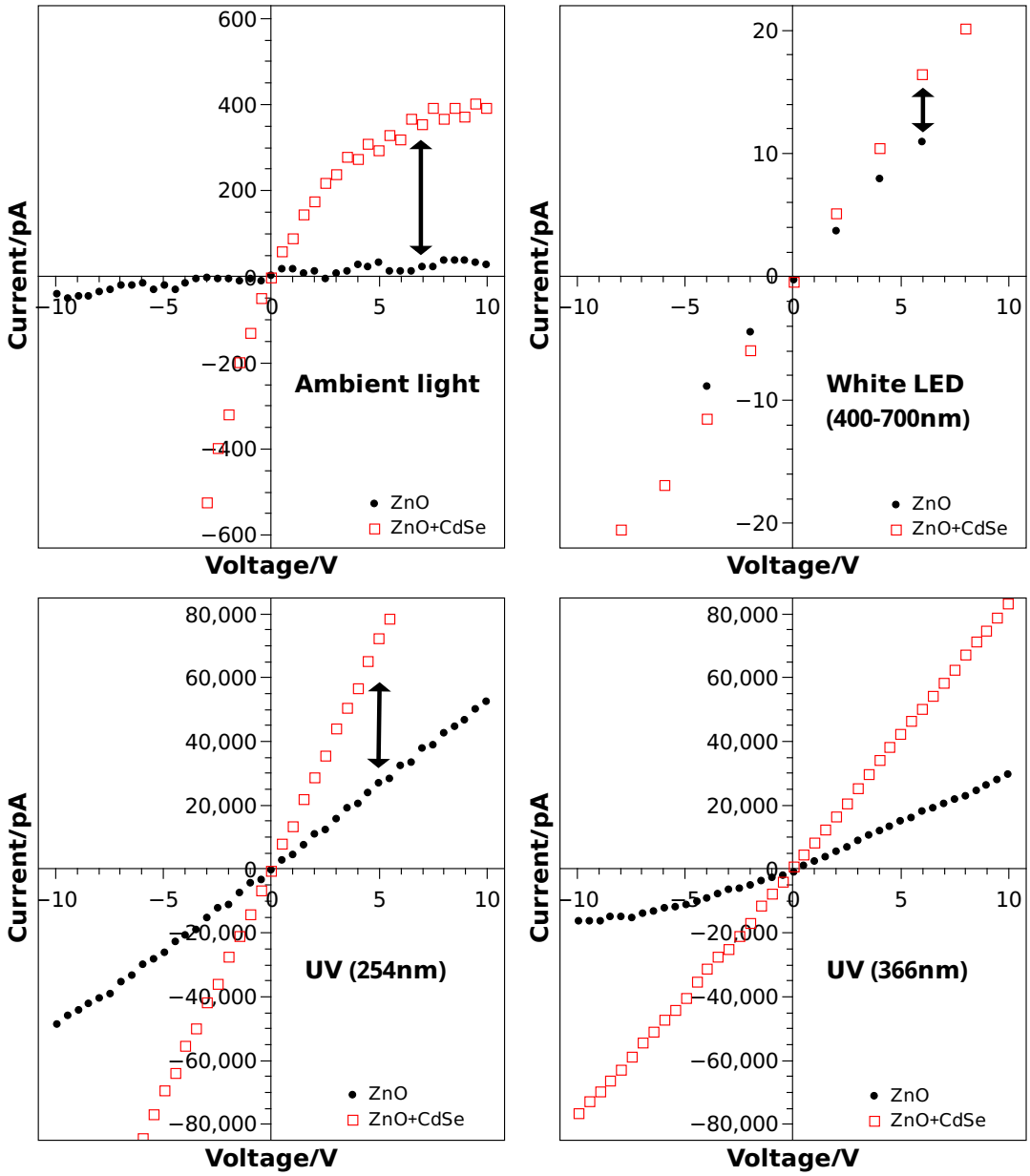

Figure 3.24: Plot of the current-voltage from the zinc oxide films, with and without L-cysteine capped CdSe CQDs, irradiated with ambient light, a white LED, UV light at 254nm and at 366nm. The black arrows point out the difference in photo-response between the zinc oxide films, with and without L-cysteine capped CdSe CQDs.

The temperature of the substrates, upon deposition, were around 17°C below the advised in [26]. It is unknown if there was still unreacted zinc acetate on the films, mixed with the zinc oxide (ZnO).

The films were irradiated by the four types of light sources indicated in Table 3.4. To simulate the sun, the measurements were performed in ambient light. A white LED typically has a white light with wavelengths ranging from 400 to 700nm, with no UV light, corresponding to energies lower than the zinc oxide's bandgap. This way, the difference in signal is solely due to sub-bandgap absorption from the CdSe CQDs. Since both the zinc oxide and the CdSe CQDs absorb in the UV region, the films were also irradiated with UV light to test their response.

Table 3.4 includes fitting data and the corresponding resistance. G is the electric conductance which corresponds to the slope of the current-voltage characteristic curve's linear regression, taken from -3V to 3V.

Table 3.4: Table with the fitting data from the current-voltage plots. G - electric conductance. r^2 - coefficient of determination. pΩ - pico ohm. * The signal was very low and full of noise.

	ZnO			
	Ambient light	**White LED**	**UV (254nm)**	**UV (366nm)**
G/pΩ^{-1}	3	2*	5150	2603
r^2	0,3018	0,9928	0,9969	0,9999
	ZnO + Cys capped CdSe CQDs			
	Ambient light	**White LED**	**UV (254nm)**	**UV (366nm)**
G/pΩ^{-1}	124	3	14300	8322
r^2	0,9539	0,9975	0.9994	0,9993

The results indicate that the presence of the CdSe CQDs in the films raises their electric conductance by up to two orders of magnitude in the case of ambient light exposure and triplicates in the case of both UV light exposures. Although the white LED flashlight had a dim light, given that its emission is above 400nm, the slightly higher photo-response from the films with CQDs can be attributed to the fact that the CQDs absorb in the visible range. Therefore, this demonstrates that the presence of CQDs in the ZnO host enables the composite material to widen its photo-response below the bandgap of the host. Sub-bandgap absorption is a possible explanation for the enhanced electric conductance, observed when the film is irradiated with the white LED. To confirm the existence of an intermediate band, described in section 1.3.3, a two-photon absorption measurement would have to be done. This technique consists in irradiating the material with two lasers. The lasers should have well defined sub-bandgap wavelengths, one that promotes the electrons from the VB to the IB and another that promotes from the IB to the CB (see Figure 1.6). If the emission corresponds to the band-gap of the matrix material, in this case the zinc oxide's, it is safe to affirm that the material has an intermediate band.[43, 44, 45]

4. Conclusions

Several different capping agents were tested to passivate the cadmium selenide nanoparticles. Some of the capping agents were never tried before, to the best of our knowledge. All capping agents were successful in chemically stabilizing the CdSe CQDs, with the exception of zinc acetate dihydrate. The stabilized nanoparticles were characterized by TEM and absorption spectroscopy. The TEM images show the existence of 2nm to 3nm quantum dots and the yellow color of the material itself which corresponds to an absorption in the range of 400 to 450nm is another evidence that the nanoparticles have 2nm to 3nm, due to the quantum confinement theory. The capping with molten bipyridine proved to be successful at temperatures up to 100°C. The uncapped CdSe CQDs cannot undergo temperatures in the same range without displaying color changes due to the fusing of the quantum dots.

Although the capped quantum dots do not show a good colloidal stability in methoxyethanol and a pellet can be observed after 24h, the addition of zinc acetate to the methoxyethanol solution significantly increases the colloidal stability and the suspension is clear, with no visible pellet, even after one day. From the DLS analysis, we were able to determine the size of colloid aggregates in methoxyethanol, with and without zinc acetate dihydrate present, and no significant differences in sizes were observed that could justify the differences in colloidal stability. The zinc acetate's function as a colloid stabilizer was not yet understood. It was hypothesized that the zinc acetate, present in the methoxyethanol solution, could have exchanged with the capping agents, leading to the observed colloidal stability. However, a test using zinc acetate as a capping agent itself, led to an immediate change in color, from yellow to red, indicative of CQD fusion. This growth induction could be exploited to shorten the time needed to grow the CdSe CQDs from 2nm to 3nm, from two days of reaction to two hours. The well defined emission peaks of these zinc acetate dihydrate capped CdSe CQDs, indicate that the growth hastening does not lead to an increase in dispersion of CQDs' sizes.

Two deposition methods were compared and the transmittance spectra from the spin-coated films were used in an attempt to characterize the film thicknesses. The spin-coating produced films did not show the desired homogeneity under the present formulation. The spray-pyrolysis method proved to be more versatile, controllable and the films were deposited more homogeneously.

To test the photo-response of the deposited films by spray-pyrolysis, the electric conductance of the films was measured and the films with embedded CdSe CQDs had a higher photo-response, under ambient and UV lights, than the films with only zinc oxide. Therefore, since the quantum dots absorb at lower energies than the zinc oxide, the enhanced photo-response could be attributed to the predicted intermediate band effect.

5. Future Perspectives

5.0.4. Colloidal Quantum Dots

5.0.4.1. Colloidal Stability

The complete and homogeneous dispersion of CQDs throughout the films is fundamental to achieve higher efficiencies. Efforts to improve the CQDs' colloidal stability, i.e., to avoid the aggregation of the 2nm CQDs in bigger structures, is desirable and a strategy to achieve that goal must be designed.

5.0.4.2. Chemical Stability VS Deposition Temperature

The film deposition typically requires the sol-gel precursor solution to react and decompose into the oxide form, at temperatures higher than the ones required to grow the uncapped CQDs. Testing the resistance to high temperature of capped CQDs should be added as a step to the methodology used.

5.0.4.3. Capping with Molten 2,2'Bipyridine

The one-step procedure described in section 3.3, could be explored to its full potential. The process can be optimized to achieve an improved extraction efficiency. Testing the solubility of the solid mixture of bipyridine and CdSe QDs in several kinds of solvents should be done to grant versatility in the deposition process.

Absorption and fluorescence spectra and TEM images should be obtained to determine the size distribution of the QDs and their bandgap and to compare with the typical capping procedures.

5.0.4.4. Testing Other Materials

The results with cadmium selenate quantum dots are very promising and should be pursued. However, it is also important to test quantum dots made of different materials, with adequate bandgaps in the desired region, to prove the generality of the approach and, with luck, to find comparable performances with cheaper and/or safer materials.

5.0.5. Film Characterization

5.0.5.1. Distribution of CQDs Embedded in the Films

The distribution of the CQDs embedded in the films has to be characterized, by confocal fluorescence microscopy, to guarantee a good dispersion of the fluorescent quantum dots throughout the films. The dispersion of the quantum dots can be correlated with the photo-electric properties of the films and used to improve the performance of the nano-structured hybrid materials.

5.0.5.2. 2-Photon Absorption Measurement

Despite the intermediate-band is a plausible explanation for the observed improvement of the photo-response, direct proof of the existence of an intermediate band is necessary. For that two-step photon absorption measurements must be employed.

Bibliography

[1] IPCC Adopted. CLIMATE CHANGE 2014 SYNTHESIS REPORT. 2014.

[2] Christian Kerschner, Christina Prell, Kuishuang Feng, and Klaus Hubacek. Economic vulnerability to Peak Oil. *Global Environmental Change*, 23(6):1424–1433, December 2013.

[3] Ian Chapman. The end of Peak Oil? Why this topic is still relevant despite recent denials. *Energy Policy*, 64:93–101, January 2014.

[4] M. Hosenuzzaman, N.A. Rahim, J. Selvaraj, M. Hasanuzzaman, A.B.M.A. Malek, and A. Nahar. Global prospects, progress, policies, and environmental impact of solar photovoltaic power generation. *Renewable and Sustainable Energy Reviews*, 41:284–297, January 2015.

[5] Chetan Solanki. *Solar Photovoltaics: Fundamentals Technologies And Applications*. Prentice-Hall Of India Pvt. Limited, 2009.

[6] Heng Liu, Alexandre Pourret, and Philippe Guyot-Sionnest. Mott and Efros-Shklovskii Variable Range Hopping in CdSe Quantum Dots Films. *ACS Nano*, 4(9):5211–5216, 2010. bibtex: doi:10.1021/nn101376u biblatexdata[eprint=http://dx.doi.org/10.1021/nn101376u].

[7] M.J. de Moura Dias Mendes, A.M. Vega, I.T. Galicia, and A.L. López. Intermediate band solar cell having solution-processed colloidal quantum dots and metal nanoparticles, April 2013. US Patent App. 13/648,757.

[8] Graham H. Carey, Illan J. Kramer, Pongsakorn Kanjanaboos, Gabriel Moreno-Bautista, Oleksandr Voznyy, Lisa Rollny, Joel A. Tang, Sjoerd Hoogland, and Edward H. Sargent. Electronically Active Impurities in Colloidal Quantum Dot Solids. *ACS Nano*, 8(11):11763–11769, November 2014.

[9] Neil C. Greenham, Xiaogang Peng, and A. Paul Alivisatos. Charge separation and transport in conjugated-polymer/semiconductor-nanocrystal composites studied by photoluminescence quenching and photoconductivity. *Physical Review B*, 54(24):17628, 1996.

[10] Steven A. McDonald, Gerasimos Konstantatos, Shiguo Zhang, Paul W. Cyr, Ethan J. D. Klem, Larissa Levina, and Edward H. Sargent. Solution-processed PbS quantum dot infrared photodetectors and photovoltaics. *Nature Materials*, 4(2):138–142, February 2005.

[11] Y. Shen, J. Bao, N. Dai, J. Wu, F. Gu, J.C. Tao, and J.C. Zhang. Speedy photoelectric exchange of CdSe quantum dots/mesoporous titania composite system. *Applied Surface Science*, 255(6):3908–3911, January 2009.

[12] Michael A. White, Jillian L. Dempsey, Gerard M. Carroll, James D. Gallagher, and Daniel R. Gamelin. Photoconductive ZnO films with embedded quantum dot or ruthenium dye sensitizers. *APL Materials*, 1(3):032107, 2013.

[13] A. Luque and S. Hegedus. *Handbook of Photovoltaic Science and Engineering*. Wiley, 2011.

[14] M. Bass and Optical Society of America. *Handbook of Optics: Fundamentals, techniques, and design*. Number v. 1 in Handbook of Optics. McGraw-Hill, 1994. bibtex: bass1994handbook.

[15] A. Luque-Lopez, F. Flores-Sinta, A. Martí-Vega, J.C. Conesa-Cegarra, P. Wahnon-Benarroch, J. Ortega-Mateo, C. Tablero-Crespo, R. Pérez-Pérez, and L. Cuadra-Rodríguez. Intermediate band semiconductor photovoltaic solar cell, September 2002. US Patent 6,444,897.

[16] Antonio Luque, Antonio Martí, and Colin Stanley. Understanding intermediate-band solar cells. *Nature Photonics*, 6(3):146–152, February 2012.

[17] M. A. Reed, J. N. Randall, R. J. Aggarwal, R. J. Matyi, T. M. Moore, and A. E. Wetsel. Observation of discrete electronic states in a zero-dimensional semiconductor nanostructure. *Phys. Rev. Lett.*, 60(6):535–537, February 1988.

[18] Yasuaki Masumoto, Toshihide Takagahara, Phaedon Avouris, Klaus von Klitzing, Hiroyuki Sakaki, and Roland Wiesendanger, editors. *Semiconductor Quantum Dots*. NanoScience and Technology. Springer Berlin Heidelberg, Berlin, Heidelberg, 2002.

[19] Saim Emin, Surya P. Singh, Liyuan Han, Norifusa Satoh, and Ashraful Islam. Colloidal quantum dot solar cells. *Solar Energy*, 85(6):1264–1282, June 2011.

[20] Mohamed Missous. Characterisation of InAs/GaAs quantum dots intermediate band photovoltaic devices. *IET Optoelectronics*, 8(2):71–75(4), April 2014.

[21] T. J. Grassman, D. B. Shah, J. A. Carlin, and S. A. Ringel. Exploration of Epitaxial Quantum Dots within Wide Band Gap Metamorphic Host Materials for Intermediate Band Solar Cells. *2013 IEEE 39TH PHOTOVOLTAIC SPECIALISTS CONFERENCE (PVSC)*, pages 284–287, 2013.

[22] Som N. Dahal, Stephen P. Bremner, and Christiana B. Honsberg. Identification of candidate material systems for quantum dot solar cells including the effect of strain. *Progress in Photovoltaics: Research and Applications*, pages n/a–n/a, 2010.

[23] Gerasimos Konstantatos. *Colloidal quantum dot optoelectronics and photovoltaics*. 2013.

[24] A. Rogach. *Semiconductor Nanocrystal Quantum Dots: Synthesis, Assembly, Spectroscopy and Applications*. Springer ebook collection / Chemistry and Materials Science 2005-2008. Springer, 2008. bibtex: rogach2008semiconductor.

[25] Wikipedia. Quantum dot — Wikipedia, The Free Encyclopedia. 2015. [Online; accessed 23-January-2015].

[26] E. Andrade, M. Miki-Yoshida, and others. Growth, structure and optical characterization of high quality ZnO thin films obtained by spray pyrolysis. *Thin Solid Films*, 350(1):192–202, 1999.

[27] Nikolai Gaponik, Dmitri V. Talapin, Andrey L. Rogach, Kathrin Hoppe, Elena V. Shevchenko, Andreas Kornowski, Alexander Eychmüller, and Horst Weller. Thiol-Capping of CdTe Nanocrystals: An Alternative to Organometallic Synthetic Routes. *The Journal of Physical Chemistry B*, 106(29):7177–7185, July 2002.

[28] Andrey L. Rogach, Andreas Kornowski, Mingyuan Gao, Alexander Eychmüller, and Horst Weller. Synthesis and Characterization of a Size Series of Extremely Small Thiol-Stabilized CdSe Nanocrystals. *The Journal of Physical Chemistry B*, 103(16):3065–3069, April 1999.

[29] Miguel ARB Castanho, Nuno C. Santos, and Luís MS Loura. Separating the turbidity spectra of vesicles from the absorption spectra of membrane probes and other chromophores. *European biophysics journal*, 26(3):253–259, 1997.

[30] Qisui Wang, Fangyun Ye, Peng Liu, Xinmin Min, and Xi Li. Conjugation and fluorescence quenching between bovine serum albumin and L-cysteine capped CdSe/CdS quantum dots. *Protein and peptide letters*, 18(4):410–414, 2011.

[31] Yingqi Cui, Zhaoyang Lou, Xinqin Wang, Shengping Yu, and Mingli Yang. A study of optical absorption of cysteine-capped CdSe nanoclusters using first-principles calculations. *Phys. Chem. Chem. Phys.*, 17(14):9222–9230, 2015.

[32] Robert G. Acres, Vitaliy Feyer, Nataliya Tsud, Elvio Carlino, and Kevin C. Prince. Mechanisms of Aggregation of Cysteine Functionalized Gold Nanoparticles. *The Journal of Physical Chemistry C*, 118(19):10481–10487, May 2014.

[33] Mikhail Bogdanov and William Dowhan. Phosphatidylethanolamine is required for in vivo function of the membrane-associated lactose permease of Escherichia coli. *Journal of Biological Chemistry*, 270(2):732–739, 1995.

[34] Imre Sóvágó, Arthur Gergely, Béla Harman, and Tamás Kiss. Complexes of sulphur-containing ligands—II: Binary and ternary complexes of D-penicillamine and L-cysteine with nickel(II) and zinc(II) ions. *Journal of Inorganic and Nuclear Chemistry*, 41(11):1629–1633, 1979.

[35] Vladimir V. Breus, Colin D. Heyes, Kyrylo Tron, and G. Ulrich Nienhaus. Zwitterionic Biocompatible Quantum Dots for Wide pH Stability and Weak Nonspecific Binding to Cells. *ACS Nano*, 3(9):2573–2580, September 2009.

[36] Yongfen Chen and Zeev Rosenzweig. Luminescent CdS Quantum Dots as Selective Ion Probes. *Analytical Chemistry*, 74(19):5132–5138, October 2002.

[37] Dale E. Moore and Kaushik Patel. Q-CdS Photoluminescence Activation on Zn^{2+} and Cd^{2+} Salt Introduction. *Langmuir*, 17(8):2541–2544, April 2001.

[38] Aldrich. Lumidot^{TM} CdSe-6, quantum dot nanoparticles kit. [Online; accessed 16-March-2015].

[39] W. William Yu, Lianhua Qu, Wenzhuo Guo, and Xiaogang Peng. Experimental Determination of the Extinction Coefficient of CdTe, CdSe, and CdS Nanocrystals. *Chemistry of Materials*, 15(14):2854–2860, July 2003.

[40] R.A. Street. Luminescence in a-si:h. In Jacques I. Pankove, editor, *Hydrogenated Amorphous SiliconOptical Properties*, volume 21, Part B of *Semiconductors and Semimetals*, pages 216 – 217. Elsevier, 1984.

[41] *Dynamic light scattering common terms defined (white paper).* Malvern Instruments Worldwide.

[42] Nor Aliya Hamizi and Mohd Rafie Johan. Optical properties of CdSe quantum dots via non-TOP based route. *International Journal of Electrochemical Science*, 7:8458–8467, 2012.

[43] Amit Nag, Arijit Kr De, and Debabrata Goswami. A Sensitive Technique for Two-Photon Absorption Measurements: Towards Higher Resolution Microscopy. *Journal of Physics: Conference Series*, 80:012034, September 2007.

[44] Tomah Sogabe, Yasushi Shoji, Mitsuyoshi Ohba, Katsuhisa Yoshida, Ryo Tamaki, Hwen-Fen Hong, Chih-Hung Wu, Cherng-Tsong Kuo, Stanko Tomić, and Yoshitaka Okada. Intermediate-band dynamics of quantum dots solar cell in concentrator photovoltaic modules. *Scientific Reports*, 4, April 2014.

[45] Mariacristina Rumi and Joseph W. Perry. Two-photon absorption: an overview of measurements and principles. *Advances in Optics and Photonics*, 2(4):451, December 2010.

Appendix A

Weights - Synthesis and Characterization

Table I: Weights of capping agents added to falcon tubes.

	Bpy	**Py**	**3-MT**	**NaAce**	**Cys**	**ZnAce**
Weight/mg	30,28	17	20,36	26,32	23,57	42,60

Table II: Weights of capped CdSe CQDs used in optical characterization, corresponding to the synthesis involving six different capping agents, in either 1mL of ORG or ZnORG.

	CdSeBpy	**CdSePy**	**CdSe3-MT**	**CdSeNaAce**	**CdSeCys**	**CdSeZnAce**	**CdSeX**
ORG	1,19mg	1,03mg	1,04mg	1,07mg	1,04mg	1,09mg	1,05mg
ZnORG	1,03mg	1,14mg	1,17mg	1,00mg	1,03mg	0,91mg	0,96mg

Table III: Weights of capped CdSe CQDs used in optical characterization, corresponding to the experiment described in section 2.1.2.2, in either 0,5mL of ORG or ZnORG.

	Reaction time		
	2h	**5h 40min**	**28h 30min**
ORG	1,99mg	1,99mg	1,07mg
ZnORG	2,07mg	2,07mg	1,34mg

Table IV: Weights of capped CdSe CQDs used in DLS analysis, both size and zeta potential determination, corresponding to the synthesis involving six different capping agents, in either 1mL of ORG or ZnORG. The CdSeNaAce sample was diluted 1:2.

	CdSeBpy	**CdSePy**	**CdSe3-MT**	**CdSeNaAce**	**CdSeCys**	**CdSeZnAce**	**CdSeX**
ORG	1,01mg	1,06mg	1,17mg	1,85mg	0,93mg	1,03mg	1,09mg
ZnORG	1,11mg	0,99mg	1,10mg	1,86mg	0,96mg	1,07mg	1,13mg

Device Parameters - Characterization

Table V: Device parameters used on the optical characterization of CdSe CQDs, from the experiment described in section 2.1.2.1, suspended in AN.

Scan Software Version	3.00(339)
Instrument	Cary 5000
Instrument Version	1.12
Start (nm)	2000,000
Stop (nm)	200,00
X Mode	
Y Mode	
UV-Vis Scan Rate (nm/min)	600,000
UV-Vis Data Interval (nm)	1,000
UV-Vis Ave. Time (sec)	0,100
UV-Vis SBW (nm)	2,000
Slit Height	Full
Beam Mode	Double
Signal-to-noise Mode	Off
UV Source	On
Vis Source	On
Third Source	Off
Source Changeover (nm)	350,00
Detector Changeover (nm)	800,00
Grating Changeover (nm)	800,00
Baseline Correction	On
Baseline Type	Baseline correction
Cycle Mode	Off
<SBW (nm)>	2,00
<Energy>	52,48
<Slit height>	Full
<Current Wavelength>	200,00

Table VI: Device parameters used on the optical characterization of CdSe CQDs, from the experiment described in section 2.1.2.1, suspended in either ORG or ZnORG.

Collection Time	7/28/2015 2:26:39 PM
Scan Software Version	4.20(468)
Instrument	Cary 100
Instrument Version	09.00
Start (nm)	800,00
Stop (nm)	200,00
UV-Vis Scan Rate (nm/min)	600,000
UV-Vis Data Interval (nm)	1,000
UV-Vis Ave. Time (sec)	0,100
UV-Vis SBW (nm)	2,0
Beam Mode	Double
Signal-to-noise Mode	Off
UV Source	On
Vis Source	On
Source Changeover (nm)	350,00
Baseline Correction	On
Baseline Type	Baseline correction
Cycle Mode	Off
<SBW (nm)>	2,00
<Energy>	155,00
<Current Wavelength>	200,00

Table VII: Device parameters used on the optical characterization of CdSe CQDs, from the experiment described in section 2.1.2.2, suspended in either ORG or ZnORG.

Scan Software Version	3.00(339)
Instrument	Cary 5000
Instrument Version	1.12
Start (nm)	2000,00
Stop (nm)	200,00
X Mode	Nanometers
Y Mode	Abs
UV-Vis Scan Rate (nm/min)	600,000
UV-Vis Data Interval (nm)	1,000
UV-Vis Ave. Time (sec)	0,100
UV-Vis SBW (nm)	2,000
Slit Height	Full
Beam Mode	Double
Signal-to-noise Mode	Off
UV Source	On
Vis Source	On
Third Source	Off
Source Changeover (nm)	350,00
Detector Changeover (nm)	800,00
Grating Changeover (nm)	800,00
Baseline Correction	On
Baseline Type	Baseline correction
Cycle Mode	Off

Appendix B

Absorption and Emission Spectra

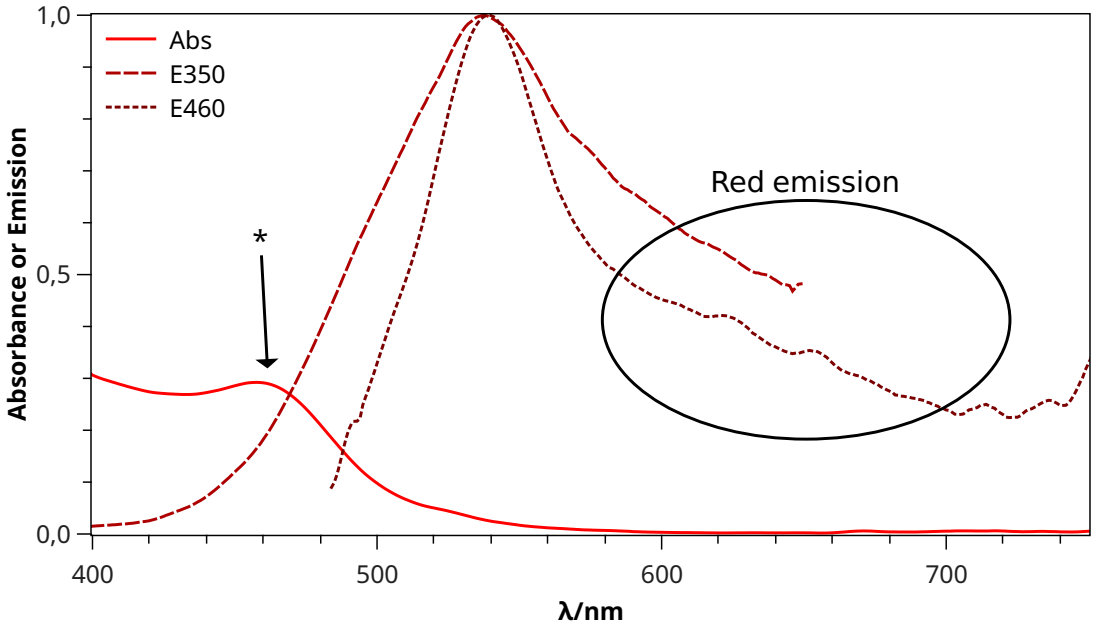

Figure I: Corrected absorption spectrum of diluted 1:10 Py capped CdSe CQDs, dispersed in ORG. The emission spectra were performed with a slit of 4nm, in right angle mode and the solution was not diluted. * - First absorption peak.

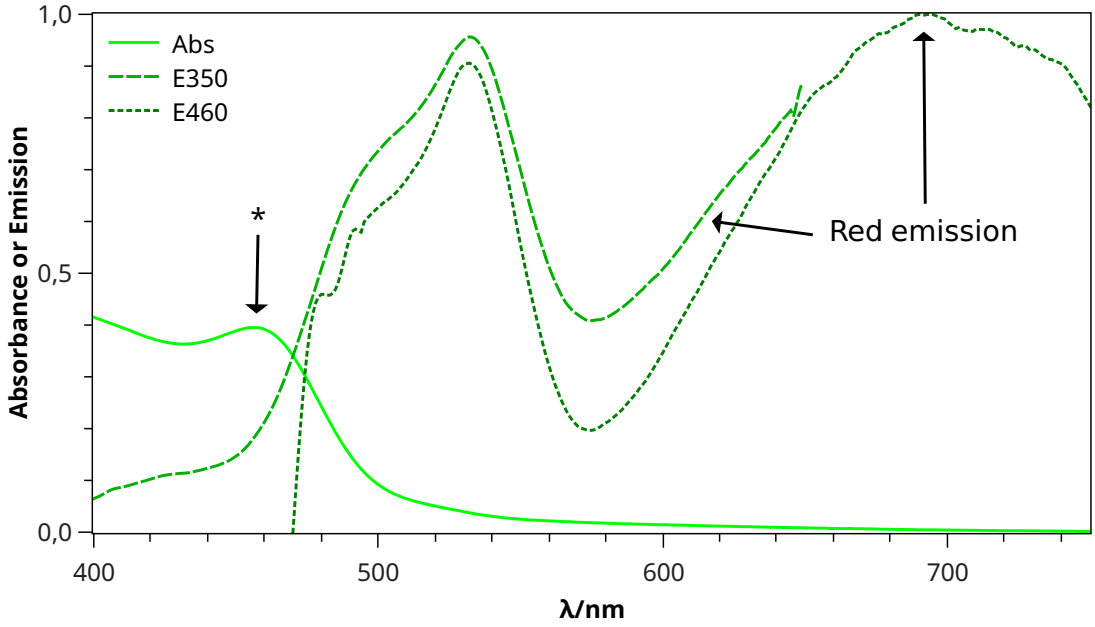

Figure II: Absorption spectrum of diluted 1:2 Py capped CdSe CQDs, dispersed in ZnORG. The emission spectra were performed with a slit of 4nm, in right angle mode and the solution was not diluted. * - First absorption peak.

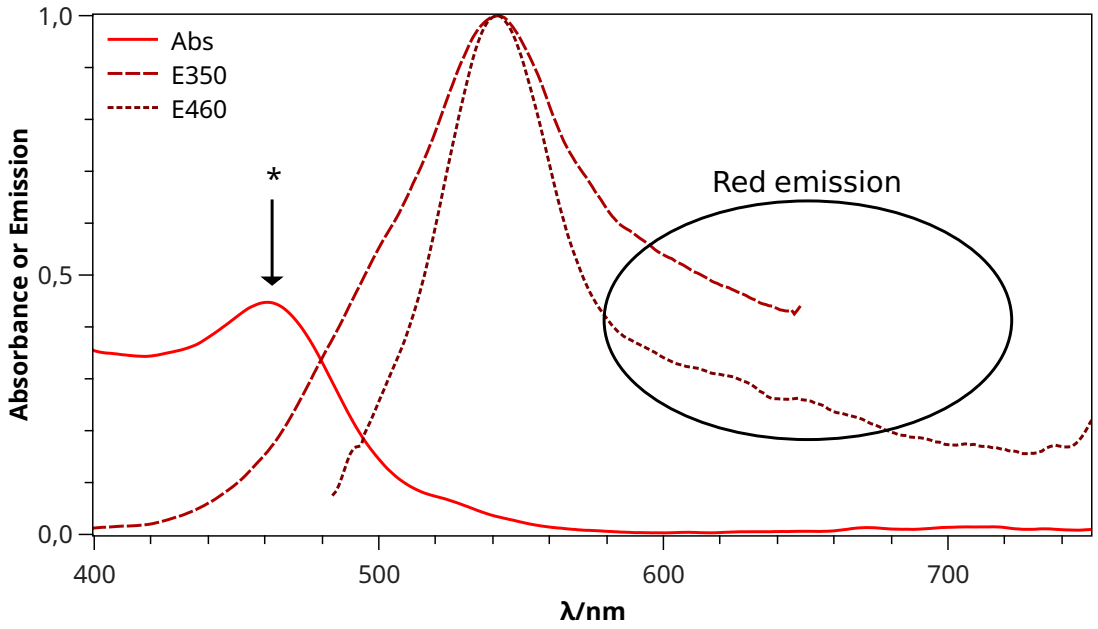

Figure III: Absorption spectrum of diluted 1:10 3-MT capped CdSe CQDs, dispersed in ORG. The emission spectra were performed with a slit of 4nm, in right angle mode and the solution was not diluted. * - First absorption peak.

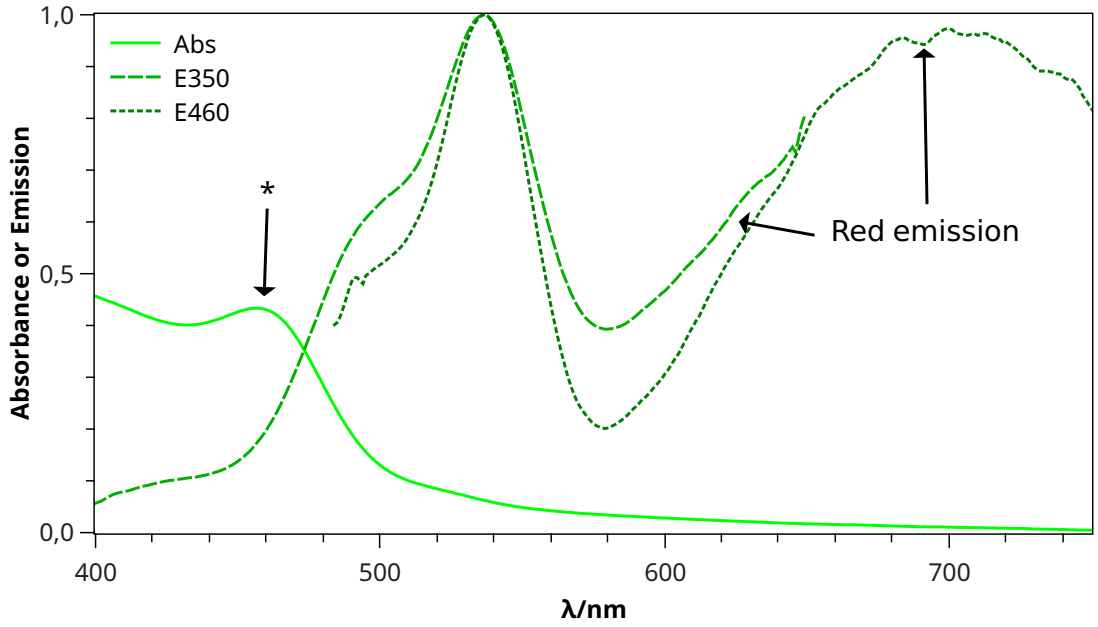

Figure IV: Absorption spectrum of diluted 1:2 3-MT capped CdSe CQDs, dispersed in ZnORG. The emission spectra were performed with a slit of 4nm, in right angle mode and the solution was not diluted. * - First absorption peak.

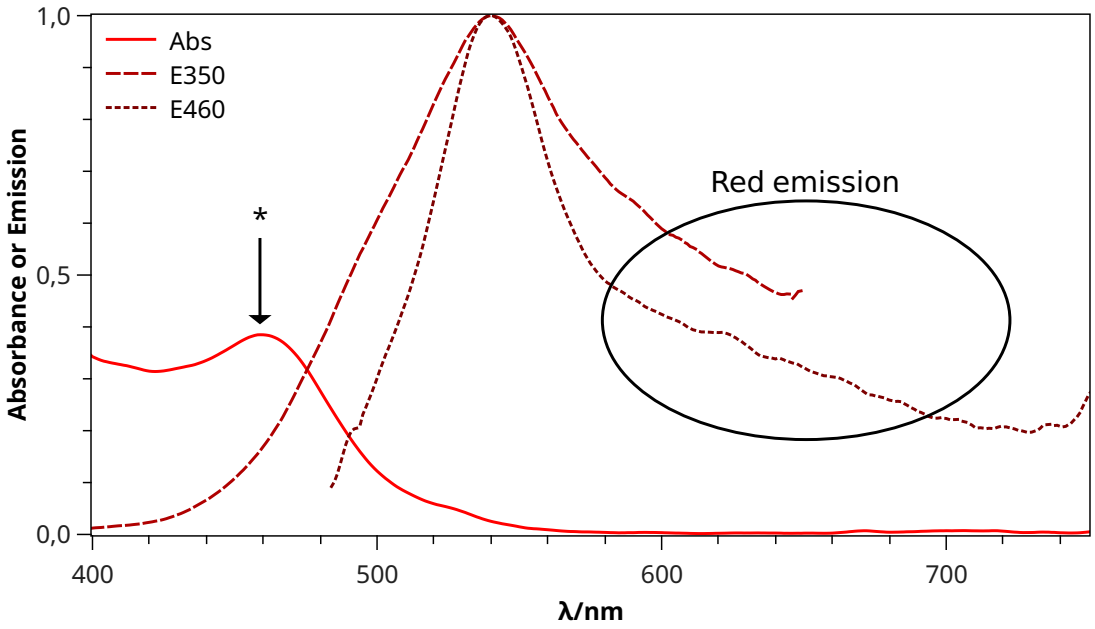

Figure V: Absorption spectrum of diluted 1:10 NaAce capped CdSe CQDs, dispersed in ORG. The emission spectra were performed with a slit of 4nm, in right angle mode and the solution was not diluted. * - First absorption peak.

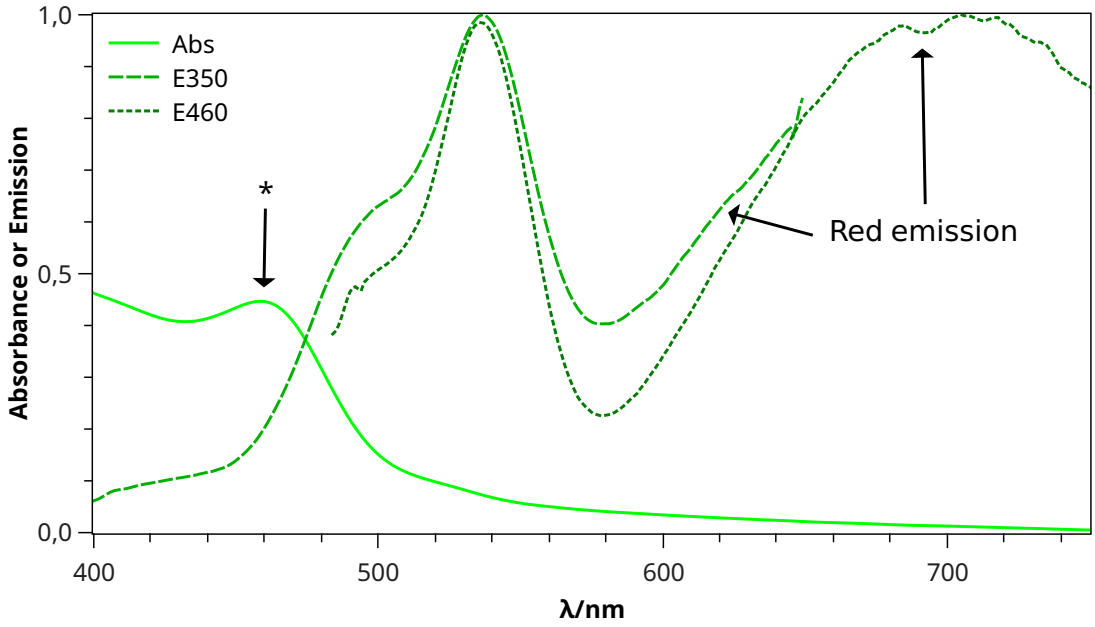

Figure VI: Absorption spectrum of diluted 1:2 NaAce capped CdSe CQDs, dispersed in ZnORG. The emission spectra were performed with a slit of 4nm, in right angle mode and the solution was not diluted. * - First absorption peak.

Absorption Spectra Differentiation

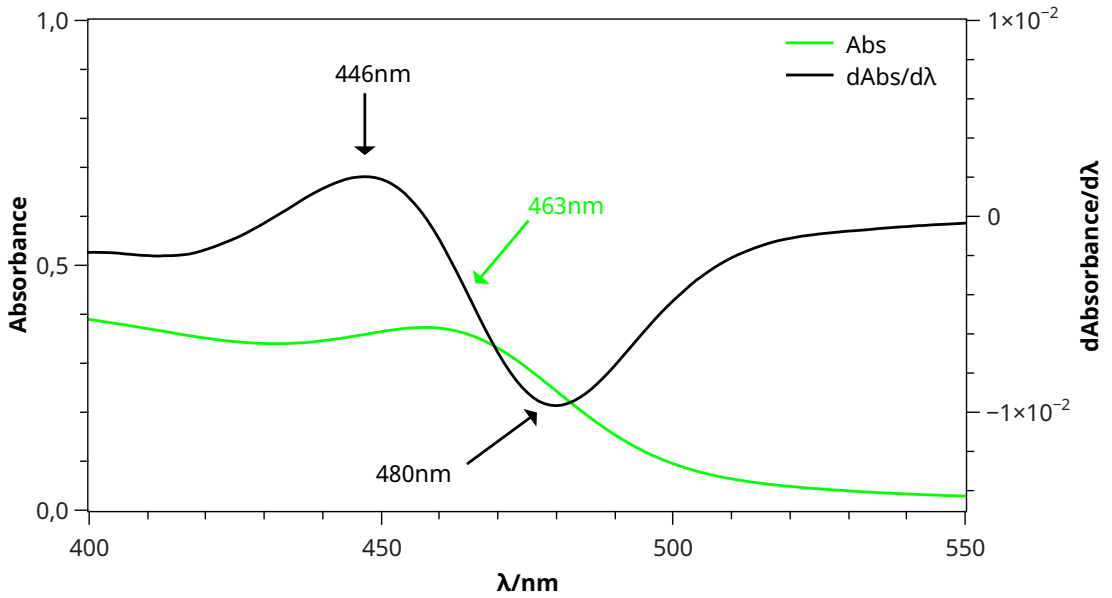

Figure VII: Absorption spectrum of diluted 1:2 bipyridine capped CdSe CQDs, dispersed in ZnORG, and the smoothed spectral derivative. The algorithm applied for smoothing was Savitzky-Golay with a polynomial order of 9 and with 25 points to the right and to the left.

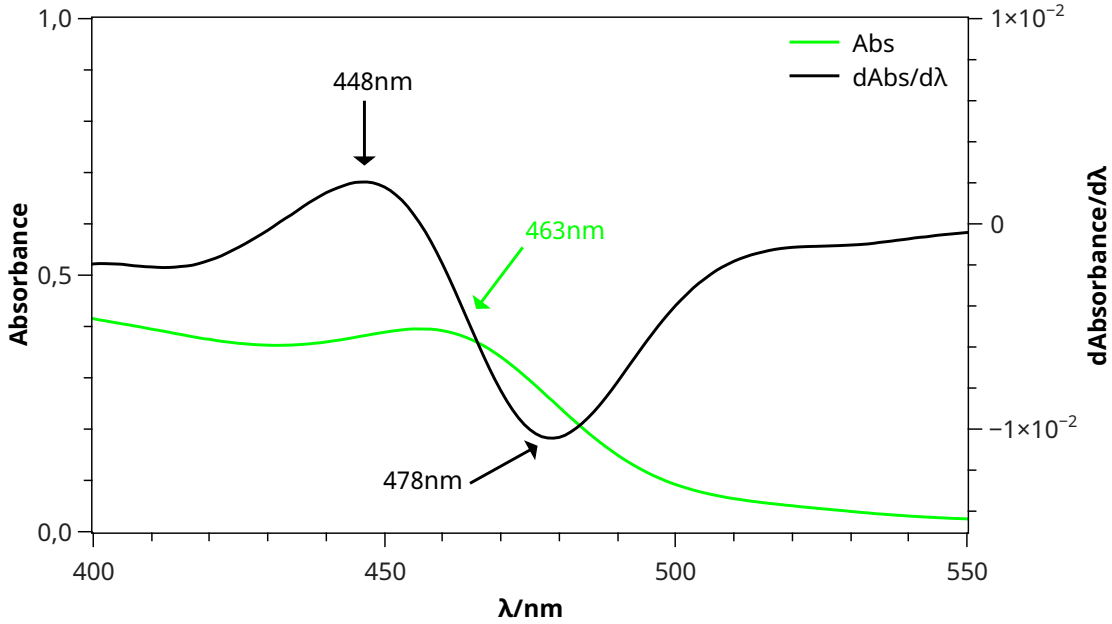

Figure VIII: Absorption spectrum of diluted 1:2 Py capped CdSe CQDs, dispersed in ZnORG, and the smoothed spectral derivative. The algorithm applied for smoothing was Savitzky-Golay with a polynomial order of 9 and with 25 points to the right and to the left.

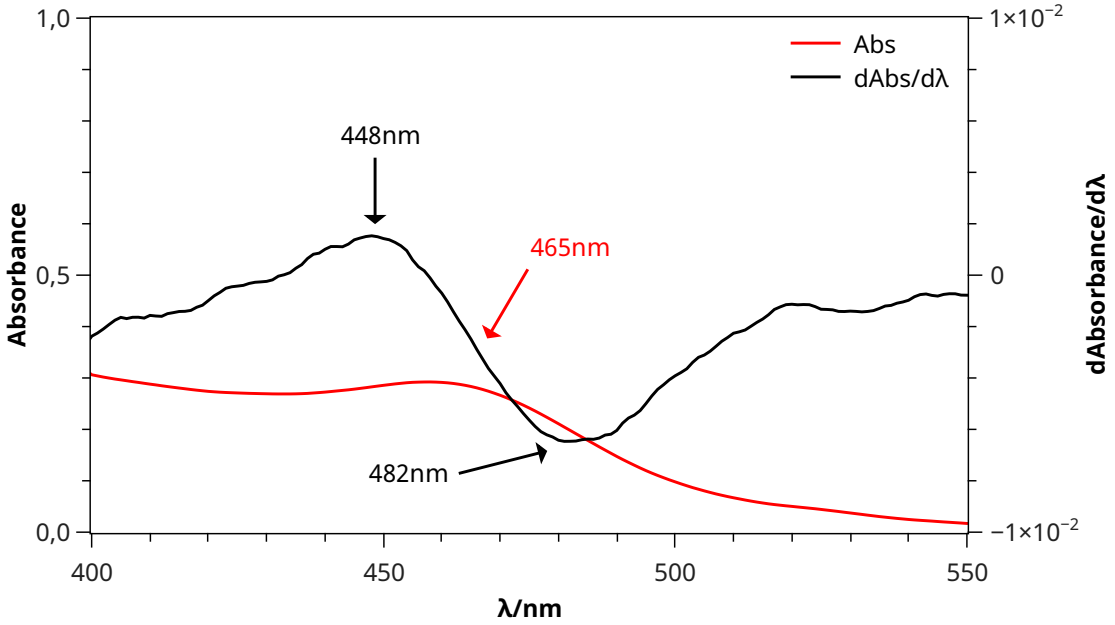

Figure IX: Corrected absorption spectrum of diluted 1:10 Py capped CdSe CQDs, dispersed in ORG, and the smoothed spectral derivative. The algorithm applied for smoothing was Savitzky-Golay with a polynomial order of 9 and with 25 points to the right and to the left and to the left.

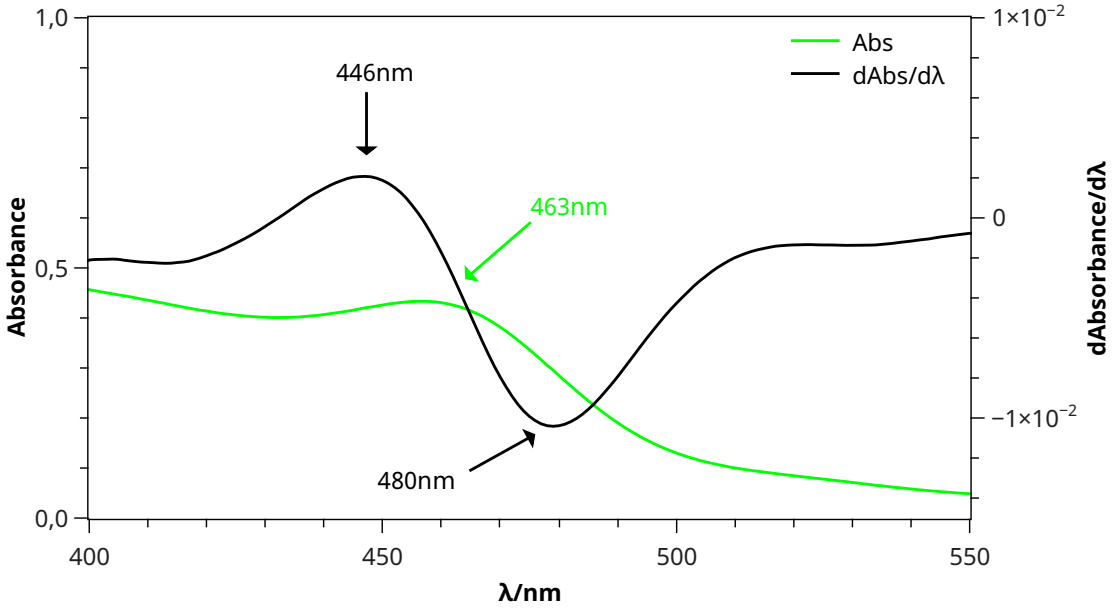

Figure X: Absorption spectrum of diluted 1:2 3-MT capped CdSe CQDs, dispersed in ZnORG, and the smoothed spectral derivative. The algorithm applied for smoothing was Savitzky-Golay with a polynomial order of 9 and with 25 points to the right and to the left.

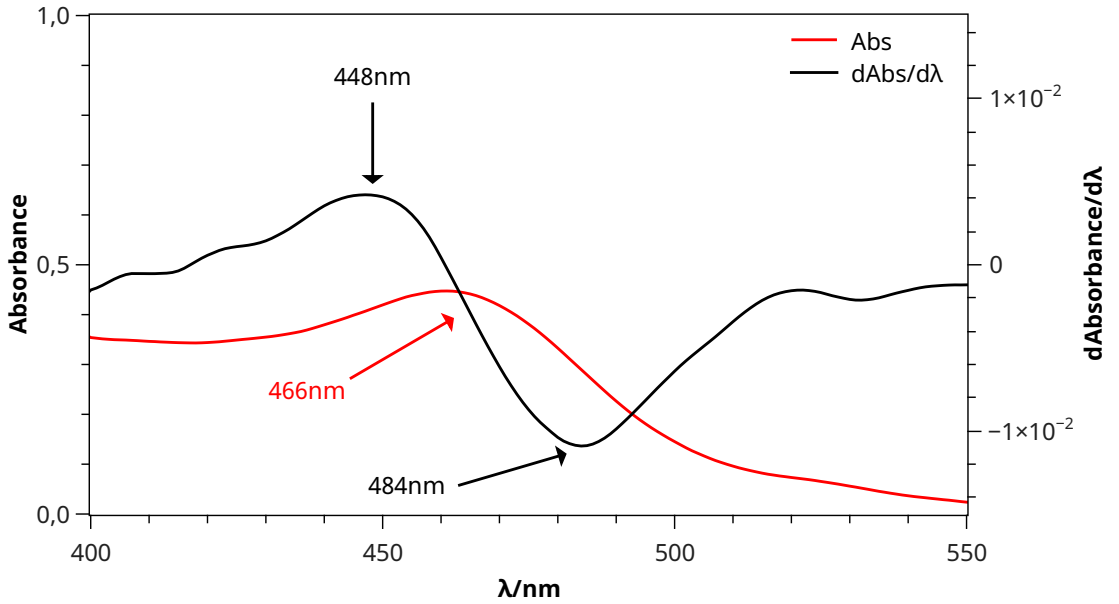

Figure XI: Absorption spectrum of diluted 1:10 3-MT capped CdSe CQDs, dispersed in ORG, and the smoothed spectral derivative. The algorithm applied for smoothing was Savitzky-Golay with a polynomial order of 9 and with 25 points to the right and to the left and to the left.

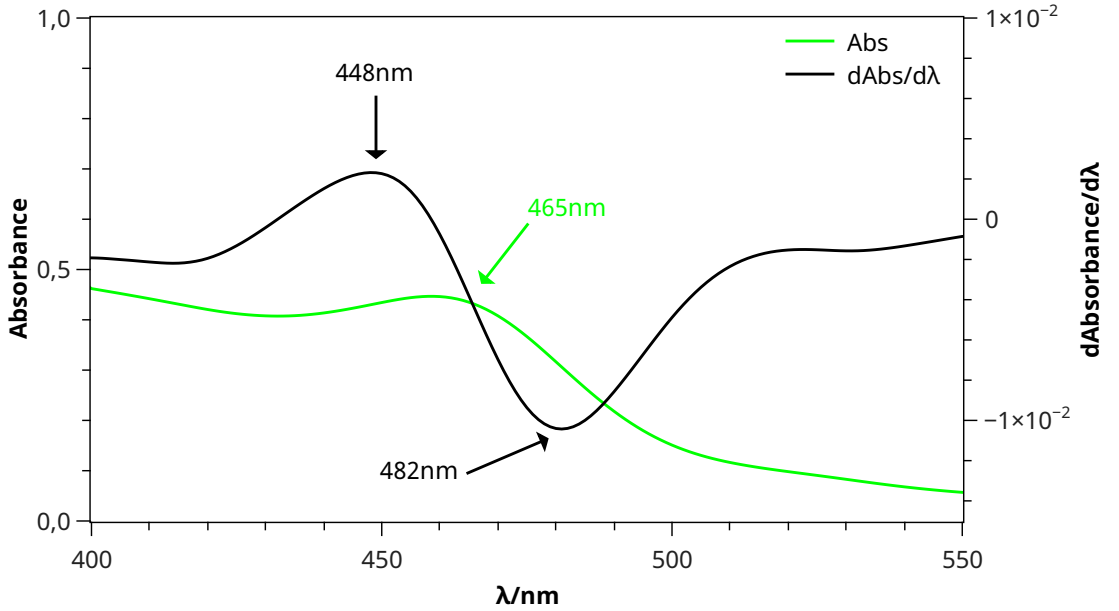

Figure XII: Absorption spectrum of diluted 1:2 NaAce capped CdSe CQDs, dispersed in ZnORG, and the smoothed spectral derivative. The algorithm applied for smoothing was Savitzky-Golay with a polynomial order of 9 and with 25 points to the right and to the left.

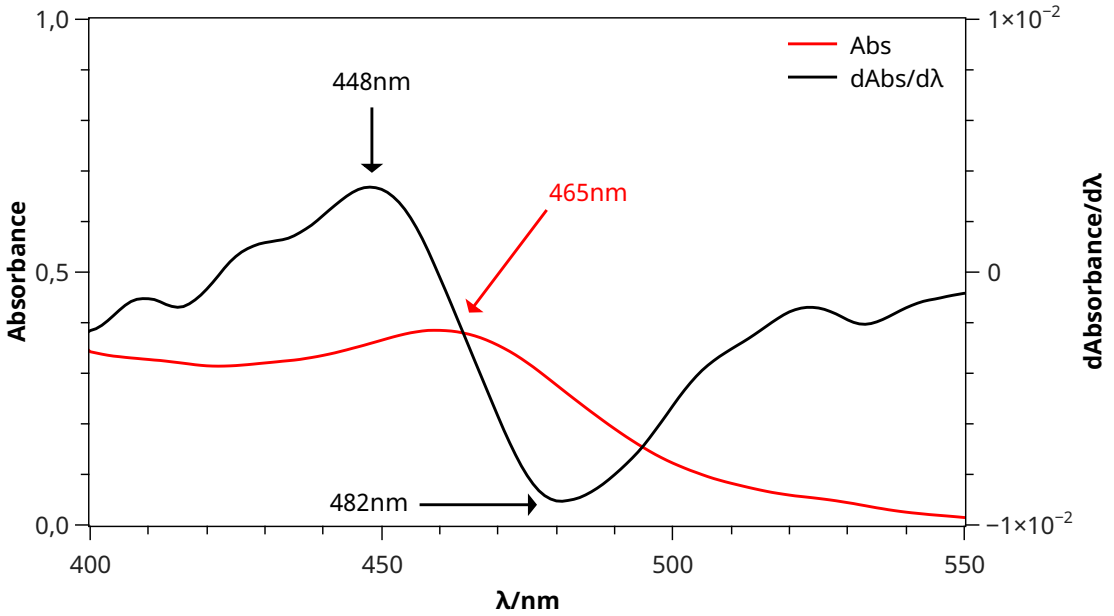

Figure XIII: Absorption spectrum of diluted 1:10 NaAce capped CdSe CQDs, dispersed in ORG, and the smoothed spectral derivative. The algorithm applied for smoothing was Savitzky-Golay with a polynomial order of 9 and with 25 points to the right and to the left and to the left.

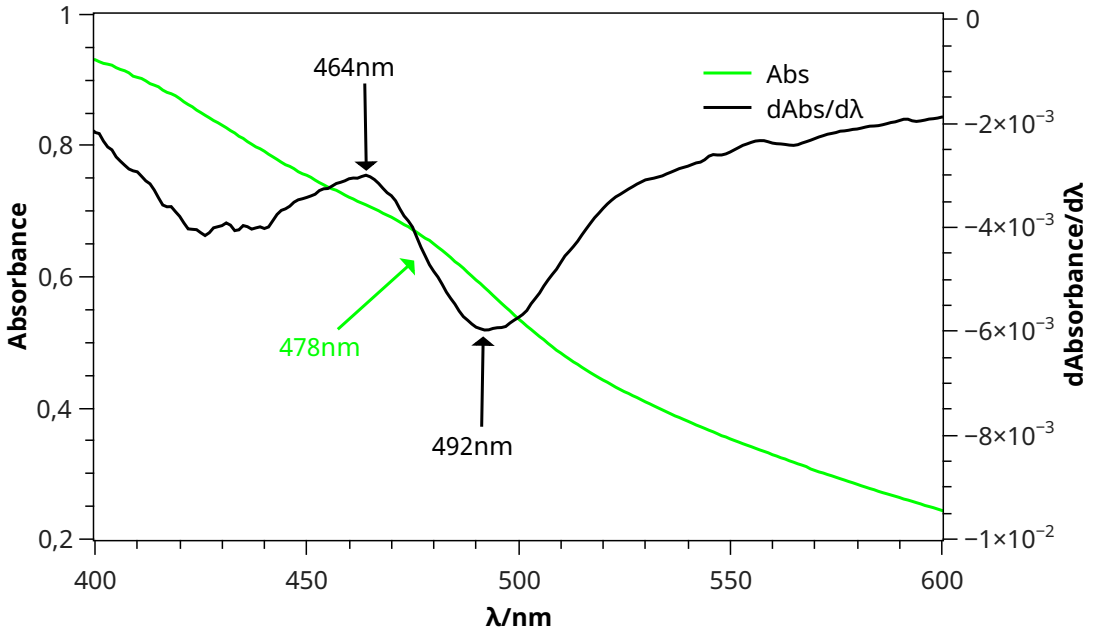

Figure XIV: Corrected absorption spectrum of diluted 1:2 Cys capped CdSe CQDs, dispersed in ORG, and the smoothed spectral derivative. The algorithm applied for smoothing was Savitzky-Golay with a polynomial order of 9 and with 25 points to the right and to the left and to the left.

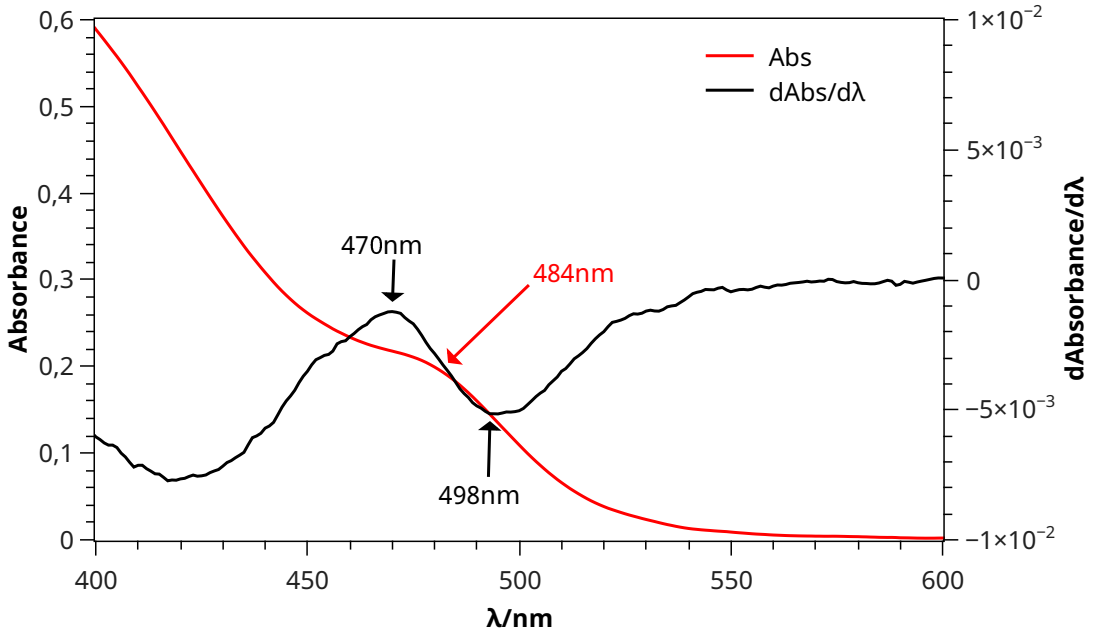

Figure XV: Absorption spectrum of diluted 1:10 Cys capped CdSe CQDs, dispersed in ORG, and the smoothed spectral derivative. The algorithm applied for smoothing was Savitzky-Golay with a polynomial order of 9 and with 25 points to the right and to the left and to the left.

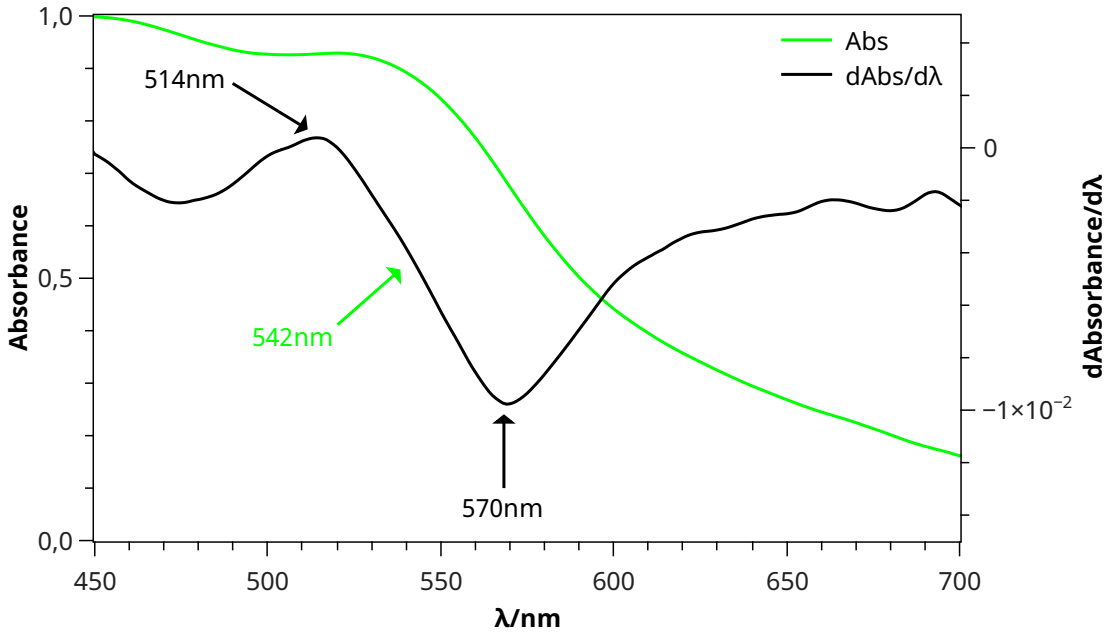

Figure XVI: Corrected absorption spectrum of diluted 1:2 ZnAce capped CdSe CQDs, dispersed in ORG, and the smoothed spectral derivative. The algorithm applied for smoothing was Savitzky-Golay with a polynomial order of 9 and with 25 points to the right and to the left and to the left.

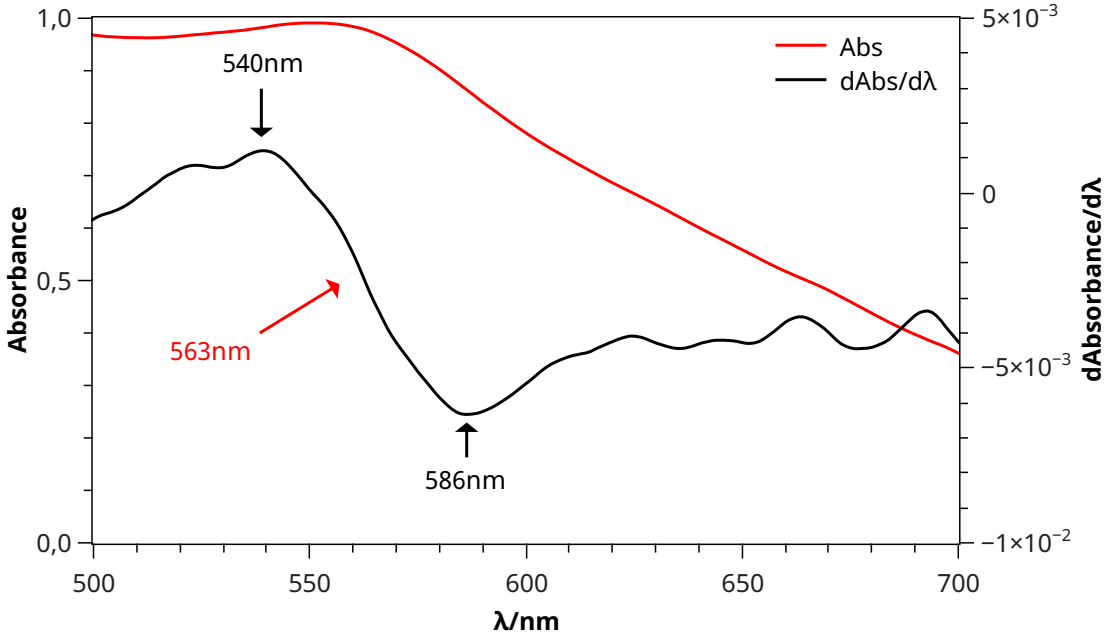

Figure XVII: Corrected absorption spectrum of diluted 1:10 ZnAce capped CdSe CQDs, dispersed in ORG, and the smoothed spectral derivative. The algorithm applied for smoothing was Savitzky-Golay with a polynomial order of 9 and with 25 points to the right and to the left and to the left.

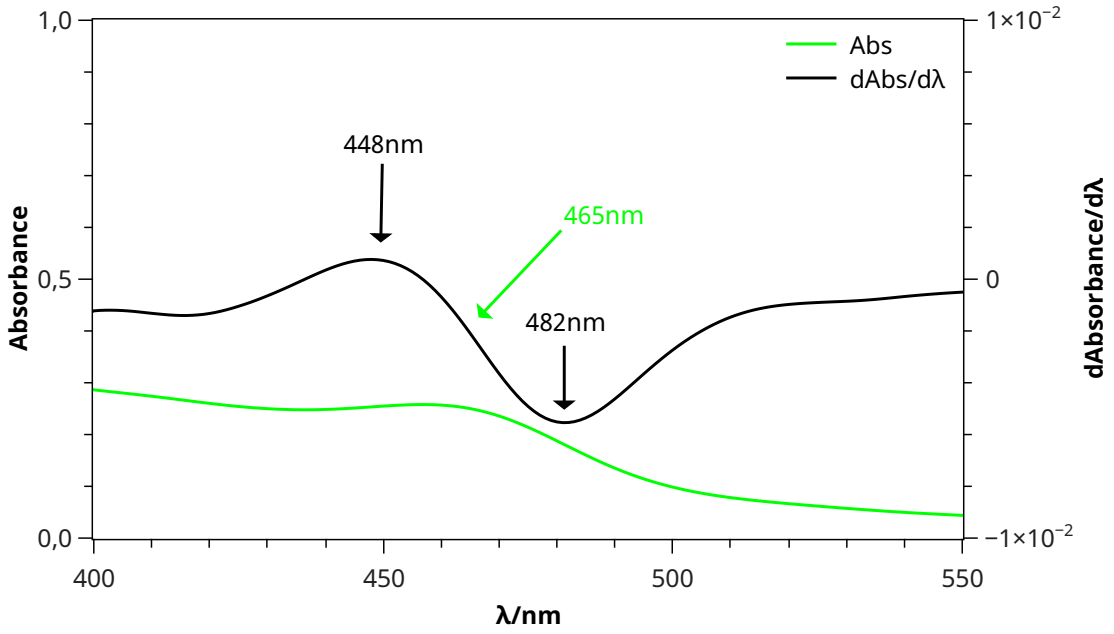

Figure XVIII: Corrected absorption spectrum of diluted 1:2 uncapped CdSe CQDs, dispersed in ORG, and the smoothed spectral derivative. The algorithm applied for smoothing was Savitzky-Golay with a polynomial order of 9 and with 25 points to the right and to the left and to the left.

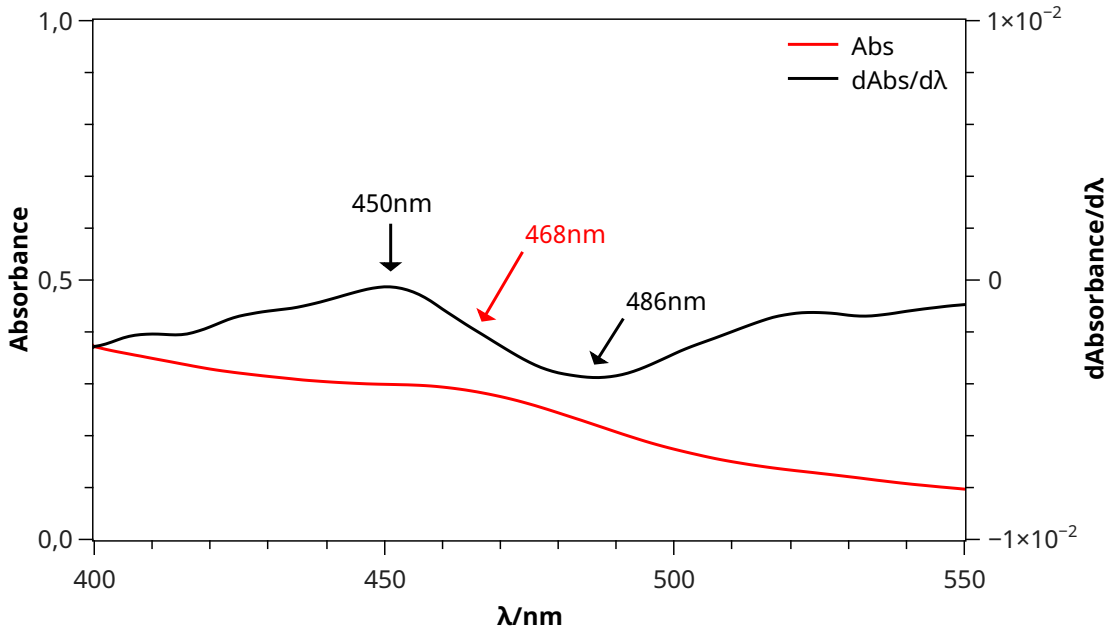

Figure XIX: Corrected absorption spectrum of diluted 1:10 uncapped CdSe CQDs, dispersed in ORG, and the smoothed spectral derivative. The algorithm applied for smoothing was Savitzky-Golay with a polynomial order of 9 and with 25 points to the right and to the left and to the left.

DLS Spectra

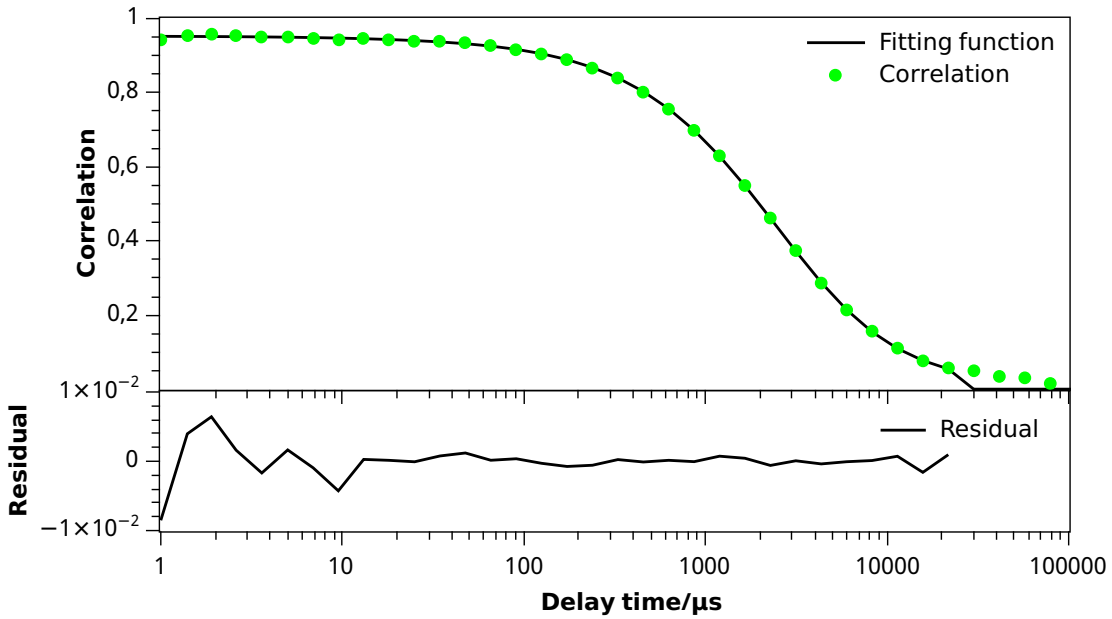

Figure XX: Graphic of the correlation data with corresponding fitting, from the DLS analysis, of uncapped CdSe CQDs, dispersed in ZnORG solution, in a quartz cell with all transparent sides, 2mm wide and with a 1cm optical path length. The solution was previously filtered with a 0,22μm filter. The signal accumulation time is 30s.

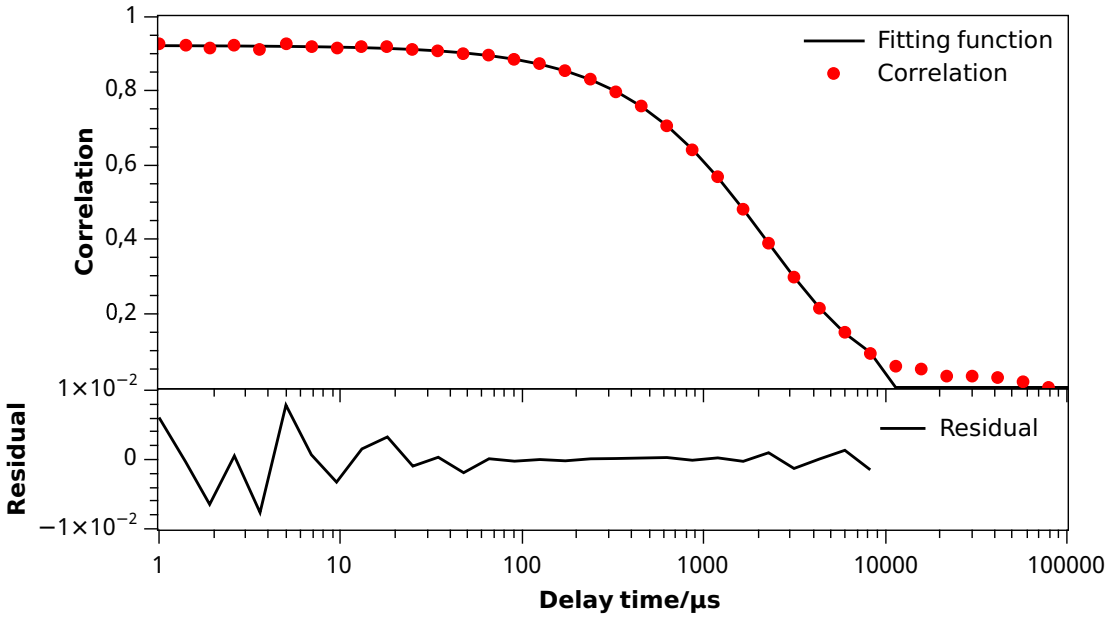

Figure XXI: Graphic of the correlation data with corresponding fitting, from the DLS analysis, of uncapped CdSe CQDs, dispersed in ORG solution, in a quartz cell with all transparent sides, 2mm wide and with a 1cm optical path length. The solution was previously filtered with a 0,22μm filter. The signal accumulation time is 30s.

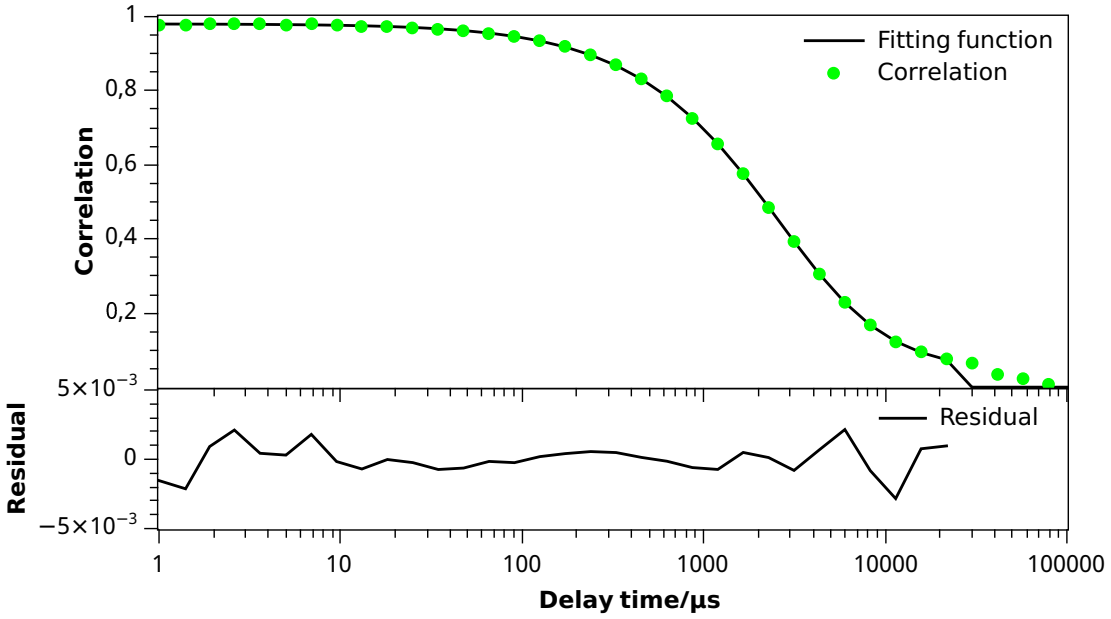

Figure XXII: Graphic of the correlation data with corresponding fitting, from the DLS analysis, of Bpy uncapped CdSe CQDs, dispersed in ZnORG solution, in a quartz cell with all transparent sides, 2mm wide and with a 1cm optical path length. The solution was previously filtered with a 0,22μm filter. The signal accumulation time is 30s.

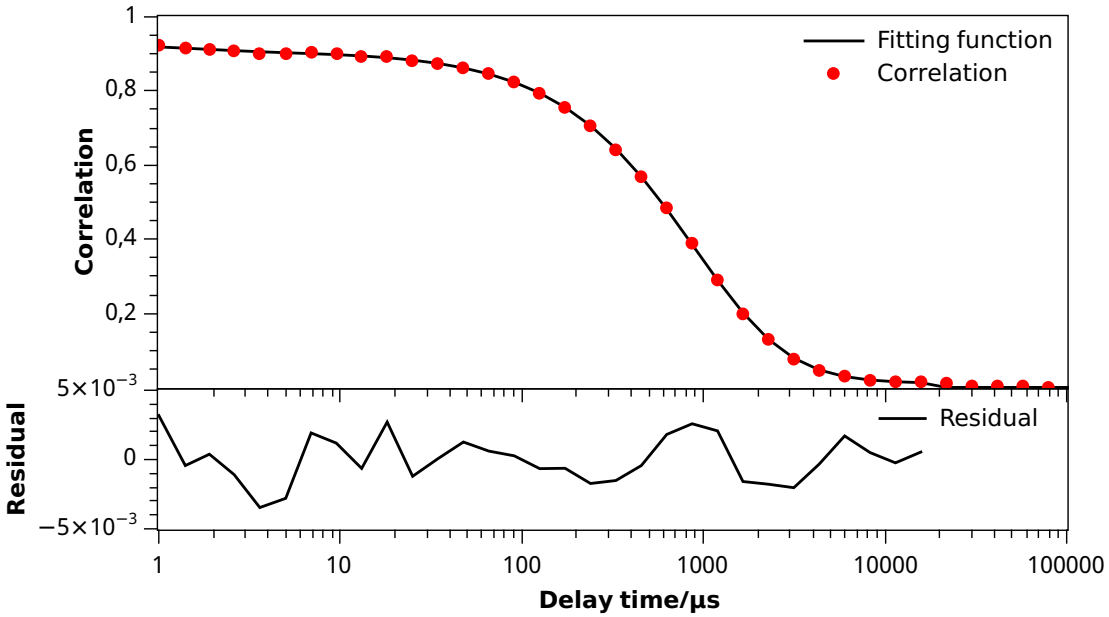

Figure XXIII: Graphic of the correlation data with corresponding fitting, from the DLS analysis, of Bpy capped CdSe CQDs, dispersed in ORG solution, in a quartz cell with all transparent sides, 2mm wide and with a 1cm optical path length. The solution was previously filtered with a 0,22μm filter. The signal accumulation time is 30s.

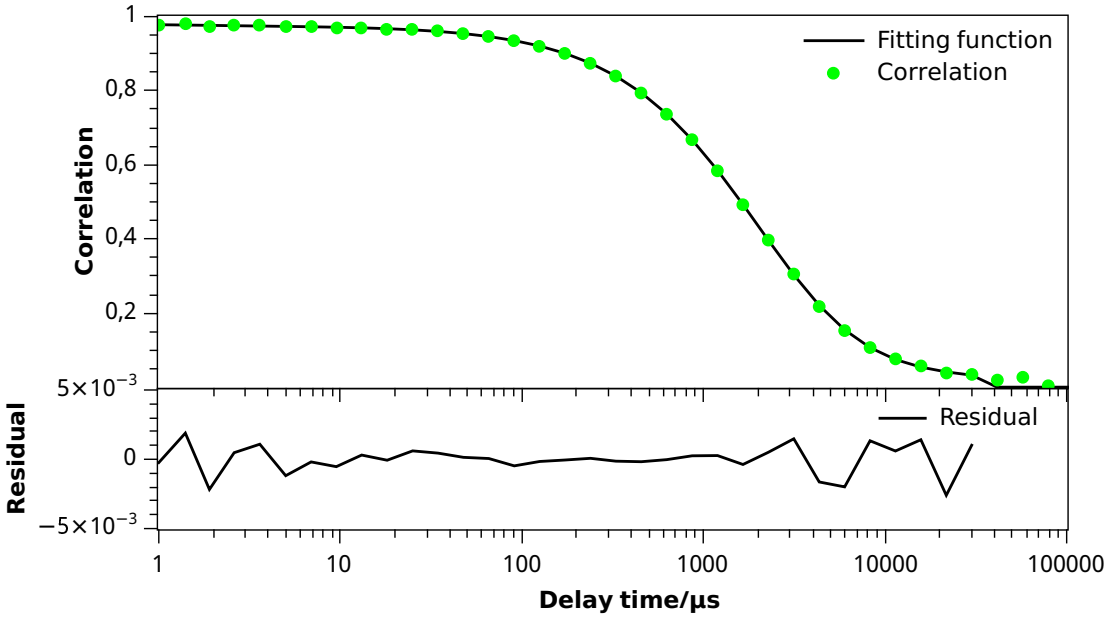

Figure XXIV: Graphic of the correlation data with corresponding fitting, from the DLS analysis, of Cys uncapped CdSe CQDs, dispersed in ZnORG solution, in a quartz cell with all transparent sides, 2mm wide and with a 1cm optical path length. The solution was previously filtered with a 0,22μm filter. The signal accumulation time is 30s.

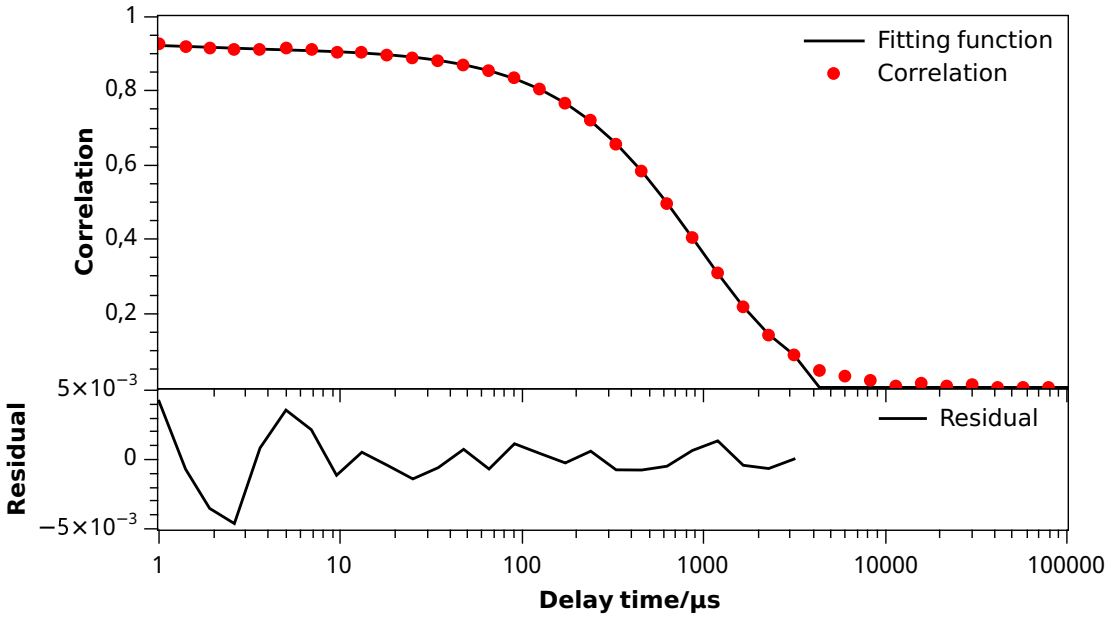

Figure XXV: Graphic of the correlation data with corresponding fitting, from the DLS analysis, of Cys capped CdSe CQDs, dispersed in ORG solution, in a quartz cell with all transparent sides, 2mm wide and with a 1cm optical path length. The solution was previously filtered with a 0,22μm filter. The signal accumulation time is 30s.

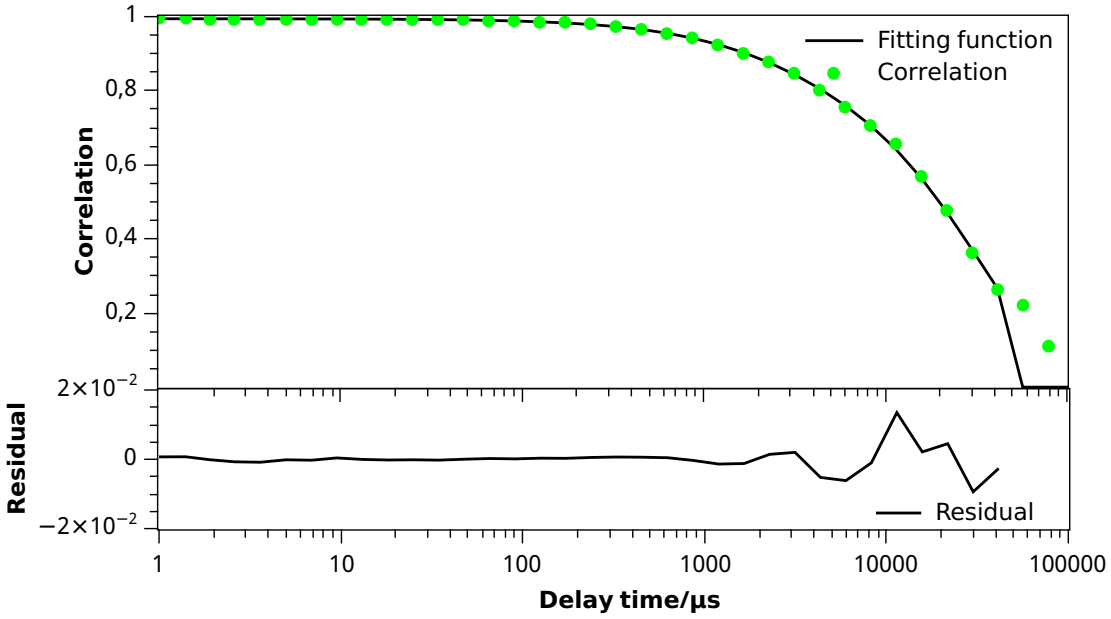

Figure XXVI: Graphic of the correlation data with corresponding fitting, from the DLS analysis, of ZnAce uncapped CdSe CQDs, dispersed in ZnORG solution, in a quartz cell with all transparent sides, 2mm wide and with a 1cm optical path length. The solution was previously filtered with a 0,22μm filter. The signal accumulation time is 30s.

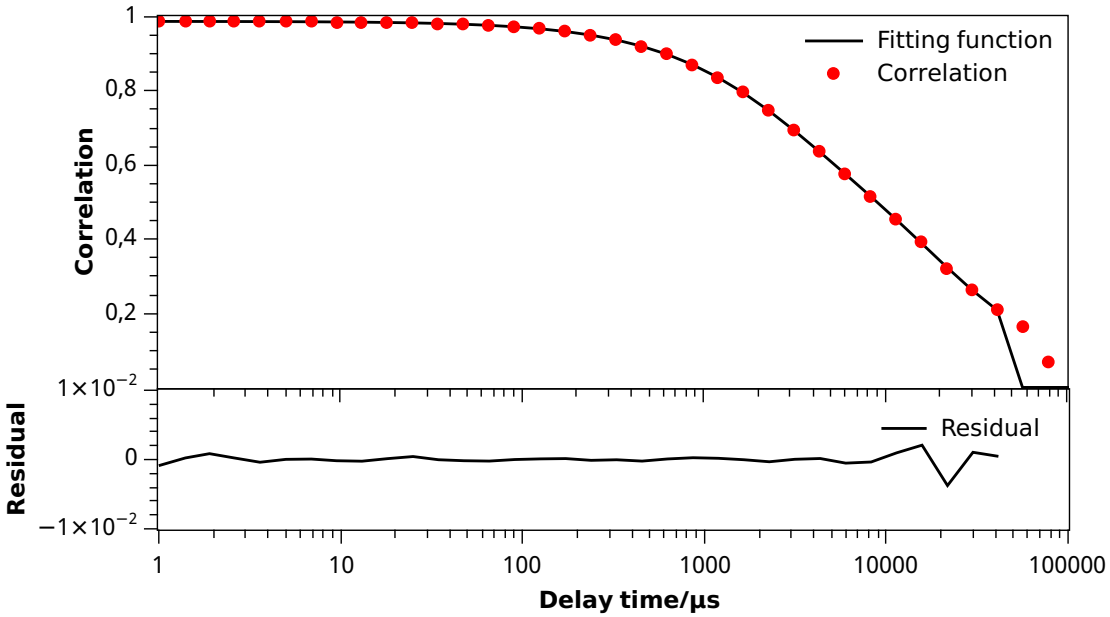

Figure XXVII: Graphic of the correlation data with corresponding fitting, from the DLS analysis, of ZnAce capped CdSe CQDs, dispersed in ORG solution, in a quartz cell with all transparent sides, 2mm wide and with a 1cm optical path length. The solution was previously filtered with a 0,22μm filter. The signal accumulation time is 30s.

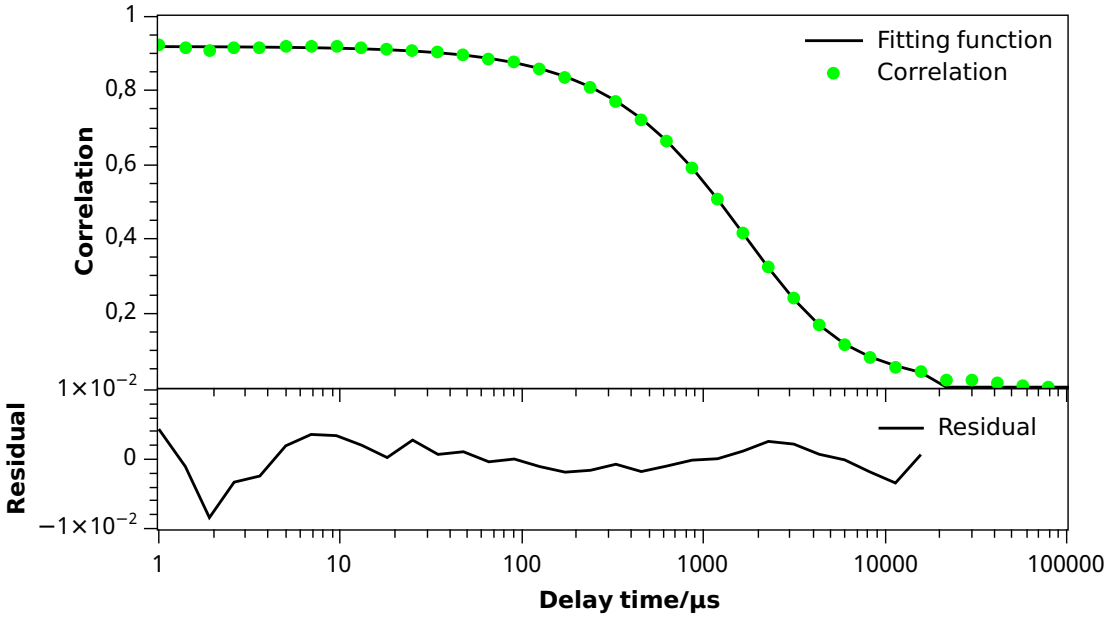

Figure XXVIII: Graphic of the correlation data with corresponding fitting, from the DLS analysis, of Py uncapped CdSe CQDs, dispersed in ZnORG solution, in a quartz cell with all transparent sides, 2mm wide and with a 1cm optical path length. The solution was previously filtered with a 0,22μm filter. The signal accumulation time is 30s.

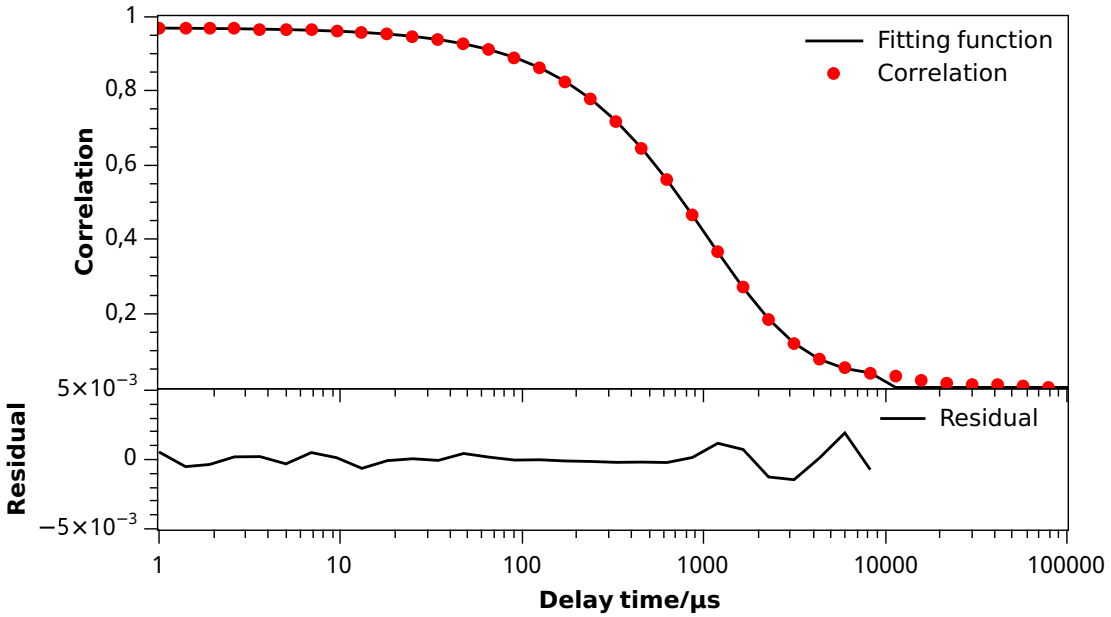

Figure XXIX: Graphic of the correlation data with corresponding fitting, from the DLS analysis, of Py capped CdSe CQDs, dispersed in ORG solution, in a quartz cell with all transparent sides, 2mm wide and with a 1cm optical path length. The solution was previously filtered with a 0,22μm filter. The signal accumulation time is 30s.

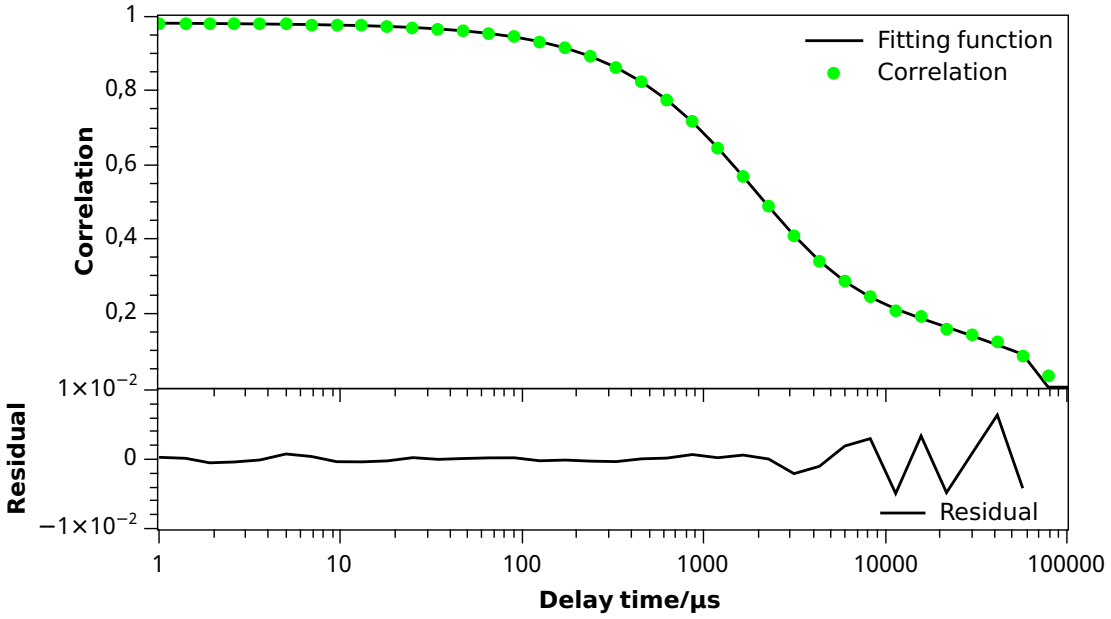

Figure XXX: Graphic of the correlation data with corresponding fitting, from the DLS analysis, of 3-MT uncapped CdSe CQDs, dispersed in ZnORG solution, in a quartz cell with all transparent sides, 2mm wide and with a 1cm optical path length. The solution was previously filtered with a 0,22μm filter. The signal accumulation time is 30s.

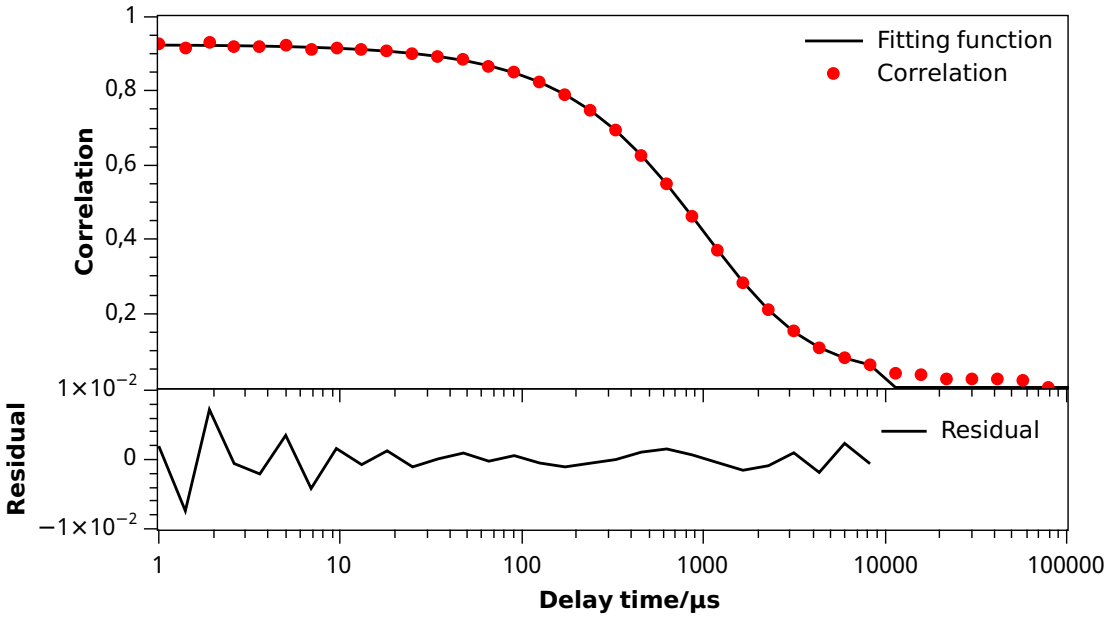

Figure XXXI: Graphic of the correlation data with corresponding fitting, from the DLS analysis, of 3-MT capped CdSe CQDs, dispersed in ORG solution, in a quartz cell with all transparent sides, 2mm wide and with a 1cm optical path length. The solution was previously filtered with a 0,22μm filter. The signal accumulation time is 30s.

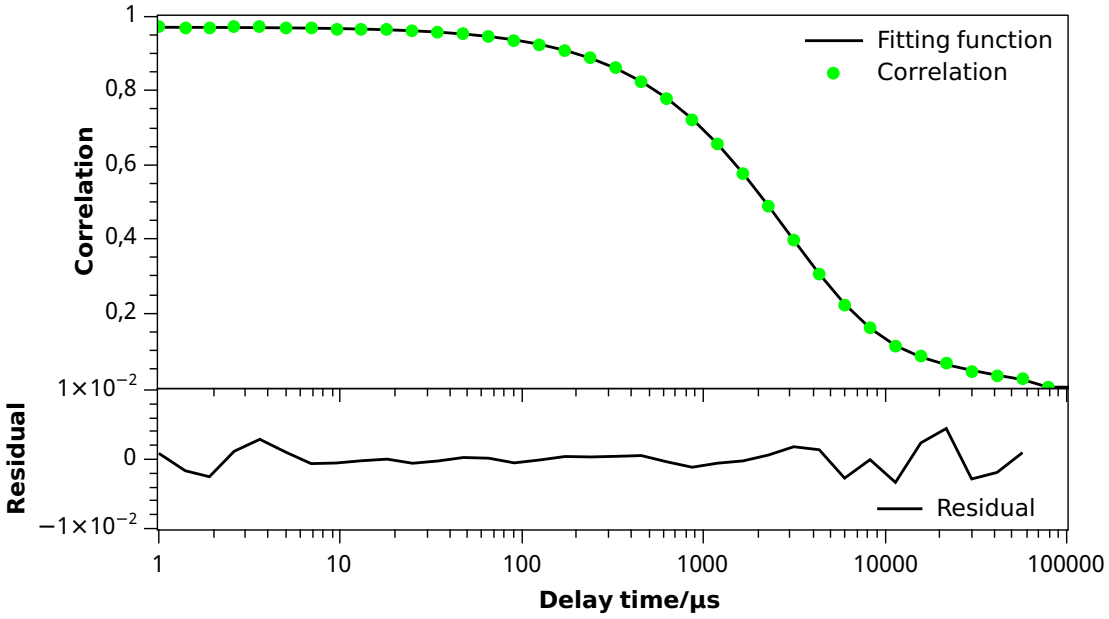

Figure XXXII: Graphic of the correlation data with corresponding fitting, from the DLS analysis, of NaAce uncapped CdSe CQDs, dispersed in ZnORG solution, in a quartz cell with all transparent sides, 2mm wide and with a 1cm optical path length. The solution was previously filtered with a 0,22μm filter. The signal accumulation time is 30s.

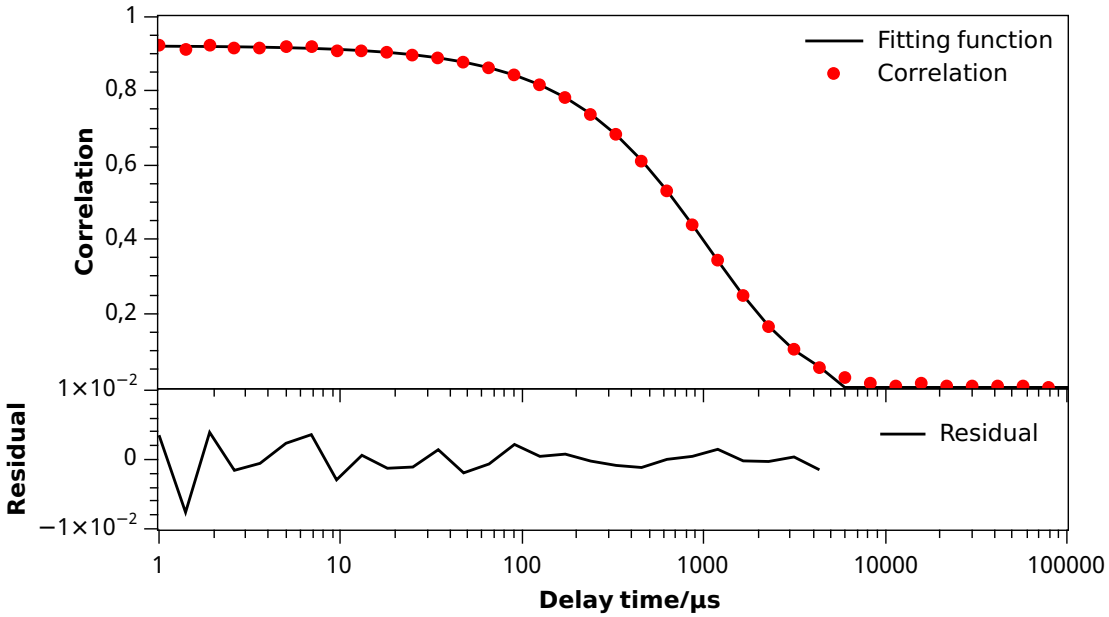

Figure XXXIII: Graphic of the correlation data with corresponding fitting, from the DLS analysis, of NaAce capped CdSe CQDs, dispersed in ORG solution, in a quartz cell with all transparent sides, 2mm wide and with a 1cm optical path length. The solution was previously filtered with a 0,22μm filter. The signal accumulation time is 30s.

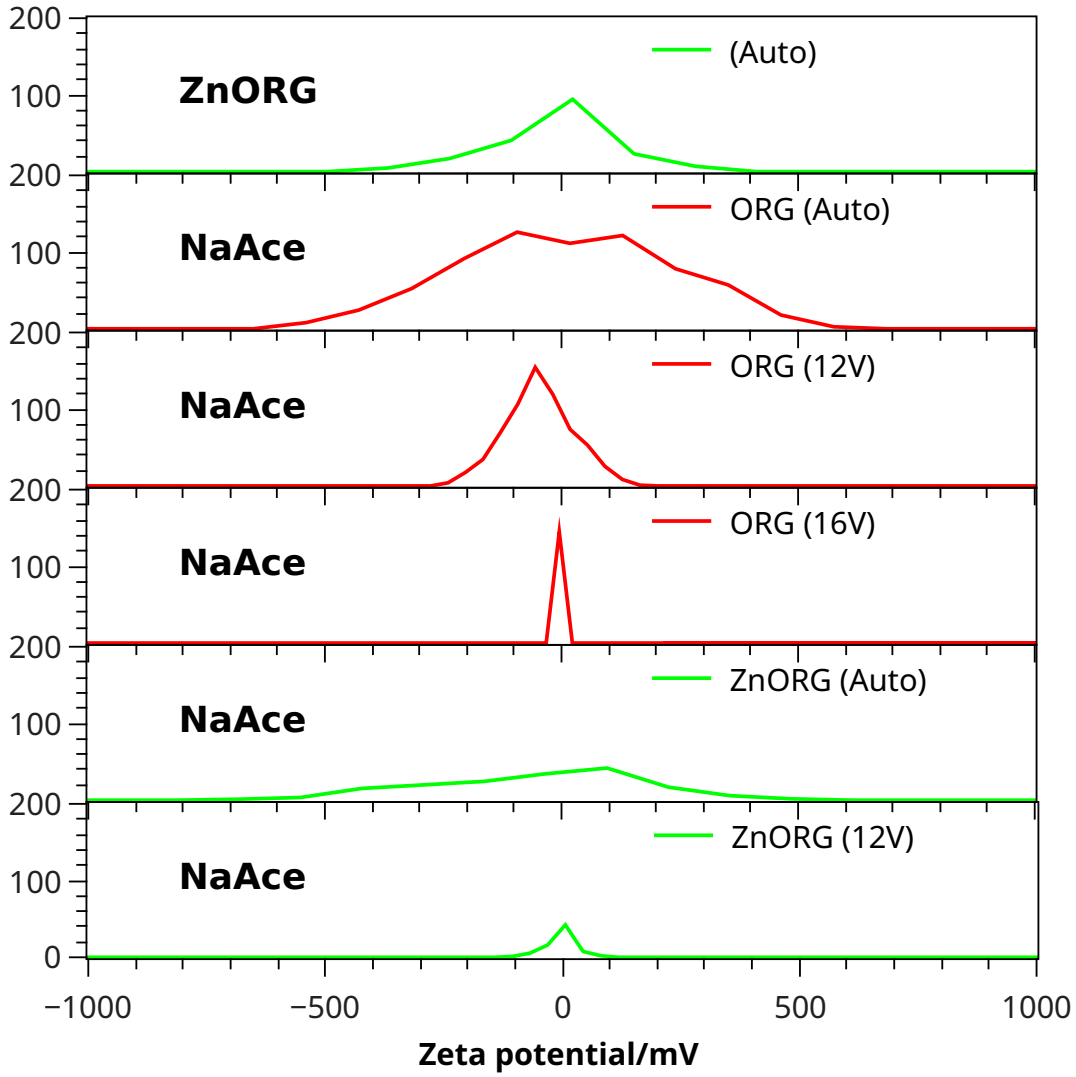

Figure XXXIV: Zeta potential graphics of ZnORG solution, NaAce capped CdSe CQDs in ORG and ZnORG. An AGILE Carbon Zeta Potential Cell was used. The solution was previously filtered with a 0,22μm filter.

Table VIII: Table with the data processed from the zeta potential analysis of ZnORG solution, NaAce capped CdSe CQDs in ORG and ZnORG. An AGILE Carbon Zeta Potential Cell was used. The solution was previously filtered with a 0,22μm filter. E. mobility is the electrophoretic mobility.

	ZnORG		
	ZnORG (Auto)	**NaAce/ZnORG (Auto)**	**NaAce/ZnORG (12V)**
Zeta potential/mV	+2,1	-4,3	-0,3
Electrode voltage/V	3,3	3,3	11,5
E. mobility/cm^2/Vs	0,000001	-0,000002	2.05
Conductivity/mS/cm	0,466	0,502	497
	ORG		
	NaAce/ORG (Auto)	**NaAce/ORG (12V)**	**NaAce/ORG (16V)**
Zeta potential/mV	+5,2	-50,3	-6,0
Electrode voltage/V	3,9	11,7	15,6
E. mobility/cm^2/Vs	0,000002	-0,000023	-0,000003
Conductivity/mS/cm	0,074	0,073	0,076

TEM Images

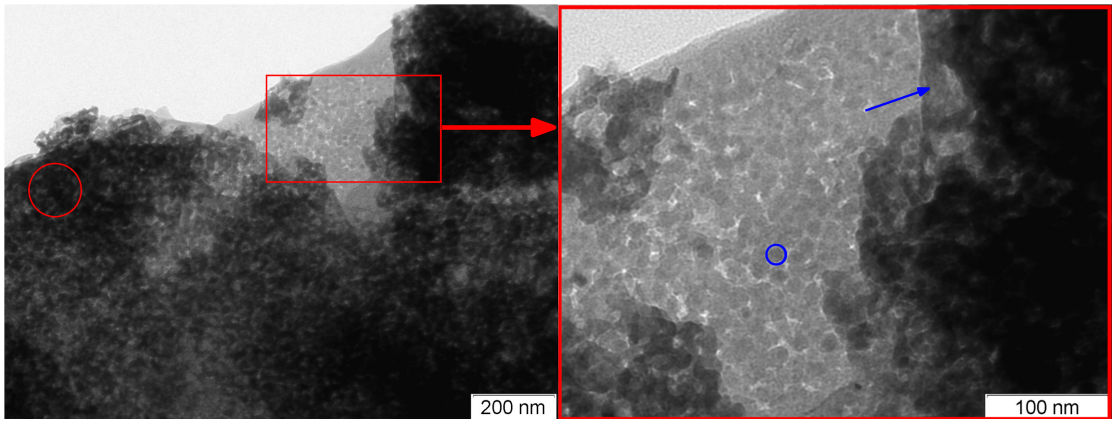

Figure XXXV: TEM image of zinc acetate dihydrate CdSe CQDs. A - the red circle points to an aggregate with a diameter ranging from 100nm to 200nm. B - zoomed image of the area represented by a red square in A. The blue circle depicts a round aggregate with a diameter of 13nm and the blue arrow points to a particle with a diameter of 2,8nm. The CQDs were suspended in absolute ethanol, with the aid of ultrasounds, and deposited on a copper grid.

Photography Color Correction

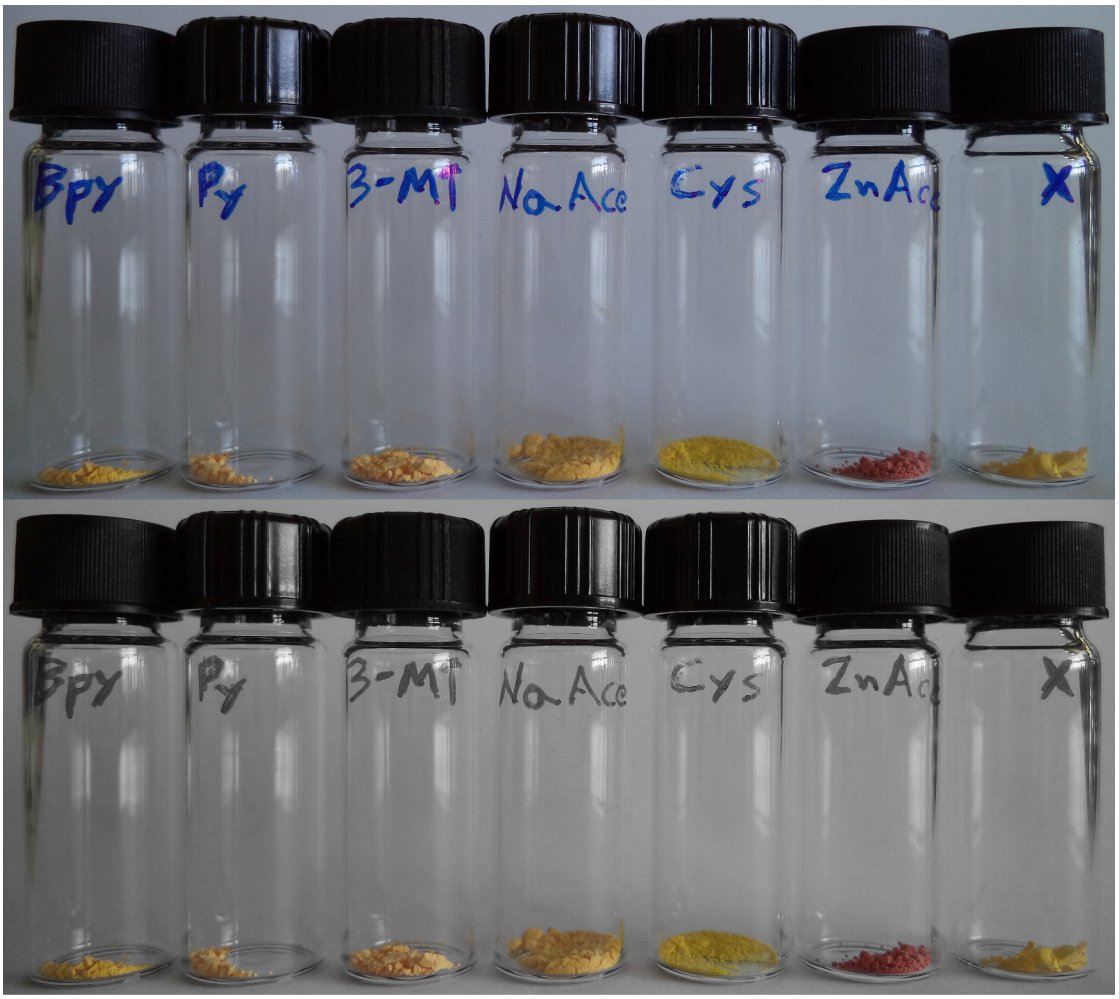

Figure XXXVI: Photography of the capped CQDs from the experiment described in section 2.1.2.1 under visible light, on the top, and the same after color removal, on the bottom.

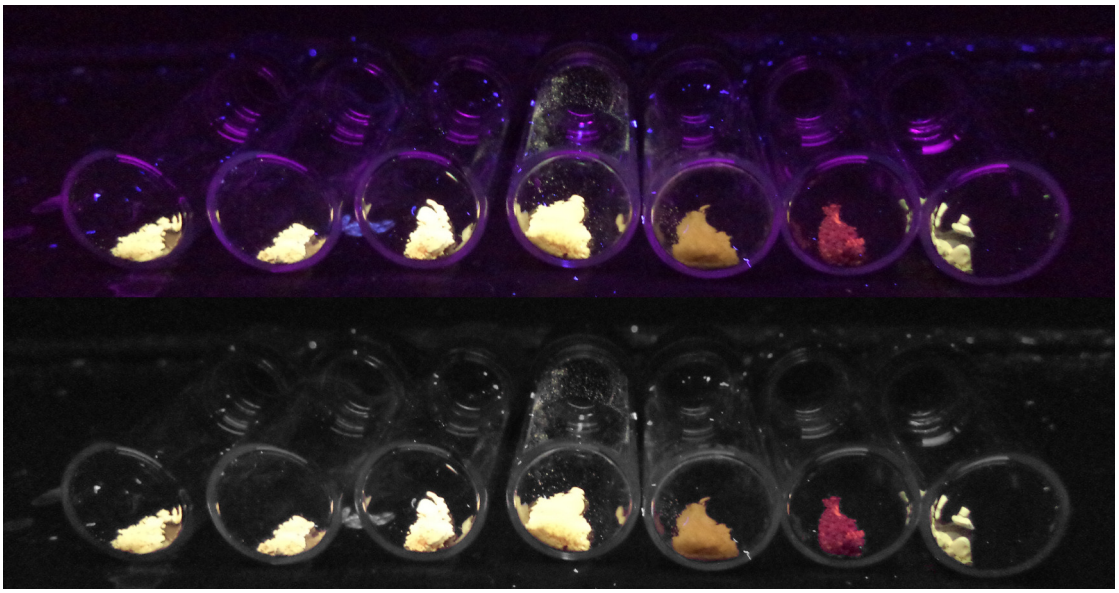

Figure XXXVII: Photography of the capped CQDs from the experiment described in section 2.1.2.1 under UV light, on the top, and the same after color removal, on the bottom.